Probing the mechanism of dihydrodipicolinate synthase

A thesis submitted in partial
fulfilment of the requirements
for the degree of

Masters of Science
at the
University of Canterbury

by

Tatiana P. Soares da Costa

Table of contents

Chapter Four: Crystal structures of DHDPS-K161A and DHDPS-K161R

Chapter Five:Discussion and conclusions

Chapter Six: Experimental

Table of contents

Abstract

Dihydrodipicolinate synthase (DHDPS, E.C. 4.2.1.52) is the enzyme that catalyses the first committed step in the lysine biosynthetic pathway, which involves the condensation reaction between (*S*)-aspartate β-semialdehyde ((*S*)-ASA) and pyruvate *via* a ping-pong mechanism, and is feedback inhibited by lysine. The major hallmark of this reaction is the formation of a Schiff base intermediate between pyruvate and the active site residue lysine 161. Surprisingly, this had never been confirmed using site-directed mutagenesis. In an attempt to investigate the necessity of this residue, two site-directed mutants were generated: DHDPS-K161A and DHDPS-K161R. They were then over-expressed, purified and characterised by steady-state kinetics, circular dichroism (CD) spectroscopy, differential scanning fluorimetry (DSF), isothermal titration calorimetry (ITC) and X-ray crystallography. Wild-type DHDPS was also over-expressed, purified and characterised in order to provide baseline data for comparison.

Unexpectedly, the mutant enzymes were still catalytically active, despite a significant decrease in activity. The k_{cat} values for DHDPS-K161A and DHDPS-K161R were 0.06±0.02 s^{-1} and 0.16±0.06 s^{-1} respectively, compared to 45±3 s^{-1} for the wild-type enzyme. Another interesting finding was a shift in the mechanism, from ping-pong to ternary-complex. This implies that the strict order of reaction sequences observed in the wild-type enzyme was relaxed in the mutant enzymes. The K_m values with respect to pyruvate increased by only 3-fold for both enzymes (0.45±0.04 mM for DHDPS-K161A and 0.57±0.06 mM for DHDPS-K161R, compared to 0.15±0.01 mM for the wild-type DHDPS), indicating a subtle change in pyruvate binding affinity; while the K_{mASA} value remained the same for DHDPS-K161R (0.12±0.01 mM) and increased by 2-fold for DHDPS-K161A (0.23±0.02 mM). Both enzymes behaved in an entirely analogous fashion to the wild-type enzyme in regards to lysine inhibition, demonstrating the lack of involvement of lysine 161 in the regulatory mechanism.

Treatment with the reducing agent sodium borohydride provided evidence that a Schiff base is not formed when pyruvate binds to either one of the mutant enzymes. DSF showed that the melting temperature for DHDPS-K161A and DHDPS-K161R upon addition of pyruvate increased to a lesser extent than for the wild-type enzyme, suggesting that stabilisation of DHDPS by pyruvate is largely dependent on Schiff base formation.

CD spectroscopy showed that the mutant enzymes had identical secondary structures in solution to the wild-type enzyme. The crystal structures of DHDPS-K161A and DHDPS-K161R were also solved to resolutions of 2.0 and 2.4 Å respectively. They showed no major rearrangement within their active sites, indicating that their attenuated catalytic activities were due to the removal of lysine 161, as opposed to gross structural alterations induced by the mutations. The crystal structure of the mutant enzymes were also solved with pyruvate bound and they showed that both mutant enzymes still had a well defined binding pocket for pyruvate that is not dependent of lysine 161. ITC experiments demonstrated that in the absence of Schiff base formation, entropic contributions may be responsible for the observed enzymatically accelerated reaction of the two DHDPS substrates, since no discernible heat was produced upon binding of pyruvate to the mutant enzymes.

Based on these results, it can be concluded that although lysine 161 is important in the DHDPS-catalysed reaction, it is not absolutely essential. The current proposed mechanism, where the tautomerisation of the Schiff base to an enamine species creates the nucleophile necessary for attack of (*S*)-ASA, had to be reconsidered and expanded. We propose that the enol form of pyruvate, which exists in equilibrium with its keto tautomer, can fulfill the role of the enamine species. NMR studies using hydrogen-deuterium exchange suggest that the rate of enolisation is unchanged in DHDPS-K161A and DHDPS-K161R catalysed mechanism, ruling out the possibility that the enolisation process could be the rate-determining step. It is likely that substrate orientation and favourable charge interactions may facilitate the interaction of an active site bound pyruvate with (*S*)-ASA and may be the major catalytic devices operating in DHDPS-

K161A and DHDPS-K161R. Removal of the Schiff base-forming residue in DHDPS could not impede catalysis completely because of the existence of this ‘back-up’ mechanism, in which lysine 161 plays no part. These conclusions may shed light into the mechanism and evolution of enzymatic activity of other class I aldolases and they underscore the functional plasticity of enzyme active sites.

List of Abbreviations

α	ratio of *V* and *V'*
a	slope of curve within T_m
A	alanine
A	concentration of substrate A
Å	Ångstrom
Amp^r	gene conferring ampicillin resistance
(*S*)-ASA	(*S*)-aspartate β-semialdehyde
ADP	adenosine-5'-diphosphate
ATP	adenosine-5'-triphosphate
B-value	estimation of atomic mobility
B	concentration of B
BSA	bovine serum albumin
^oC	degrees Celsius
c	product of the receptor concentration and the binding constant, K_b
CBPHA	*trans*-2'-carboxybenzalpyruvate hydratase-aldolase
CD	circular dichroism
DAP	*meso*-diaminopimelate
*dap*A	gene encoding dihydrodipicolinate synthase
*dap*B	gene encoding dihydrodipicolinate reductase
Da	dalton
DHDPR	dihydrodipicolinate reductase
DHDPS	dihydrodipicolinate synthase
DNA	deoxyribonucleic acid
DOGDH	D-5-keto-4-deoxyglucarate dehydratase
ddNTP	2',3'-dideoxynucleic acid triphosphate
DSF	differential scanning fluorimetry
dH_2O	distilled water
dsDNA	double stranded DNA

E	glutamate
ε	extinction coefficient
E. coli	*Escherichia coli*
g	gram
G	glycine
H	histidine
ΔH	change in enthalpy
HBPHA	*trans-o*-hydroxybenzylidenepyruvate hydratase-aldolase
HEPES	*N*-2-hydroxyethylpiperazine-*N'*-2-ethane sulfonic acid
HIC	hydrophobic interaction chromatography
HTPA	(4*S*)-4-hydroxy-2,3,4,5-tetrahydro-(2*S*)-dipicolinate
I	isoleucine
I	inhibitor
$I_{0.5}$	inhibitor concentration giving 50% inhibition
IR	infrared
ITC	isothermal titration calorimetry
IPTG	isopropyl β-D-thiogalactopyranoside
J	coupling between two nuclear spins
K	lysine
kbp	kilobase
kcal	kilocalorie
k_{cat}	catalytic constant
kDa	kilodalton
kV	kilovolt
KDGA	D-2-keto-3-deoxygluconate aldolases
K_b	binding constant
K_i	inhibition constant
K_m	Michaelis-Menten constant
K_{sA}	binding constant for substrate A to the free enzyme form
lac	operon encoding β-galactosidase
L	litre

LB	Luria-Bertani broth
LL	minimum intensity
µCal	microcalorie
µg	microgram
µL	microlitre
µmol	micromole
M	moles per litre
$[M]_{t\,(0)}$	initial macromolecular concentration
mA	milliamp
mg	milligram
MHz	megahertz
mL	millilitre
mM	millimoles per litre
MOPS	3-morpholinopropanesulfonic acid
nm	nanometre
N	asparagine
N	primer length
n	number of binding sites
N^{ε}	nitrogen atom attached to an amino acid's alpha carbon
$NaBH_4$	sodium borohydride
NAL	*N*-acetyl neuraminate lyase
$NADP^+$	nicotinamide adenine dinucleotide phosphate
NADPH	nicotinamide adenine dinucleotide phosphate, reduced form
ng	nanogram
N-OG	*N*-octyl-β-*R*-glucopyranoside
NMR	nuclear magnetic resonance
OG1	hydroxyl group attached to an amino acid's alpha carbon
OH	hydroxyl group
PAGE	polyacrylamide gel electrophoresis
PCR	polymerase chain reaction
pJG001	pBluescript plasmid containing the *dap*A gene encoding DHDPS

pSD002	pETM11 plasmid containing the *dap*B gene encoding DHDPR
P_i	inorganic phosphate
PYR	pyruvate
ppm	parts per million
R	arginine
recA	gene encoding for the RecA protein
rpm	revolution per minute
rmsd	root mean square deviation
S	concentration of substrate
s	second
S.E.	standard error
ΔS	change in entropy
SDS	sodium dodecyl sulfate
T	threonine
T	temperature
TAE	tris-acetyl EDTA electrophoresis buffer
Tet^r	tetracycline resistance gene
TCA	trichloroacetic acid
T_m	melting temperature
Tris.HCl	tris (hydroxymethyl) methylamine hydrochloride salt
UL	maximum intensity
UV	ultraviolet
v	initial rate
V	maximum rate of reaction
V'	maximum rate of reaction in the presence of saturating inhibitor
v/v	volume per volume
w/v	weight per volume
WT	wild-type
X-gal	5-bromo-4-chloro-3-indolyl-β-*δ*-galactosidase
Y	fluorescence intensity at temperature *T*
Y	tyrosine

Acknowledgements

First of all, I would like to say a huge thank you to my supervisor Juliet for always seeing the bright side of things, for the great ideas, guidance, friendship and let's not forget, the great parties.

A big thanks also goes to the present and past members of the purple lab. Ren, you are an inspiration. Thanks for your time, support and enthusiasm. Sean, it's been a pleasure working with you despite your awful taste in music. Thanks for always answering my questions with a smile on your face and for the great chats about everything, ranging from enzymes to Spice Girls. Grant, I will never forget our conversations, I am so glad I met someone who is into shoes as much as I am☺ Andrew, thanks for helping me with all things related to chemistry. Let's not forget all the girls from the lab who kept the boys on their toes: Sophie (mini-me), Shiva (I will miss our 3 hour lunches), Genevieve (the best cake maker I know), Pam (the best Lorne room mate), Sarah, Susie and of course, Jackie, for keeping me in line.

A special thanks goes out to Gareth for all the late night chats, for teaching me about growth-retarded salmon and for being the best office companion ever! Big kudos to Nikki and Julia for their unparallel support and great coffee breaks! Yes, we made it ☺

I also would like to thank Geoff for teaching me the wonders of X-ray crystallography and for making my stay in Palmerston North so enjoyable.

Lastly, thanks to Mum and Dad for supporting me throughout my years at uni, for putting up with my bad mood after frustrating days in the lab and for always believing in me.

Chapter One

Introduction

The subject of this thesis is the enzyme dihydrodipicolinate synthase (DHDPS) from *Escherichia coli*. This enzyme catalyses the first committed step of the diaminopimelate pathway of lysine biosynthesis in plants and bacteria, and is feedback inhibited by the end product, lysine.

The work described in this thesis focuses specifically on the elucidation of the role of an active site residue in this enzyme, lysine 161. This is achieved using site-directed mutagenesis, followed by characterisation of the variant forms of the enzyme using steady-state kinetics, far-ultraviolet (UV) circular dichroism (CD) spectroscopy, differential scanning fluorimetry (DSF), isothermal titration calorimetry (ITC), and X-ray crystallography.

1.1 Background

The identification of the novel amino acid, *meso*-diaminopimelate (DAP), found in bacterial hydrolysates[1,2] led to the investigation of the bacterial biosynthetic pathway of lysine.[3] This included the discovery of the enzyme that catalyses the first unique step in this pathway, DHDPS.[4,5]

Lysine is an essential amino acid and is part of the aspartate family, which also includes methionine, threonine, and isoleucine.[6,7] The biosynthesis of aspartate-derived amino acids is restricted to bacteria, plants and some fungi and, as such, they are essential amino

acids in animal nutrition.[8] Lysine is often the most limiting amino acid nutritionally.[9] Thus, this pathway has been the focus of research for several years, much of which is ultimately aimed at the improvement of crop growth as well as enhancement of lysine production in crops.[7,9] In addition, a branch of research has focused on the inhibition of DHDPS, which is a validated drug target[10-12] because it occurs at a branchpoint in the lysine biosynthetic pathway and its inhibition has the potential to create novel herbicides and antibiotics.[6,13] Neither area has yet met with much success, in part because the catalytic and regulatory mechanisms of the enzyme are not fully understood.

1.2 Biosynthesis of the aspartate family of amino acids

The first step in the synthesis of aspartate-derived amino acids involves the phosphorylation of (*S*)-aspartate to (*S*)-β-aspartyl phosphate, with subsequent reduction to (*S*)-aspartate β-semialdehyde ((*S*)-ASA) in an NADPH-dependent reaction (Figure 1.1). (*S*)-ASA resides at the branchpoint of the biosynthetic pathways of the four aspartate-derived amino acids, as it either enters the diaminopimelate (DAP) pathway to produce (*S*)-lysine, or is reduced by homoserine dehydrogenase to give (*S*)-homoserine, the precursor to (*S*)-methionine, (*S*)-threonine, and (*S*)-isoleucine.[6,14]

1.3 Dihydrodipicolinate synthase

1.3.1 Genetic studies

The *dap*A locus in *E. coli*, which encodes for DHDPS, was mapped to 53 minutes on the *E. coli* chromosome,[15] cloned[16] and sequenced.[15] Based on the nucleotide sequence, a subunit molecular weight of 31,372 Da was deduced for the *E. coli* DHDPS. Unlike six of the nine enzymes present in the lysine biosynthetic pathway, the intracellular levels of DHDPS are not regulated at the genetic level by (*S*)-lysine.[17] The *dap*A gene has also been cloned and sequenced from a number of other bacterial[18-21] and plant sources.[22-26]

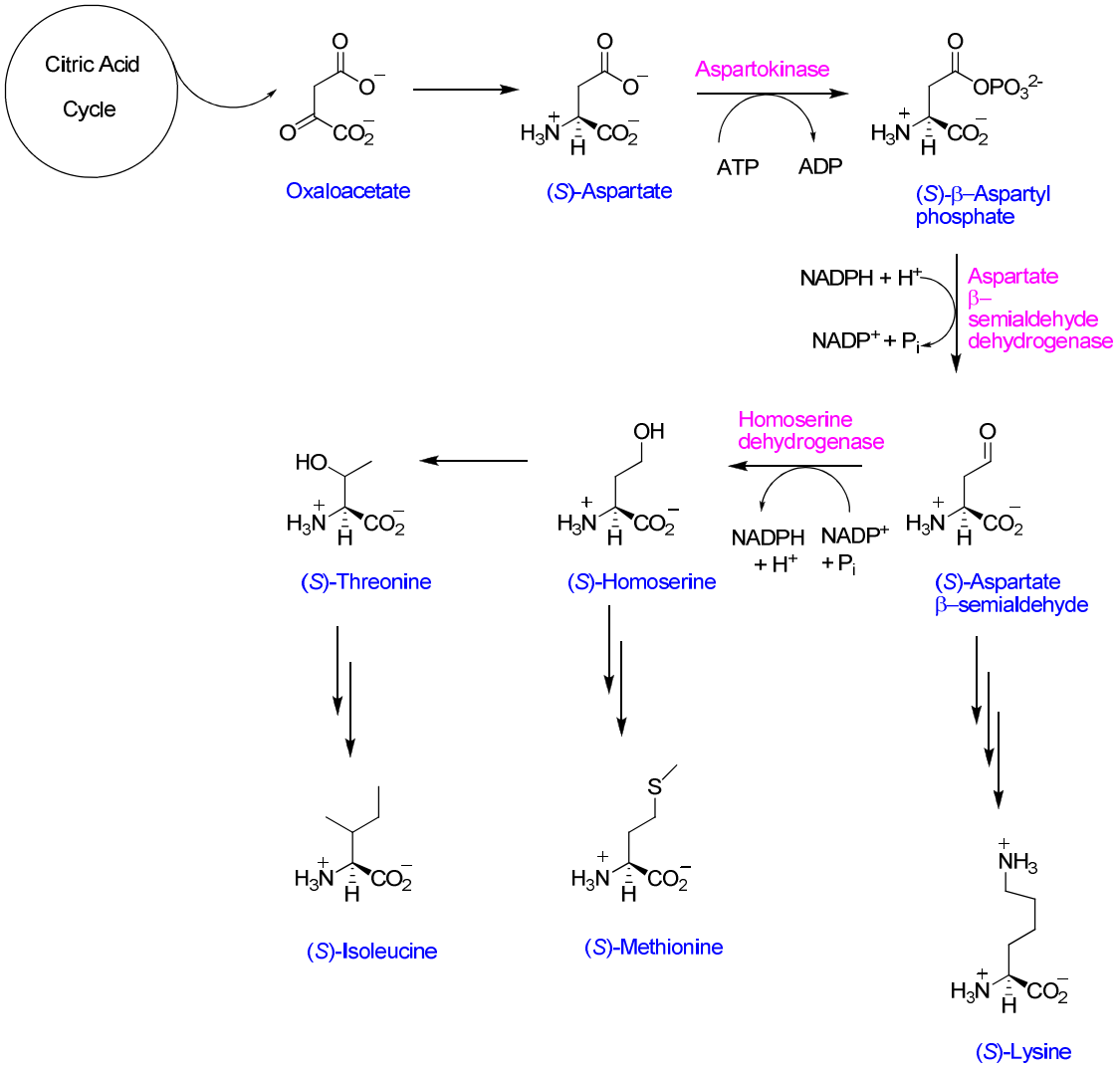

Figure 1.1 *Biosynthesis of the aspartate family of amino acids.*[27]

1.3.2 Structural studies of *E. coli* DHDPS

The crystal structure of *E. coli* DHDPS was first determined by Mirwaldt *et al.* (1995) at a resolution of 2.5 Å, but it has been refined since to a resolution of 1.9 Å (Figure 1.2).[28] The enzyme is homotetrameric, consisting of a dimer of tight dimers with weak contacts between the two tight dimers compared to the intradimeric contacts.[29] Each monomer contains two domains: the N-terminal domain consists of residues 1 to 224 and folds into a $(\beta/\alpha)_8$ barrel, which contains the active site; the C-terminal domain consists of residues

224 to 292, forming three α-helices, the role of which remains to be resolved.[30] This is a similar structure to other class I aldolases including *N*-acetylneuraminate lyase (NAL), which is mechanistically related to DHDPS.[31]

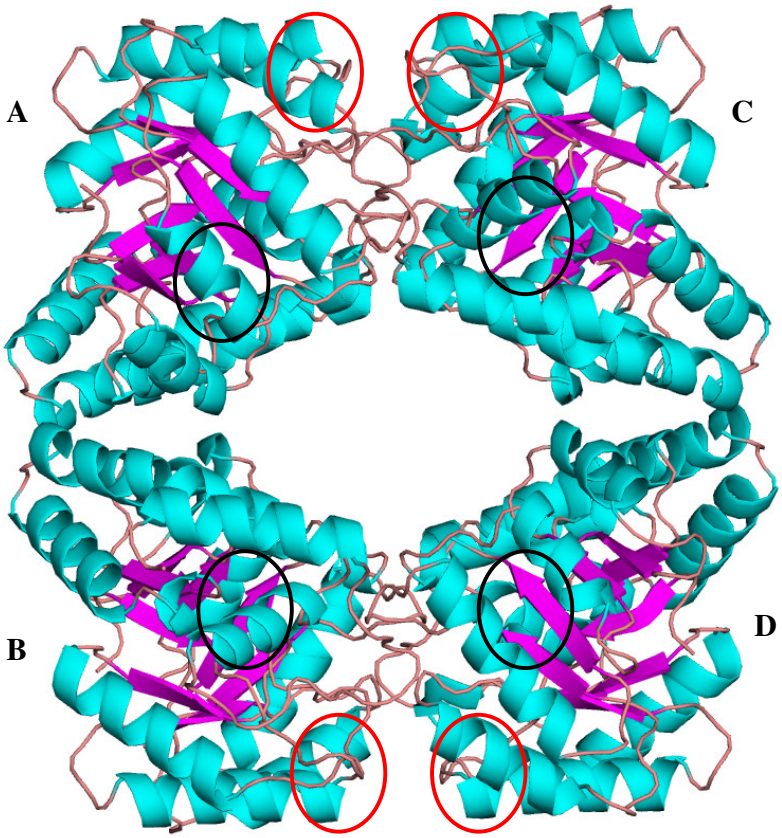

Figure 1.2 *The tetrameric structure of* E. coli *DHDPS, showing the four monomers labelled A-D. Monomers A/C and B/D associate tightly to form tight dimers, which self-associate to form a tetramer.[28] β-Sheets are coloured purple and α-helices are coloured cyan. The active sites are indicated by the black circles and the lysine binding sites are indicated by the red circles. This figure was produced using PyMol.[32]*

The active site

E. coli DHDPS has four complete active sites. Based on the X-ray crystal structure of the *E. coli* enzyme[29,30] and sequence homologies from DHDPS of other sources,[33] it was proposed that a catalytic triad made up of residues Y133, T44 and Y107 is involved in

relaying protons in and out of the active site.[27] This was confirmed by site-directed mutagenesis experiments, where the mutation of Y133 and Y107 to a phenylalanine and the mutation of T44 to a valine, resulted in enzymes that had substantially reduced catalytic activities.[27] K161, which is the pyruvate binding residue, defines the catalytic site. It is situated at the C-terminal end of the β-barrel, in a cavity defined by the interface of the other monomer of the tight-dimer. This residue is in close proximity to Y133. R138 lies at the entrance to the active site cavity and its role in binding the carboxyl group of (*S*)-ASA has also been shown by site-directed mutagenesis.[34]

The allosteric binding site

Lysine binds at the exterior cleft of the tetramer formed at the tight-dimer interface. Several residues have to subtly rearrange in order to accommodate the binding; most notably H53, H56, E84, Y106, and Y107 from the opposite subunit.[28,35]

The dimer-dimer interface

Monomers A/C and B/D associate tightly to form dimers, which more loosely associate to form the tetrameric structure of wild-type DHDPS (Figure 1.2). The tight dimer interface includes the highly conserved residues Y106 and Y107. Their side chains interdigitate in the crystal structure of all DHDPS solved thus far, resulting in a hydrophobic, sandwich-like stacking of their aromatic rings.[30]

The loose interface between monomers A/B and C/D is thought to involve a limited number of residues, resulting in a weak association.[30,36] L197 is one of these residues and its mutation to an aspartate prevents the tight dimers from associating into a tetramer, due to the introduction of negative charge where there are normally hydrophobic interactions. The introduction of steric bulk at this position, by exchanging the leucine residue to a tyrosine, also results in a dimeric form of DHDPS.[36] These mutant enzymes displayed less than 3% of the activity of the wild-type enzyme, indicating that the tetrameric structure of *E. coli* DHDPS is important for catalysis.

1.3.3 Reaction mechanism catalysed by DHDPS

The current proposed catalytic mechanism of the DHDPS-catalysed reaction can be divided into three main steps. The first step involves Schiff base formation with pyruvate. (*S*)-ASA then binds to the active site, where it undergoes an aldol condensation reaction, followed by the release of the product (4*S*)-4-hydroxy-2,3,4,5-tetrahydro-(2*S*)-dipicolinic acid (HTPA).[29]

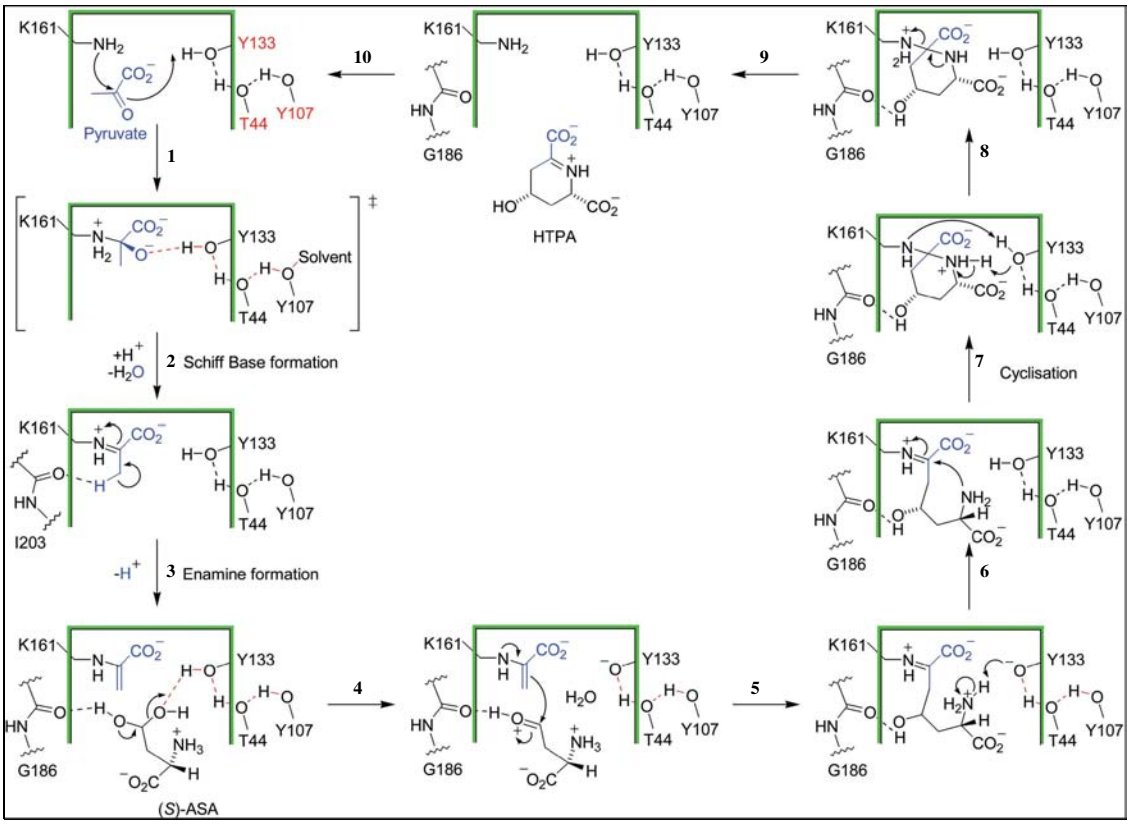

Figure 1.3 *Mechanism of the DHDPS-catalysed reaction.*[37]

Schiff base formation

Schiff base formation is initiated by nucleophilic attack of the ε-amino group of the highly conserved K161 residue in the active site upon the keto group of pyruvate, resulting in the release of water (Figure 1.3, steps 1 and 2). Y133 is proposed to play a major role in this part of the reaction *via* stabilisation of the oxyanion intermediate and as a proton donor.[29]

Aldol condensation reaction

The binding of pyruvate to the Schiff base is followed by tautomerisation to an enamine (Figure 1.3, step 3), which undergoes condensation with (*S*)-ASA (Figure 1.3, steps 4 and 5). (*S*)-ASA can exist in two different forms in solution (Figure 1.4). There is some debate as to whether (*S*)-ASA binds as the free aldehyde or as the hydrated form; the latter appears to be gaining general acceptance.[29,30,38-40] It has been observed that the hydrate of (*S*)-ASA is the predominant species in aqueous solution[39,41] and that the active site can accommodate and coordinate this species.[13,29] Assuming that the hydrate form of (*S*)-ASA is the species involved in this reaction, Y133 is in position to protonate one of the hydroxyl groups (Figure 1.3, step 4), while G186 coordinates the other one. The catalytic triad stabilises the tyrosine anion *via* a proton-relay to bulk solvent.[27,29]

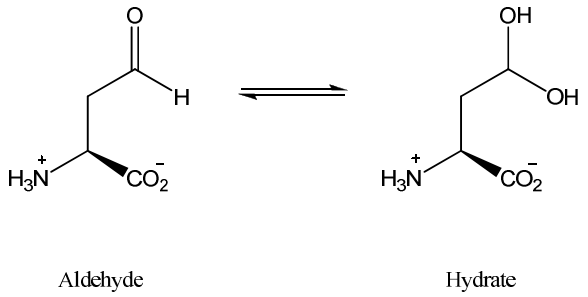

Figure 1.4 *Two possible structures of (*S*)-ASA structure in solution.*

Cyclisation and product release

Nucleophilic attack by the amine of the (*S*)-ASA moiety on the Schiff base results in cyclisation (Figure 1.3, step 7), followed by the release of the product (Figure 1.3, step 9). For the final steps of the reaction, deprotonation of the attacking amino group and transfer of a proton to the ε-amino group of K161 are necessary (Figure 1.3, step 6). Y133 is proposed to play a central role in these steps, as it is in position to coordinate the attacking amino group both before and after nucleophilic attack. Proton transfer to the ε-amino group of K161 is also proposed to be mediated through the proton-relay triad.[27,29]

It was previously assumed that the product released was the dehydrated adduct 2,3-dihydrodipicolinate (Figure 1.5).[4] However, NMR studies have shown that the cyclic hydroxy imine product HTPA is released, and that the release of water had not occurred.[29] This suggests that HTPA undergoes a non-enzymatic dehydration reaction under physiological conditions to generate 2,3-dihydrodipicolinate. However, this remains under debate, since the basic conditions used in the NMR experiment may have influenced the dehydration chemistry and accounted for the accumulation of the hydroxyl intermediate.[6]

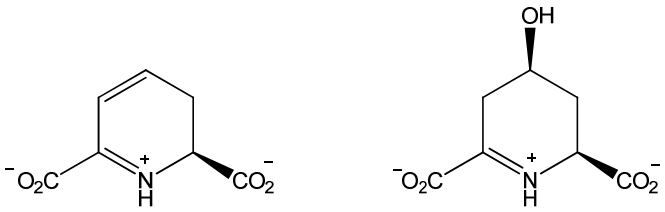

2,3-dihydrodipicolinate HTPA

Figure 1.5 *Two possible products of the DHDPS-catalysed reaction.*

1.3.4 Kinetic studies

A ping-pong mechanism has been proposed for DHDPS based on kinetic studies.[4,27,42-45] This mechanism, also known as the substituted enzyme mechanism or the double displacement mechanism, requires that the two substrates, (*S*)-ASA and pyruvate, bind to the enzyme in a defined order, through a covalent enzyme-substrate intermediate, and that two independent products are released.[46] This is consistent with the mechanism proposed in Figure 1.3, with H_2O as the first released product (step 2).

The reported Michaelis-Menten constants (K_m) of DHDPS from *E. coli* for pyruvate range between 0.11-0.25 mM, whereas for (*S*)-ASA the values range between 0.11-0.12 mM.[4,29,37,45] Higher K_m values for (*S*)-ASA have been observed for DHDPS from bacterial sources compared to that from plant sources. The values of K_m for pyruvate vary considerably within plant and bacterial species.[29]

The observation of substrate inhibition by (*S*)-ASA at high concentrations is another area that has caused debate. Stahly (1969)[47] first reported inhibition by (*S*)-ASA and suggested that it affected pyruvate binding, but not the maximal velocity, as predicted by a ping-pong mechanism. Further studies have agreed with Stahly's work.[44,48-50] However, (*S*)-ASA inhibition of DHDPS has not been observed in this laboratory.[40,45] The difference in results with respect to inhibition by (*S*)-ASA demanded a re-evaluation of the data. Dobson *et al.* (2004)[40] compared alternative preparations of (*S*)-ASA and suggested that apparent substrate inhibition is caused by an as yet unidentified inhibitor present in impure preparations and not by (*S*)-ASA. It was concluded that previous experiments documenting substrate inhibition could have resulted from artifacts associated with the ozonolysis preparation of (*S*)-ASA.

1.3.5 Regulation of DHDPS by (*S*)-lysine

Inhibition of the DHDPS-catalysed reaction by (*S*)-lysine was first observed in *E. coli* in 1962.[51] This work suggested that (*S*)-lysine is a competitive inhibitor with respect to (*S*)-ASA. Evidence from kinetic and structural studies have since supported the idea that lysine is an allosteric inhibitor;[4,29,35,42] however, the exact mechanism by which lysine exerts its regulatory effect is still open to debate.

There have been three mechanisms proposed to explain how DHDPS is regulated by lysine. The first proposal involves the re-orientation of Y107, which is part of the catalytic triad, when lysine is bound.[29,35] The second hypothesis is that upon re-orientation of Y107, the flexibility of R138, which binds to the carboxyl group of (*S*)-ASA, is compromised and this could inhibit DHDPS activity. It has been argued that in the final stages of the catalysis, cyclisation requires some flexibility in R138 so that the Schiff base can be formed.[29,34] The third mechanism of inhibition proposed involves (*S*)-lysine blocking the proton shuttle through a water channel, which connects the active site to the bulk solvent *via* a series of hydrogen bonds when lysine is bound.[27]

The level of inhibition of DHDPS by (*S*)-lysine varies widely and can be grouped into three classes:[29]

(i) Plant enzymes, which are strongly inhibited by lysine with an $I_{0.5}$ between 0.01 and 0.05 mM.[23,52-54]

(ii) Enzymes from *E. coli*,[4] *Bacillus sphaericus*,[55] and *Methanobacterium thermoautotropicum*,[56] which are only weakly inhibited with an $I_{0.5}$ between 0.25 and 1.0 mM.

(iii) DHDPS from most Gram-positive bacteria and *Thermotoga*[57] (Gram-negative), which appear not to be inhibited at all, with an $I_{0.5}$ of more than 10 mM.[58-61]

1.3.6 Related enzyme *N*-acetylneuraminate lyase (NAL)

Like DHDPS, *N*-Acetylneuraminate lyase (NAL) is a member of the $(\beta/\alpha)_8$ barrel proteins and the class I aldolase family. NAL is involved in the regulation of intracellular sialic acid concentration,[31] catalysing the aldol cleavage of *N*-acetylneuraminate to form *N*-acetylmannosamine and pyruvate *via* a Schiff base intermediate. *E. coli* DHDPS displays significant sequence homology with respect to *E. coli* NAL, revealing important residues for their tertiary structure, active site and lysine binding site. This sequence similarity is not restricted to the enzyme from *E. coli*, and several proteins from the NAL sub-family, from a variety of species have been shown to exhibit significant interspecies sequence and structural homology.[33]

E. coli DHDPS residues T44, T45, Y133, K161, G186, Y107 and Y203 are conserved in *E. coli* NAL. Alignment of the structures of DHDPS and NAL indicates these residues have the same spatial positioning. This led to the conclusion that the mechanism of Schiff base formation and the subsequent aldol reaction is likely to be conserved in both enzymes.[29] Current opinion favours the entire $(\beta/\alpha)_8$ barrel protein family as having arisen from one ancestral protein, or from a limited number of ancestors, due to the deduced sequence similarity within the family.[33]

When lysine 161 was substituted to an alanine in *Clostridium perfringens* NAL by site-directed mutagenesis, activity was completely removed.[62] However, when the residue was mutated to an arginine, 3% of the original activity was still maintained. It was proposed that residual activity could be detected because the guanidinium group of arginine should still allow the formation of the Schiff base, but at a much slower rate than with the amino group of lysine 161. This is because this group is stabilised mesomerically and thus, the NH_2 group of arginine is less nucleophilic than that of lysine. Although arginine has been shown to allow Schiff base formation in the work by Morris *et al.* (1996)[63] using sodium borohydride to trap the intermediate, no further experimental work was conducted by Kruger *et al.* (2001)[62] to confirm the ability of the NAL-K161R to form the covalent intermediate.

1.4 Summary and aims of this project

Although the mechanism of DHDPS has been studied in considerable detail, the absolute necessity for the active site lysine residue, K161, has, strikingly, never been established like in the NAL enzyme. The primary aim of this thesis is to address this gap in our understanding of DHDPS. The results of this study may shed some light on the evolutionary relationship between the two enzymes.

The elucidation of the role of this residue has been achieved by generating and purifying two site-directed mutants of lysine 161, followed by their characterisation using steady-state kinetics, far-UV CD, DSF and ITC, which are all described in Chapter three. Chapter two deals with the over-expression, purification and kinetic description of wild-type DHDPS to provide baseline data for comparison with those obtained for the mutant enzymes, as well as including the over-expression and purification of DHDPR, which is the coupling enzyme used in the DHDPS kinetic assays. Chapter four includes the crystal structure of the mutants generated in order to detect any changes in the tertiary structure induced by the mutations. Chapter five is a discussion chapter, which brings together all

the information gathered in Chapters three and four. Chapter six contains all the experimental work pertaining to Chapters two to four.

1.5 References

1. Work, E., A new naturally occurring amino acid. *Nature* **1950,** 165, 74-75.
2. Work, E., The isolation of diaminopimelic acid from *Corynebacterium diphteriae* and *Mycobcterium tuberculosis*. *Journal of Biochemistry* **1951,** 49, 17-23.
3. Gilvarg, C., Biosythesis of diaminopimelic acid. *Fin Lakaresallsk Handl* **1960,** 19, 948-952.
4. Yugari, Y.; Gilvarg, C., The condensation step in diaminopimelate synthesis. *Journal of Biological Chemistry* **1965,** 240, 4710-4716.
5. Shedlarski, J. G.; Gilvarg, C., The pyruvate-aspartic semialdehyde condensing enzyme of *Escherichia coli*. *Journal of Biological Chemistry* **1970,** 245, 1362-1373.
6. Cox, R. J.; Sutherland, A.; Vederas, J. C., Bacterial diaminopimelate metabolism as a target for antibiotic design. *Bioorganic Medical Chemistry* **2000,** 8, 843-871.
7. Viola, R. E., The central enzymes of the aspartate family of amino acid biosynthesis. *Accounts of Chemical Research* **2001,** 34, 339-349.
8. Keeler, S. J.; Maloney, C. L.; Webber, P. Y.; Patterson, C.; Hirata, L. T.; Falco, S. C.; Rice, J. A., Expression of the *de novo* high-lysine alpha-helical-coiled-coil proteins may significantly increase the accumulated levels of lysine in mature seeds of transgenic tobacco plants. *Plant Molecular Biology* **1997,** 34, 15-29.
9. Bright, S. W. J.; Shewry, R., Improvement of protein quality in cereals. *Critical Review of Plant Sciences* **1983,** 1, 49-93.
10. Monaghan, R. L.; Barrett, J. F., Antibacterial drug discovery- then, now and the genomics future. *Biochemical Pharmacology* **2006,** 71, (7), 901-909.
11. Pucci, M. J., Use of genomics to select antibacterial targets. *Biochemical Pharmacology* **2006,** 71, (7), 1066-1072.

12. Mills, S. D., When will the genomics investment pay off for antibacterial discovery? *Biochemical Pharmacology* **2006,** 71, (7), 1096-1102.
13. Hutton, C. A.; Perugini, M. A.; Gerrard, J. A., Inhibition of lysine biosynthesis: an evolving antibiotic strategy. *Molecular BioSystems* **2007,** 3, 458-465.
14. Scapin, G.; Blanchard, J. S., Enzymology of bacterial lysine biosynthesis. *Advances in Enzymology and Related Areas of Molecular Biology* **1998,** 72, 279-297.
15. Richaud, F.; Richaud, C.; Ratet, P.; Patte, J., Chromosomal location and nucleotide sequence of the *Escherichia coli dap*A gene. *Journal of Bacteriology* **1986,** 166, 297-300.
16. Richaud, F.; Richaud, C.; Haziza, C.; Patte, J., Isolement et purification de genes d'*Escherichia coli* K12 impliques dans la biosynthese de la lysine. *Comptes Rendus de l'Acaddmie des Sciences. La vie des Sciences* **1981,** 293, 507-512.
17. Bouvier, J.; Richaud, C.; Richaud, F.; Patte, J.; Stragier, P., Nucleotide sequence and expression of *Escherichia coli dap*B gene. *Journal of Biological Chemistry* **1984,** 258, 14829-14834.
18. Cremer, J.; Eggeling, L.; Sahm, H., Cloning the *dap*A *dap*B cluster of the lysine-secreting bacterium *Corynebacterium glutamicum*. *Molecular & General Genetics* **1990,** 220, (3), 478-480.
19. Chen, N. Y.; Jian, S. Q.; Klein, D. A.; Paulus, H., Organization and nucleotide-sequence of the *Bacillus subtilis* diaminopimelate operon, a cluster of genes encoding the 1st 3 enzymes of diaminopimelate synthesis and dipicolinate synthase. *Journal of Biological Chemistry* **1993,** 268, (13), 9448-9465.
20. Pisabarro, A.; Malumbres, M.; Mateos, L. M.; Oguiza, J. A.; Martin, J. F., A cluster of three genes (*dap*A, *orf*2, and *dap*B) of *Brevibacterium lactofermentum* encodes dihydrodipicolinate synthase, dihydrodipicolinate reductase, and a third polypeptide of unknown function. *Journal of Bacteriology* **1993,** 175, (9), 2743-2749.
21. Garcia-Rodriguez, F. M.; Zekri, S.; Toro, N., Characterization of the *Sinorhizobium meliloti* genes encoding a functional dihydrodipicolinate synthase

(*dap*A) and dihydrodipicolinate reductase (*da*pB). *Archives of Microbiology* **2000,** 173, (5-6), 438-444.

22. Kaneko, T.; Hashimoto, T.; Kumpaisal, R.; Yamada, Y., Molecular cloning of wheat dihydrodipicolinate synthase. *Journal of Biological Chemistry* **1990,** 265, (29), 17451-17455.
23. Frisch, D. A.; Gengenbach, B. G.; Tommey, A. M.; Sellner, J. M.; Somers, D. A.; Myers, D. E., Isolation and characterization of dihydrodipicolinate synthase from maize. *Plant Physiology* **1991,** 96, (2), 444-452.
24. Silk, G. W.; Matthews, B. F.; Somers, D. A.; Gengenbach, B. G., Cloning and expression of the soybean *dap*A gene encoding dihydrodipicolinate synthase. *Plant Molecular Biology* **1994,** 26, (3), 989-993.
25. Vauterin, M.; Jacobs, M., Isolation of a popular and an *Arabidopsis thaliana* dihydrodipicolinate synthase cDNA clone. *Plant Molecular Biology* **1994,** 25, (3), 545-550.
26. Ghislain, M.; Frankard, V.; Jacobs, M., A dinucleotide mutation in dihydrodipicolinate synthase of *Nicotiana sylvestris* leads to lysine overproduction. *Plant Journal* **1995,** 8, (5), 733-743.
27. Dobson, R. C. Investigating the catalytic and regulatory mechanism of dihydropicolinate synthase. D. Phil. Thesis. University of Canterbury, 2003.
28. Dobson, R. C.; Griffin, M. D.; Jameson, G. B.; Gerrard, J. A., The crystal structures of native and (*S*)-lysine-bound dihydrodipicolinate synthase from *Escherichia coli* with improved resolution show new features of biological significance. *Acta Crystallographica Section D-Biological Crystallography* **2005,** 61, (Pt 8), 1116-1124.
29. Blickling, S.; Renner, C.; Laber, B.; Pohlenz, H. D.; Holak, T. A.; Huber, R., Reaction mechanism of *Escherichia coli* dihydrodipicolinate synthase investigated by X-ray crystallography and NMR spectroscopy. *Biochemistry* **1997,** 36, (1), 24-33.
30. Mirwaldt, C.; Korndorfer, I.; Huber, R., The crystal structure of dihydrodipicolinate synthase from *Escherichia coli* at 2.5 Å resolution. *Journal of Molecular Biology* **1995,** 246, (1), 227-239.

31. Izard, T.; Lawrence, M. C.; Malby, R. L.; Lilley, G. G.; Colman, P. M., The three-dimensional structure of *N*-acetylneuraminate lyase from *Escherichia coli*. *Structure* **1994,** 2, 361-369.

32. Delano, W. L. *The PyMOL Molecular Graphics System.* 2002.

33. Lawrence, M. C.; Barbosa, J.; Smith, B. J.; Hall, N. E.; Pilling, P. A.; Ooi, H. C.; Marcuccio, S. M., Structure and mechanism of a sub-family of enzymes related to *N*-acetylneuraminate lyase. *Journal of Molecular Biology* **1997,** 266, (2), 381-399.

34. Dobson, R. C.; Devenish, S. R.; Turner, L. A.; Clifford, V. R.; Pearce, F. G.; Jameson, G. B.; Gerrard, J. A., Role of arginine 138 in the catalysis and regulation of *Escherichia coli* dihydrodipicolinate synthase. *Biochemistry* **2005,** 44, (39), 13007-13013.

35. Blickling, S.; Knablein, J., Feedback inhibition of dihydrodipicolinate synthase enzymes by *L*-lysine. *Biological Chemistry* **1997,** 378, (3-4), 207-210.

36. Griffin, M. D. Why is dihydrodipicolinate synthase a tetramer? D. Phil. Thesis. University of Canterbury, 2005.

37. Dobson, R. C.; Valegard, K.; Gerrard, J. A., The crystal structure of three site-directed mutants of *Escherichia coli* dihydrodipicolinate synthase: further evidence for a catalytic triad. *Journal of Molecular Biology* **2004,** 338, (2), 329-339.

38. Shames, S.; Wedler, F., Homoserine kinase of *Escherichia coli*: kinetic mechanism and inhibition by L-aspartate semialdehyde. *Archives of Biochemistry and Biophysics* **1984,** 235, 359-370.

39. Coulter, C. V.; Gerrard, J. A.; Kraunsoe, J. A. E.; Moore, D. J.; Pratt, A. J., (*S*)-Aspartate semi-aldehyde: synthetic and structural studies. *Tetrahedron* **1996,** 52, (20), 7127-7136.

40. Dobson, R. C.; Gerrard, J. A.; Pearce, F. G., Dihydrodipicolinate synthase is not inhibited by its substrate, (*S*)-aspartate beta-semialdehyde. *Biochemistry Journal* **2004,** 377, (Pt 3), 757-762.

41. Tudor, D. W.; Lewis, T.; Robins, D. J., Synthesis of the trifluoroacetate salt of aspartic-acid β-semialdehyde, an intermediate in the biosynthesis of *L*-lysine, *L*-threonine, and *L*-methionine. *Synthesis* **1993,** 11, 1061-1062.

42. Laber, B.; Gomis-Ruth, F. X.; Romao, M. J.; Huber, R., *Escherichia coli* dihydrodipicolinate synthase. Identification of the active site and crystallization. *Biochemistry Journal* **1992,** 288, (Pt 2), 691-695.

43. Borthwick, E. B.; Connell, S. J.; Tudor, D. W.; Robins, D. J.; Shneier, A.; Abell, C.; Coggins, J. R., *Escherichia coli* dihydrodipicolinate synthase: characterization of the imine intermediate and the product of bromopyruvate treatment by electrospray mass spectrometry. *Biochemistry Journal* **1995,** 305, (Pt 2), 521-524.

44. Karsten, W. E., Dihydrodipicolinate synthase from *Escherichia coli*: pH dependent changes in the kinetic mechanism and kinetic mechanism of allosteric inhibition by L-lysine. *Biochemistry* **1997,** 36, (7), 1730-1739.

45. Coulter, C. V.; Gerrard, J. A.; Kraunsoe, J. A. E.; Pratt, A. J., *Escherichia coli* dihydrodipicolinate synthase and dihydrodipicolinate reductase: kinetic and inhibition studies of two putative herbicide targets. *Pesticide Science* **1999,** 55, 887-895.

46. Cornish-Bowden, A., *Fundamentals of enzyme kinetics*. Portland Press: London, 1999.

47. Stahly, D. P., Dihydrodipicolinic acid synthase of *Bacillus licheniformis*. *Biochimie et Biophysica Acta* **1969,** 191, 439-451.

48. Mazelis, M.; Whatley, F. R.; Whatley, J., The enzymology of lysine biosynthesis in higher plants. The occurrence, characterization and some regulatory properties of dihydrodipicolinate synthase. *FEBS Letters* **1977,** 84, (2), 236-240.

49. Wallsgrove, R. M.; Mazelis, M., The enzymology of lysine biosynthesis in higher plants: complete localization of the regulatory enzyme dihydrodipicolinate synthase in the chloroplasts of spinach leaves. *FEBS Letters* **1981,** 116, (2), 189-192.

50. Kumpaisal, R.; Hashimoto, T.; Yamada, Y., Purification and characterization of dihydrodipicolinate synthase from wheat suspension cultures. *Plant Physiology* **1987,** 85, (1), 145-151.

51. Yugari, Y.; Gilvarg, C., Coordinated end-product inhibition in lysine synthesis in *Escherichia coli Biochimie et Biophysica Acta* **1962,** 62, 612-614.

52. Kumpaisal, R.; Hashimoto, T.; Yamada, Y., Inactivation of wheat dihydrodipicolinate synthase by 3-bromopyruvate. *Agricultural and Biological Chemistry* **1989,** 53, 355-359.

53. Ghislain, M.; Frankard, V.; Jacobs, M., Dihydrodipicolinate synthase of *Nicotiana sylvestris*, a chloroplast-localized enzyme of the lysine pathway. *Planta* **1990,** 180, 480-486.

54. Dereppe, C.; Bold, G.; Ghisalba, O.; Ebert, E.; Schar, H. P., Purification and characterization of dihydrodipicolinate synthase from pea. *Plant Physiology* **1992,** 98, (3), 813-821.

55. Bartlet, A. T. M.; White, P. J., Regulation of the enzymes of lysine biosynthesis in *Brevibacterium lactofermentum* NCTC 9602 during vegetative growth. *Journal of General Microbiology* **1986,** 132, 3169-3177.

56. Bakhiet, N.; Forney, F. W.; Stahly, D. P.; Daniels, L., Lysine biosynthesis in *Methanobacterium thermoautotropicum* is by the diaminopimelic acid pathway. *Current Microbiology* **1984,** 10, 195-198.

57. Pearce, F. G.; Perugini, M. A.; McKerchar, H. J.; J.A., G., Dihydrodipicolinate synthase from *Thermotoga maritima*. *Biochemical Journal* **2006,** 400, 359-366.

58. Webster, F. H.; Lechowich, R. V., Partial purification and characterization of dihydrodipicolinic acid synthetase from sporulating *Bacillus megaterium*. *Journal of Bacteriology* **1970,** 101, (1), 118-126.

59. Yamakura, F.; Ikeda, Y.; Kimura, K.; Sasakawa, T., Partial purification and some properties of pyruvate-aspartic semialdehyde condensing enzyme from sporulating *Bacillus subtilis*. *Journal of Biochemistry (Tokyo)* **1974,** 76, (3), 611-621.

60. Hoganson, D. A.; Stahly, D. P., Regulation of dihydrodipicolinate synthase during growth and sporulation of Bacillus cereus. *Journal of Bacteriology* **1975,** 124, (3), 1344-1350.

61. Selli, A.; Crociani, F.; Di Gioia, D.; Fava, F.; Crisetig, G.; Matteuzzi, D., Regulation of dihydrodipicolinate synthase and diaminopimelate decarboxylase

activity in *Bacillus stearothermophilus*. *Italian Journal of Biochemistry* **1994,** 43, (1), 29-35.

62. Kruger, D.; Schauer, R.; Traving, C., Characterization and mutagenesis of the recombinant *N*-acetylneuraminate lyase from *Clostridium perfringens* - insights into the reaction mechanism. *European Journal of Biochemistry* **2001,** 268, (13), 3831-3839.

63. Morris, A.; Davenport, R. C.; Tolan, D. R., A lysine to arginine substitution at position 146 of rabbit aldolase changes the rate-determining step to Schiff base formation. *Protein Engineering* **1996,** 9, (1), 61-67.

Chapter Two

Purification and kinetic analysis of wild-type DHDPS

2.1 Introduction

In order to examine the consequences of site-directed mutations on the kinetic properties of DHDPS, the kinetic properties of the wild-type enzyme first had to be determined. Thus, it was necessary to purify wild-type DHDPS. In addition, the assay used to collect the initial rate data uses dihydrodipicolinate reductase (DHDPR) as the coupling enzyme, so this enzyme also had to be purified. Strains of *E. coli* were available that had been transformed with the plasmids pBluescript and pETM11, containing the *dap*A[1] and *dap*B genes (courtesy of Sean Devenish) respectively. These strains provide a simple and convenient means for over-expression of each of the enzymes.

Following purification, two methods were used to assess the activity of DHDPS: the *o*-aminobenzaldehyde assay and the coupled assay. The former method yields qualitative results, which were useful for following the purification of DHDPS, while the coupled assay was used to obtain accurate measurements of the initial rate of the enzyme-catalysed reaction.[2,3]

2.2 Over-expression and purification of DHDPR

DHDPR was over-expressed and purified using methods reported previously by Dobson *et al.* (2004).[4] The *dap*B gene had already been cloned into the pETM11 plasmid and transformed into the BL21 (DE3) strain for induced expression of the N-terminal His-tagged DHDPR protein (courtesy of Sean Devenish). The successful transformants were identified by conferred resistance to the antibiotic kanamycin. Protein expression was induced by the addition of isopropyl β-D-1-thiogalactopyranoside (IPTG), followed by overnight growth. The cells were harvested by centrifugation and washed with buffer. Disruption of the cell was achieved by sonication, which allowed the release of proteins, including DHDPR. Following centrifugation, the supernatant containing the crude enzyme was applied to a His-trap column. The success of the purification was assessed by SDS-PAGE and staining with Coomassie brilliant blue, which revealed a single band at the expected mass of 29 kDa (Figure 2.1). The increase in purity was reflected in an increase in specific activity (Table 2.1).

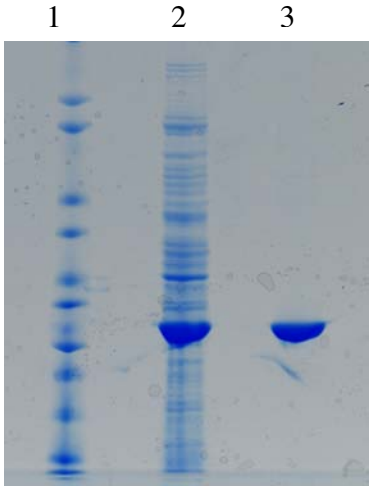

Figure 2.1 *SDS-PAGE following the purification of DHDPR. Lanes:* ***1****, Sigmamarker, wide molecular weight range of the bands (from top) 97, 84, 66, 55, 45, 36, 29, 24, 20, 10.2 and 6.5 kDa;* ***2****, crude cell extract;* ***3****, eluant from His-Trap column.*

Table 2.1 *Purification of DHDPR (from 3 L of culture).*

	Protein[a] (mg)	**Total activity**[b] (units[c])	**Specific activity** (units mg^{-1})	**Yield total** (%)	**Degree of purification** (fold)
Crude	2688	5908	2.20	100	
His-Trap	514	3790	7.37	64	3.4

[a] Protein concentrations determined using the Bradford assay.
[b] Activity determined using the quantitative coupled assay for DHDPR activity.
[c] 1 unit is defined as the consumption of 1 µmol NADPH s^{-1}.

2.3 Over-expression and purification of DHDPS

The purification of DHDPS was based on the methods originally reported by Yugari and Gilvarg (1995),[2] as modified by Dobson *et al.* (2004).[4] *E. coli* DHDPS was over-expressed from the AT997recA$^-$ strain that had been transformed with the pBluescript plasmid pJG001.[5] Chapter three (section 3.3.1) details the reasons for the choice of this *E. coli* strain. The successful transformants were identified by conferred resistance to ampicillin and tetracycline antibiotics. The cells were grown overnight and harvested by centrifugation. The proteins were released from the cells by sonication and activity was detected using the *o*-aminobenzaldehyde assay, as described in section 2.4.1. DHDPS shows a relative thermostability, which enabled the introduction of the heat shock procedure as a purification step. Following heat shock to remove much of the protein in solution, ion exchange (Q-Sepharose) and hydrophobic interaction (phenyl-Sepharose) were utilized to further purify the protein. The success of these purification steps were assessed by SDS-PAGE with Coomassie brilliant blue staining, which revealed a single band corresponding to the expected monomeric mass of approximately 31.2 kDa (Figure 2.2). The purification procedure resulted in an increase specific activity of over 10-fold (Table 2.2).

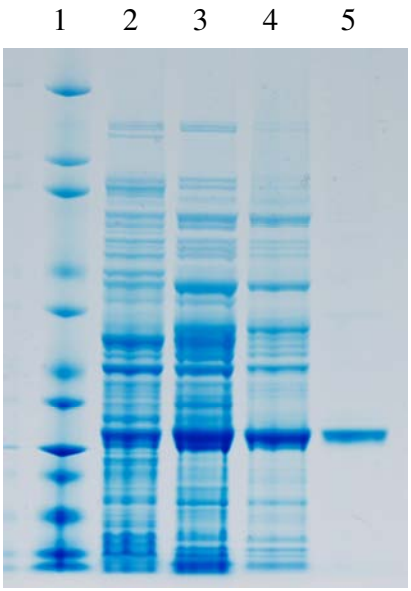

Figure 2.2 *SDS-PAGE following the purification of wild-type DHDPS. Lanes:* ***1****, Sigma marker, wide molecular weight range of the bands (from top) 97, 84, 66, 55, 45, 36, 29, 24, 20, 10.2 and 6.5 kDa;* ***2****, crude cell extract;* ***3****, heat shock;* ***4****, eluant from Q-Sepharose;* ***5****, eluant from phenyl-Sepharose.*

Table 2.2 *Purification of wild-type DHDPS (from 5 L of culture).*

	Protein[a] (mg)	**Total activity**[b] (units[c])	**Specific activity** (units mg^{-1})	**Yield total** (%)	**Degree of purification** (fold)
DHDPS					
Crude	2048	334	0.16	100	
Heat shock	1376	247	0.18	74	1.1
Q-Sepharose	569	216	0.38	65	2.1
phenyl-Sepharose	106	187	1.76	56	4.6

[a] Protein concentrations determined using the Bradford assay.
[b] Activity determined using the quantitative coupled assay for DHDPS activity.
[c] 1 unit is defined as the consumption of 1 µmol NADPH s^{-1}.

2.4 Methods used to measure DHDPS activity

2.4.1 *o*-Aminobenzaldehyde assay

The reaction between DHDPS and its substrates in the presence of *o*-aminobenzaldehyde results in the formation of an unknown purple product (Figure 2.3) during an incubation period of about 30 minutes, the formation of which can be monitored at 540 nm.[2,3] The intensity of the purple colouration can be increased by the addition of an acid after the incubation period. This qualitative assay is useful to detect DHDPS activity during the purification steps due to its high specificity and sensitivity to the enzyme. However, since it is only semi-quantitative,[2] this method was not used for quantitative kinetic measurements.

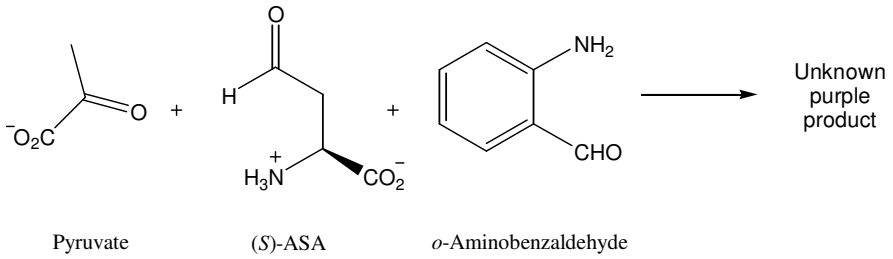

Figure 2.3 o-*Aminobenzaldehyde assay.*[2,3]

2.4.2 Coupled assay

The reaction of DHDPS cannot be followed directly using the spectrophotometer but it can be followed indirectly by coupling it to the next reaction in the lysine biosynthetic pathway, which is catalysed by DHDPR. This reaction utilises NADPH, so a spectrophotometric assay can be used that exploits the large absorbance of reduced NADPH at 340 nm (Figure 2.4).[6] Provided that the activity of DHDPR is high enough, the rate of NADPH oxidation recorded will correspond exactly to the rate of the DHDPS-catalysed reaction. This quantitative assay described originally in Borthwick *et al.* (1995)[7] and Coulter *et al.* (1999),[8] but later modified by Dobson (2004),[4] was used to

determine the kinetic parameters of wild-type DHDPS, which will be discussed in the next section.

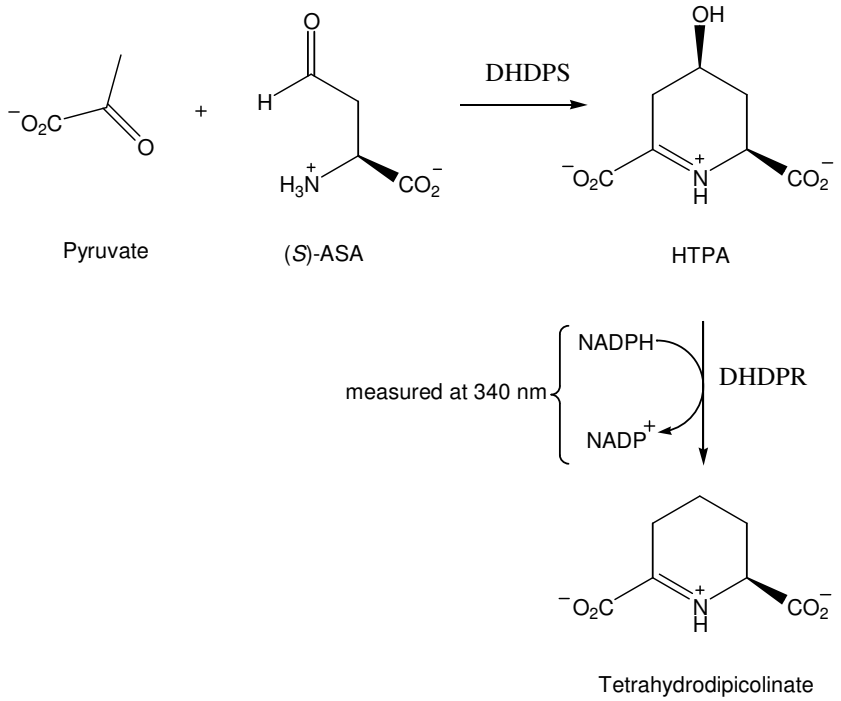

Figure 2.4 *The coupled assay used to quantitatively measure DHDPS activity. The oxidation of NADPH by the coupling enzyme, DHDPR, is monitored at 340 nm.*[7,8]

2.5 Enzyme kinetics of *E. coli* DHDPS

Initial rate data were collected using the coupled assay, with DHDPR present in 10-fold excess. The substrate concentrations used ranged between 0.2 x K_m and 10 x K_m according to the method of Cornish-Bowden.[6] Thus, the concentration of (*S*)-ASA and pyruvate used varied between 0.04 mM and 1.25 mM. The rates were collected in duplicate and the experiment carried out on two independent occasions. No rate of reaction was observed between the two substrates in the absence of enzyme at the range of concentrations mentioned above; indicating that any rates observed in these assays

would be attributed to the enzyme-catalysed reaction. The computer programme Enzfitter (Biosoft Cambridge, UK) was used to analyse the initial rate data.

As mentioned in Chapter one (section 1.3.4), DHDPS displays a ping-pong kinetic mechanism, also known as the double displacement mechanism. In the case of DHDPS, pyruvate binds to the enzyme first *via* the formation of a covalent enzyme-substrate intermediate, followed by the release of water and the formation of a Schiff base. The second substrate, (*S*)-ASA, then binds to the Schiff base to release the final product, HTPA.[5,9] Overall, two independent products are released (Figure 1.3).

The kinetic data obtained for wild-type DHDPS were fitted to both the ping-pong model (Equation (2.1)) and the ternary-complex model (Equation (2.2)). A ternary-complex mechanism implies that there is no longer a strict order of reaction sequences like in the ping-pong mechanism. The data were fitted to both models because the mutants generated may have a change in mechanism, and a comparison point was needed.

Equation (2.1)[6] $\upsilon = VAB / (K_{mB}A + K_{mA}B + AB)$

Equation (2.2)[6] $\upsilon = VAB / (K_{mB}A + K_{mA}B + AB + K_{sA}K_{mB})$

V is the maximal velocity, K_{mA} and K_{mB} are the Michaelis-Menten constants for the two substrates, A and B are the substrate concentrations and υ is the initial velocity. K_{sA} is the binding constant for substrate A to the free enzyme form. The better model was chosen, based on the statistical parameters obtained for each fit (Table 2.3).

Table 2.3 *Comparison of the statistical parameters obtained when kinetic data for wild-type DHDPS were fitted to the ping-pong and ternary-complex models.*

Statistical Parameter	Ping-pong model	Ternary-complex model
R^2	0.98	0.95
S.E. of fit	0.039	0.056
F-Value	860	253
p-value	3.8×10^{-25}	2.1×10^{-18}

The kinetic data fitted better to the classical ping-pong model with an R^2 value of 0.98 and lower standard errors and *p*-values than those obtained for the ternary-complex model. The kinetic values (Table 2.4) are consistent with values published in the literature. The $K_{mPyruvate}$ of (0.14-0.16) mM is similar to those published, which range between 0.11 mM[8] and 0.25 mM.[2] The K_{mASA} values obtained using the coupled assay vary between 0.11 and 0.14 mM,[2,5,8-10] which is identical to the value obtained in this work. The catalytic turnover number (k_{cat}) of 45±3 s^{-1} agrees with values obtained by other workers in this laboratory.[5,11]

Table 2.4 *Kinetic parameters of wild-type DHDPS determined using the ping-pong model.*

Parameter	Wild-type DHDPS
k_{cat} (s^{-1})	45±3
$K_{mPyruvate}$ (mM)	0.15±0.01
K_{mASA} (mM)	0.12±0.01
$k_{cat}/K_{mPyruvate}$ ($M^{-1}s^{-1}$)	(3.0±0.4) x 10^5
k_{cat}/K_{mASA} ($M^{-1}s^{-1}$)	(3.8±0.6) x 10^6

The Enzfitter programme was also used to generate the direct plot, Lineweaver-Burk plot (1/rate *vs* 1/[substrate]), Eadie-Hofstee plot (rate/[substrate] *vs* rate) and a percentage residual plot of the data. The ping-pong model clearly fitted the data well, as evidenced by a tight grouping of points about the Lineweaver-Burk plots (Figures 2.5B and 2.6B) and Eadie-Hofstee plots (Figures 2.5C and 2.6C), except at the lowest substrate concentrations, where experimental error is largest.[6] The residual plots (Figures 2.5D and 2.6D) showed random scattering, indicating that there were no systematic experimental errors.

Figure 2.5 *Kinetic analysis of wild-type DHDPS with respect to* (S)*-ASA. (A) is a direct plot, (B) is the Lineweaver-Burk plot, (C) is the Eadie-Hofstee plot, and (D) is a percentage residual plot of the data.* R^2*=0.98 and* p (F) *<0.01*

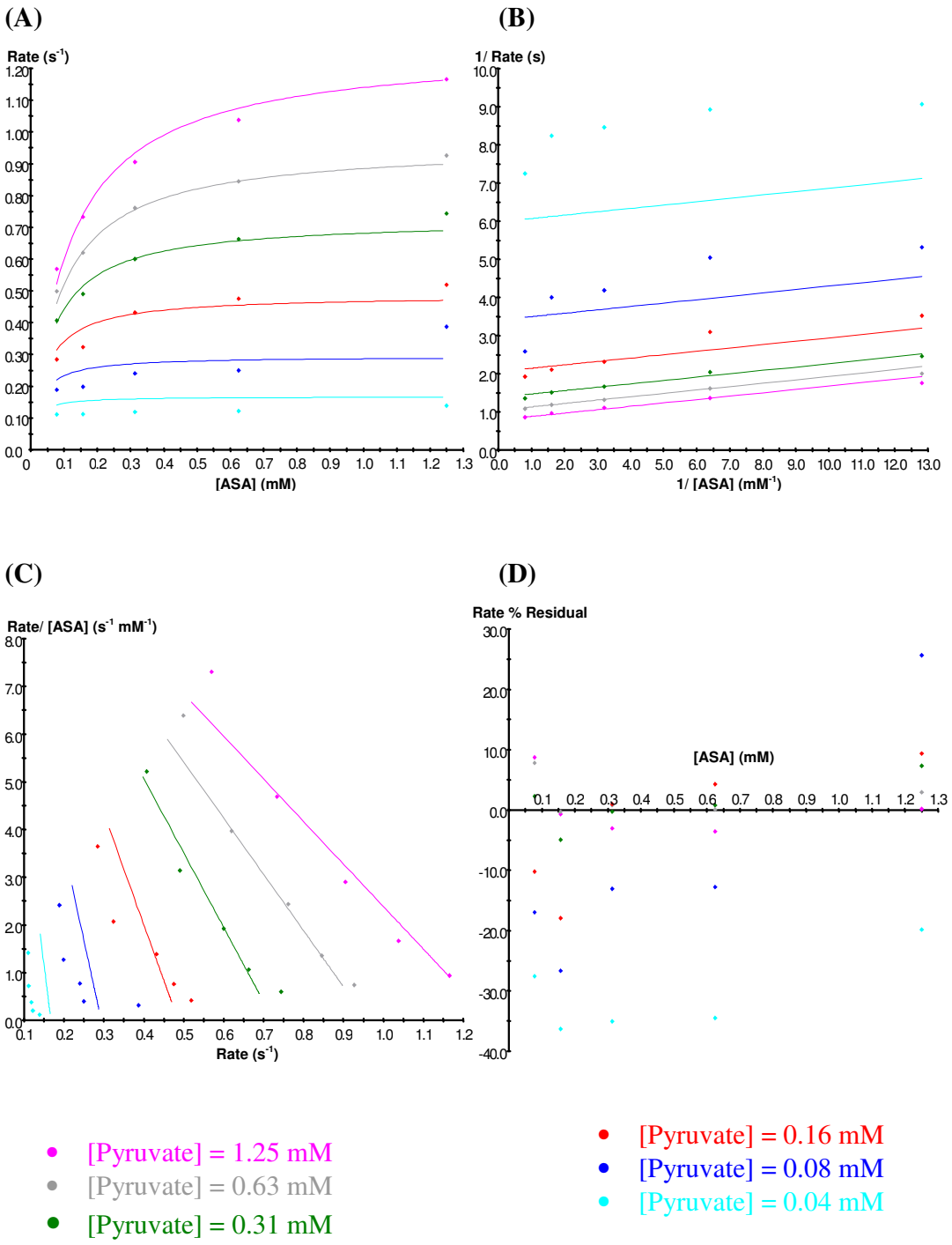

Figure 2.6 *Kinetic analysis of wild-type DHDPS with respect to pyruvate. (A) is a direct plot, (B) is the Lineweaver-Burk plot, (C) is the Eadie-Hofstee plot, and (D) is a percentage residual plot of the data.* R^2*=0.98 and* p (F) *<0.01*

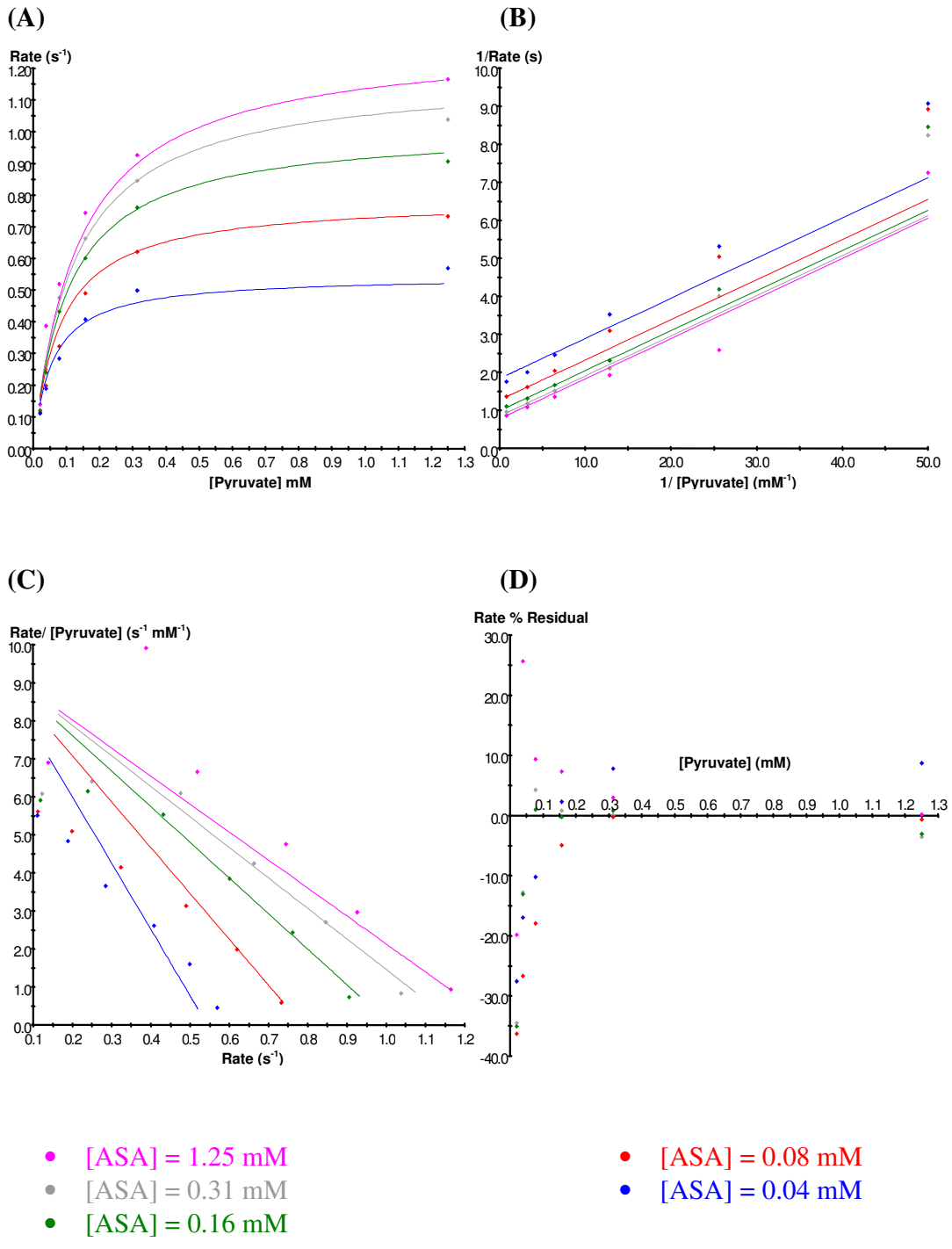

2.6 Lysine inhibition studies of wild-type *E. coli* DHDPS

Lysine, the end-product of the biosynthetic pathway, has been found to be an allosteric inhibitor of DHDPS, as described in Chapter one (section 1.3.5). However, the precise regulatory mechanism is not completely understood. DHDPS displays different types of inhibition with respect to each of its substrates. The inhibition of DHDPS with respect to pyruvate has been determined to be partial and uncompetitive,[5] but lysine has been found to be a partial non-competitive inhibitor with respect to (*S*)-ASA.[5,10,11]

Data were collected by keeping one of the substrates at a saturating concentration and varying the concentration of the other substrate and lysine, as described in Cornish-Bowden (1999).[6] The lysine concentrations used varied between 0 mM and 5 mM. The concentrations of pyruvate varied between 0.04 mM and 2.5 mM, and for (*S*)-ASA, between 0.04 mM and 1.25 mM.

Once again, the rates were collected in duplicate and the experiment repeated. The computer programme Enzfitter was used to analyse the initial rate data and to generate the plots, using the equations for partial uncompetitive (Equation (2.3)) and partial non-competitive inhibition (Equation (2.4)).

Partial uncompetitive inhibition

Equation (2.3), which describes partial uncompetitive inhibition, was used to fit the data collected when (*S*)-ASA was kept at a constant concentration.

Equation (2.3)[6] $$\upsilon = 1/ [1/ (V K_i + V'I)] [I+ K_i (1+ K_s/S)]$$

Where V is the maximal velocity in the absence of the inhibitor, V' is the maximal velocity in the presence of the inhibitor at a saturating concentration, I is the inhibitor concentration, S is the substrate concentration, K_i is the inhibitor constant, K_s is the substrate binding constant and υ is the initial velocity.

This type of inhibition demonstrates that the higher the lysine concentration, the lower the V and K_s values will be, since the inhibitor is binding to the enzyme-substrate complex only.[6]

The data obtained fitted Equation (2.3) well, with a K_i value of (0.11-0.13) mM (Table 2.5 and Figure 2.7), which is in good agreement with values published in the literature.[10,12] The enzyme was found to be 92% inhibited at saturating levels of (*S*)-lysine, which is exactly what was observed by Dobson *et al.* (2004).[12]

Table 2.5 *Lysine inhibition studies of wild-type DHDPS with respect to pyruvate. (*S*)-ASA was kept at a constant concentration of 1.25 mM.*

Parameter	Wild-type
Inhibition type	Partial uncompetitive
α (%)[1]	8±1
K_i (mM)	0.12±0.01

[1] α is the ratio of the maximal velocity without the inhibitor (V) to the maximal velocity at saturating levels of the inhibitor (V').[12]

Figure 2.7 *Lysine inhibition studies of wild-type DHDPS with respect to pyruvate. (A) is a direct plot, (B) is the Lineweaver-Burk plot, (C) is the Eadie-Hofstee plot, and (D) is a percentage residual plot of the data.* R^2*=0.98 and* p (F) *<0.01*

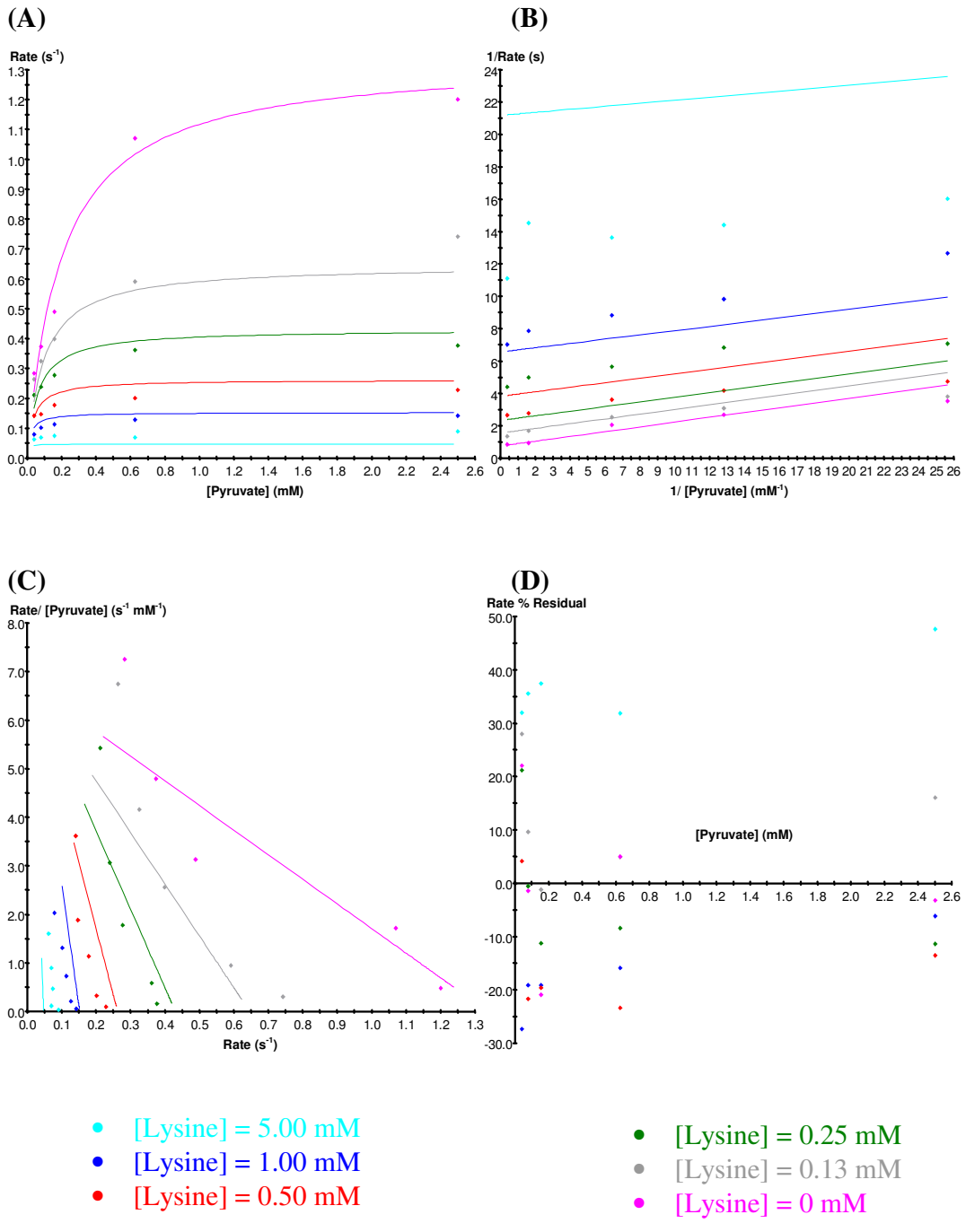

Partial non-competitive inhibition

Lysine has been found to be a partial non-competitive inhibitor of DHDPS with respect to (*S*)-ASA, so the following equation was used to fit the kinetic data:

Equation (2.4)[6] $\upsilon = 1/ \{[(K_i+I) / [VK_i + V'I)] (1+K_s/S)\}$

Enzymes that display this type of inhibition have reduced V but unchanged K_m with increasing concentration of the inhibitor.[6]

The data fitted well to Equation (2.4), with an R^2 value of 0.98 and p (F) <0.01. DHDPS retained 8% of its original activity in the presence of saturating levels of the inhibitor and the K_i value obtained was 0.18±0.02 mM (Table 2.6 and Figure 2.8), which is in good agreement with values obtained in the literature.[10,13]

Table 2.6 *Lysine inhibition studies of wild-type DHDPS with respect to (*S*)-ASA. Pyruvate was kept at a constant concentration of 2.5 mM.*

Parameter	Wild-type
Inhibition type	Partial non-competitive
α (%)	8±1
K_i (mM)	0.18±0.02

[1] α is the ratio of the maximal velocity without the inhibitor (V) to the maximal velocity at saturating levels of the inhibitor (V').[12]

Figure 2.8 *Lysine inhibition studies of wild-type DHDPS with respect to* (S)*-ASA. (A) is a direct plot, (B) is the Lineweaver-Burk plot, (C) is the Eadie-Hofstee plot, and (D) is a percentage residual plot of the data.* R^2*=0.98 and* p (F) *<0.01.*

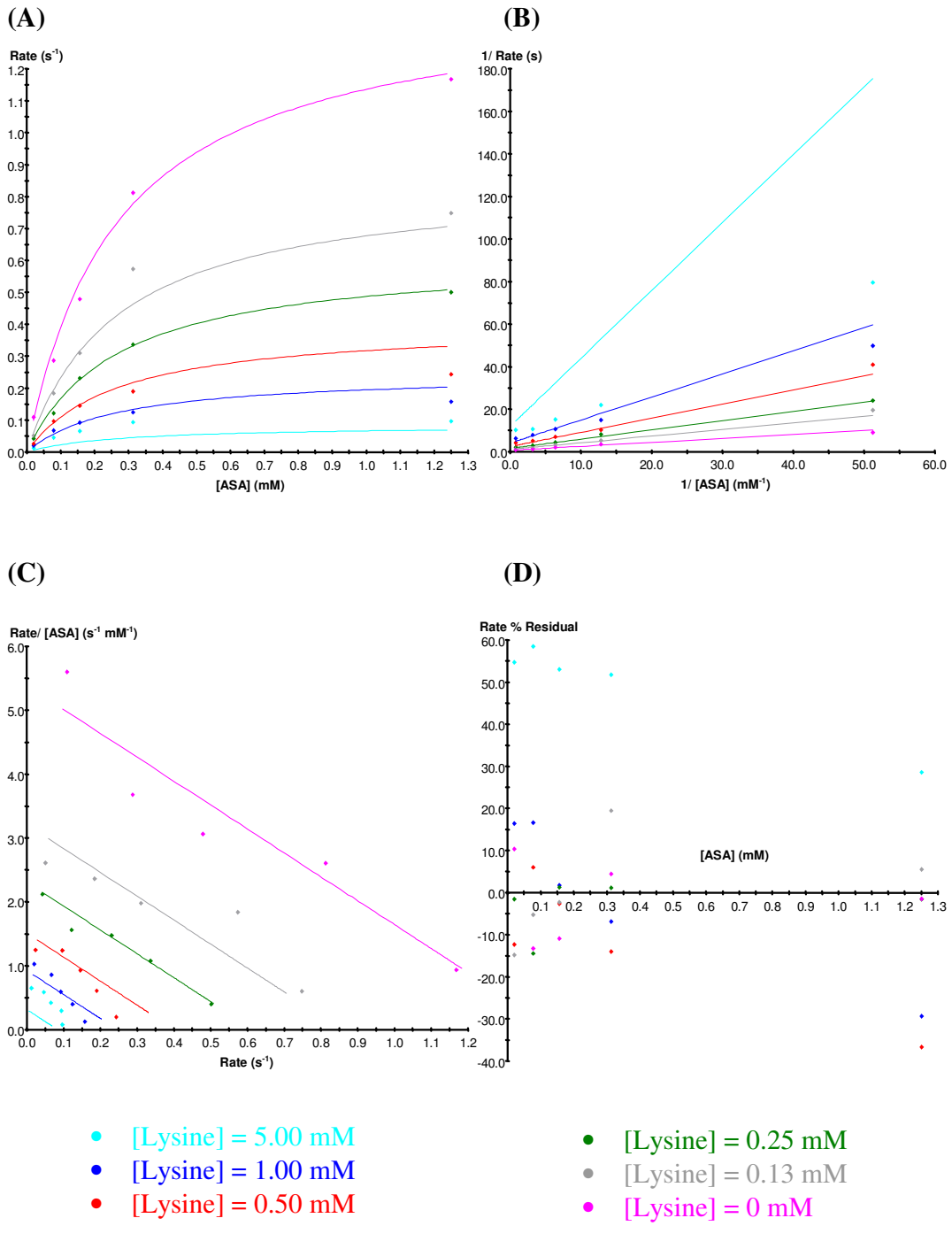

2.7 Summary

DHDPS and DHDPR were both purified and the former was also kinetically characterised in this chapter using the coupled assay. The data obtained fitted the ping-pong mechanism better than the ternary-complex model, as evidenced by a higher R^2 value for the fit as well as a higher *F*-value and lower standard errors and *p*-value (Table 2.3). The K_m value for (*S*)-ASA was 0.12±0.01 mM, while for pyruvate, it was 0.15±0.01 mM. The catalytic turnover number was 45±3 s^{-1}.

In addition, lysine inhibition studies were carried out on DHDPS. Partial uncompetitive inhibition was observed when varying the concentration of pyruvate, with a K_i value of 0.12±0.01 mM. DHDPS displayed partial non-competitive inhibition with respect to (*S*)-ASA, with a K_i ranging between 0.16 and 0.20 mM. The enzyme still retains 8% activity with respect to each substrate at saturating levels of the inhibitor.

The values obtained in this chapter are consistent with those published in the literature and they provide the baseline data required for the characterisation of the mutants generated in the following chapter.

2.8 References

1. Gerrard, J. A. Studies on dihydrodipicolinate synthase. D. Phil. Thesis. Oxford University, 1992.
2. Yugari, Y.; Gilvarg, C., The condensation step in diaminopimelate synthesis. *Journal of Biological Chemistry* **1965,** 240, 4710-4716.
3. Shedlarski, J. G.; Gilvarg, C., The pyruvate-aspartic semialdehyde condensing enzyme of *Escherichia coli*. *Journal of Biological Chemistry* **1970,** 245, 1362-1373.

4. Dobson, R. C.; Valegard, K.; Gerrard, J. A., The crystal structure of three site-directed mutants of *Escherichia coli* dihydrodipicolinate synthase: further evidence for a catalytic triad. *Journal of Molecular Biology* **2004,** 338, (2), 329-339.
5. Dobson, R. C. Investigating the catalytic and regulatory mechanism of dihydropicolinate synthase. D. Phil. Thesis. University of Canterbury, 2003.
6. Cornish-Bowden, A., *Fundamentals of enzyme kinetics*. Portland Press, London: 1999.
7. Borthwick, E. B.; Connell, S. J.; Tudor, D. W.; Robins, D. J.; Shneier, A.; Abell, C.; Coggins, J. R., *Escherichia coli* dihydrodipicolinate synthase: characterization of the imine intermediate and the product of bromopyruvate treatment by electrospray mass spectrometry. *Biochemistry Journal* **1995,** 305, (Pt 2), 521-524.
8. Coulter, C. V.; Gerrard, J. A.; Kraunsoe, J. A. E.; Pratt, A. J., *Escherichia coli* dihydrodipicolinate synthase and dihydrodipicolinate reductase: kinetic and inhibition studies of two putative herbicide targets. *Pesticide Science* **1999,** 55, 887-895.
9. Blickling, S.; Renner, C.; Laber, B.; Pohlenz, H. D.; Holak, T. A.; Huber, R., Reaction mechanism of *Escherichia coli* dihydrodipicolinate synthase investigated by X-ray crystallography and NMR spectroscopy. *Biochemistry* **1997,** 36, (1), 24-33.
10. Karsten, W. E., Dihydrodipicolinate synthase from *Escherichia coli*: pH dependent changes in the kinetic mechanism and kinetic mechanism of allosteric inhibition by L-lysine. *Biochemistry* **1997,** 36, (7), 1730-1739.
11. Griffin, M. D. Why is dihydrodipicolinate synthase a tetramer? D. Phil. Thesis. University of Canterbury, 2005.
12. Dobson, R. C.; Griffin, M. D.; Roberts, S. J.; Gerrard, J. A., Dihydrodipicolinate synthase (DHDPS) from *Escherichia coli* displays partial mixed inhibition with respect to its first substrate, pyruvate. *Biochimie* **2004,** 86, (4-5), 311-315.
13. Dobson, R. C.; Gerrard, J. A.; Pearce, F. G., Dihydrodipicolinate synthase is not inhibited by its substrate, (*S*)-aspartate beta-semialdehyde. *Biochemistry Journal* **2004,** 377, (Pt 3), 757-762.

Chapter Three

Site-directed mutagenesis and characterisation of lysine 161 mutants

3.1 Introduction

DHDPS is a member of the class I aldolases and a common feature in the enzymes from this family is the presence of a lysine residue within the active site that forms a Schiff base intermediate with the substrate. From the X-ray crystal structure of DHDPS from *E. coli*, and alignment of all DHDPS sequences, it was deduced that it is lysine 161 that forms the intermediate with the first substrate, pyruvate.[1,2] Alignment of the structures of DHDPS and the homologous enzyme, NAL, indicates that lysine 161 has the same spatial positioning. This led to the conclusion that the mechanism of Schiff base formation is likely to be conserved in both enzymes, as discussed in Chapter one (section 1.3.6).[2]

Kruger *et al.* (2001)[3] used site-directed mutagenesis to substitute lysine 161 from *Clostridium perfringens* NAL to an alanine and found that enzyme activity was completely removed. However, when the residue was mutated to an arginine, activity could still be detected. Although lysine 161 has been unequivocally implicated in Schiff base formation in the DHDPS catalytic mechanism, the effect of mutating this residue, in a manner similar to that investigated by Kruger *et al.* (2001)[3] for NAL, had not yet been investigated. In this chapter, the generation of the alanine and arginine site-directed mutants is described, to assess whether lysine 161 is absolutely essential for catalysis of DHDPS and, consequently, to assess the importance of the Schiff base in the reaction mechanism. Site-directed mutagenesis is a powerful technique as it allows the

introduction of specific changes in the amino acid sequence of an enzyme by utilising the polymerase chain reaction (PCR) and it is much less structurally disruptive than chemical modification.[4]

The two mutants were purified to obtain material suitable for biochemical characterisation. Their kinetic parameters were determined using the coupled assay, and the results compared to those obtained for wild-type DHDPS, in Chapter two. In addition, far-ultraviolet circular dichroism spectroscopy, differential scanning fluorimetry and isothermal titration calorimetry were used to characterise the wild-type and mutant enzymes in this chapter.

3.2 Site-directed mutagenesis

The QuikChange site-directed mutagenesis kit (Stratagene) was used to introduce the specific changes in the *dap*A gene.

3.2.1 Mutagenic primer design

The primers were designed from the gene sequence of *E. coli* DHDPS determined by Gerrard.[5] The primers used are shown in Table 3.1.

Table 3.1 *Forward primers used for site-directed mutagenesis showing the codon changed underlined.*

Primer name	Forward primer
DHDPS-K161A#1	5'GGC GAA AGT AAA AAT ATT ATC GGA ATC GCA GAG GCA ACA GGG G3'
DHDPS-K161R#1	5'GGC GAA AGT AAA AAT ATT ATC GGA ATC AGA GAG GCA ACA GGG G3'

Reactions were set up using a constant primer concentration with two template DNA concentrations to optimise amplification. Following temperature cycling, the product was digested with *Dpn* I endonuclease (incubation at 37°C for 2 hours). The nicked vector DNA incorporating the desired mutations was then transformed into *Epicurian coli* XL 1-Blue chemically competent cells using the heat shock method.[6]

3.2.2 Sequencing

The mutant plasmids were sequenced to ensure the desired mutation had been introduced and that the integrity of *dap*A was intact after site-directed mutagenesis. Sequencing was performed by the Auckland Genomics Unit, using plasmid DNA prepared by the standard alkaline lysis plasmid preparation method, described in Chapter six (section 6.2.9). The electropherograms show that each sequence contained the desired change (Figure 3.1).

DHDPS-K161A **DHDPS-K161R**

Figure 3.1 *Electropherograms showing the desired changes in the plasmid underlined.*

3.3 Over-expression and purification of DHDPS mutants

3.3.1 Choice of *E. coli* strain and over-expression of the *dap*A gene

It is essential to exclude the possibility of contamination with wild-type enzyme when dealing with the low residual activity of enzymes lacking a key catalytic group such as

lysine 161. Traces of wild-type enzyme may arise in the preparation, either as a contaminant or because of natural errors of miscorporation.[7] To prevent the possibility of interference from wild-type enzyme derived from the host chromosome, which would affect the biochemical assays during kinetic characterisation, the over-expression of DHDPS mutants was performed in the *E. coli* strain AT997recA$^-$.

The strain AT997 contains a non-functional DHDPS gene (*dap*A$^-$), which has been found to be complemented by pJG001. In addition, the strain was made recA$^-$ to avoid homologous recombination between a plasmid-borne *dap*A mutant gene and the *E. coli* genome.[8] The strain was grown and maintained in LB in the presence of tetracycline in a medium supplemented with DAP, to allow easy selection and confirmation of the *dap*A$^-$ phenotype. The DHDPS activity from this strain was examined prior to transformation to ensure that the enzyme being produced from the chromosome was indeed non-functional.

3.3.2 Transformation of *E. coli* AT997recA$^-$ with DHDPS mutant plasmids

The ability of transformants to complement the *dap*A$^-$ phenotype was assessed by growing them in the absence of DAP. Each mutant plasmid rescued the AT997recA$^-$ strain, suggesting that they retained sufficient DHDPS activity for survival.

3.3.3 Purification of DHDPS mutants

The AT997recA$^-$ cells that were transformed with the mutant plasmids were grown overnight and harvested by centrifugation. Each protein was purified as described in section 2.3. The increase in purity was reflected in an increase in specific activity for each of the mutants (Table 3.2). The success of these purification steps was assessed by SDS-PAGE with Coomassie brilliant blue staining, which revealed a single band corresponding to the expected monomeric mass of approximately 31.2 kDa in each case (Figure 3.2).

Table 3.2 *Purification of DHDPS mutants (from 5 L of culture).*

	Protein[a] **(mg)**	**Total activity**[b] **(units**[c]**)**	**Specific activity (units mg^{-1})**	**Yield total (%)**	**Degree of purification (fold)**
DHDPS-K161A					
Crude	2078	4.23	0.00200	100	
Heat shock	1246	2.51	0.00202	59	1.0
Q-Sepharose	758	1.95	0.00257	78	1.3
phenyl-Sepharose	127	1.12	0.00886	58	3.4
DHDPS-K161R					
Crude	2186	16.5	0.00754	100	
Heat shock	1345	10.3	0.00765	62	1.0
Q-Sepharose	445	7.13	0.0160	43	2.1
phenyl-Sepharose	103	3.12	0.0304	19	4.0

[a] Protein concentrations determined using the Bradford assay.
[b] Activity determined using the quantitative coupled assay for DHDPS activity.
[c] 1 unit is defined as the consumption of 1 µmol NADPH s^{-1}.

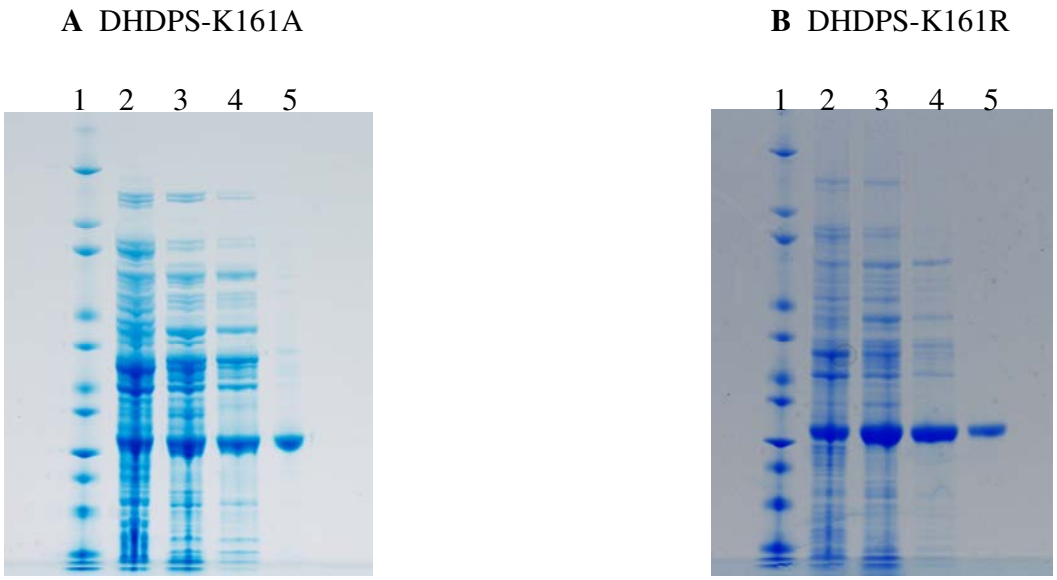

Figure 3.2 *SDS-PAGE following the purification of the DHDPS mutants.*

A ***DHDPS-K161A*** *Lanes: 1, Sigmamarker, wide molecular weight range of the bands (from top) 97, 84, 66, 55, 45, 36, 29, 24, 20, 10.2 and 6.5 kDa; 2, crude cell extract; 3, heat shock; 4, eluant from Q-Sepharose; 5, eluant from phenyl-Sepharose.*

B ***DHDPS-K161R*** *Lanes: 1, Sigmamarker; 2, crude cell extract; 3, heat shock; 4, eluant from Q-Sepharose; 5, eluant from phenyl-Sepharose.*

3.4 Stability of DHDPS-K161A and DHDPS-K161R

It is not uncommon for an enzyme to lose its activity under *in vitro* conditions. Neglecting enzyme inactivation can result in errors in both estimating the kinetic parameters and reporting the mechanisms of enzyme action.[9] Therefore, it is important to know if enzyme inactivation is affecting an enzyme assay. The most commonly used method to determine the stability of an enzyme under assay conditions is to compare progress curves of the product formation at different enzyme concentrations. If the enzyme is stable, the plots of synthesised product against time, multiplied by the enzyme concentration should be superimposable. This test was developed by Michaelis and

Davidsohn,[10] and later systematically adapted by Selwyn.[11] Both DHDPS mutants were stable under the assay conditions and therefore suitable for kinetic analysis (Figure 3.3).

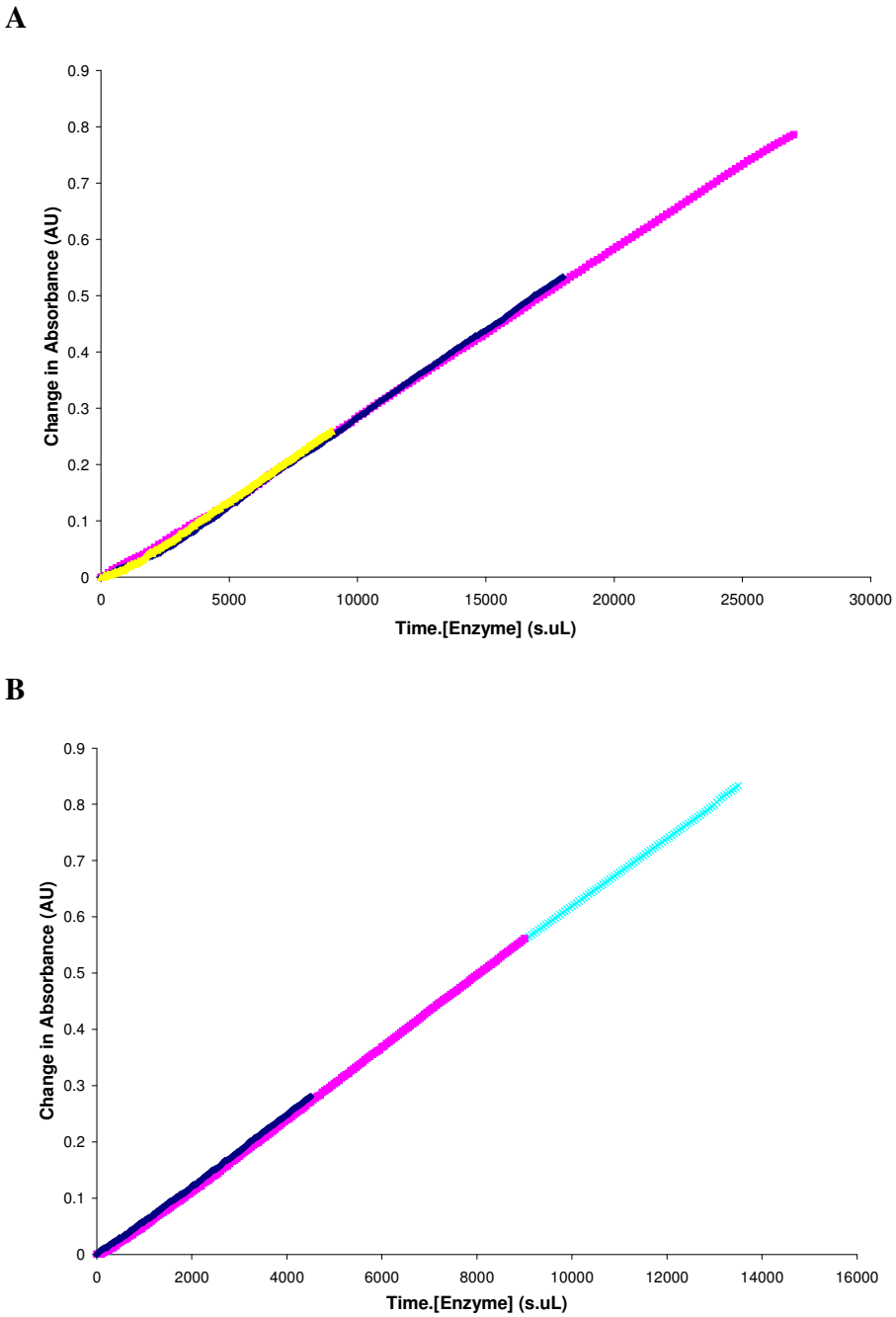

Figure 3.3 *Selwyn's test for enzyme stability:* ***A****, DHDPS-K161A: 50 µL (▲), 100 µL (♦) and 150 µL (■);* ***B****, DHDPS-K161R: 25 µL (♦), 50 µL (■) and 75 µL (x).*

3.5 Enzyme kinetics of *E. coli* DHDPS K161 mutants

The kinetic data were fitted to the ping-pong model (Equation (1)) and the ternary-complex model (Equation (2)) as described in section 2.5. Both models showed the same standard errors associated with the kinetic constants and the same R^2 values, unlike the pattern observed in the wild-type enzyme (Tables 3.3 and 3.4). Thus, the *F*- and *p*-values were used to determine which model gave the better fit, which was the ternary-complex mechanism.

Table 3.3 *Comparison of the statistical parameters obtained when kinetic data for DHDPS-K161A were fitted to the ping-pong and ternary-complex models.*

Statistical Parameter	Ping-pong model	Ternary-complex model
R^2	0.99	0.99
S.E. of fit	4.4×10^{-5}	4.4×10^{-5}
F-Value	860	1300
p-value	1.1×10^{-30}	2.6×10^{-32}

Table 3.4 *Comparison of the statistical parameters obtained when kinetic data for DHDPS-K161R were fitted to the ping-pong and ternary-complex models.*

Statistical Parameter	Ping-pong model	Ternary-complex model
R^2	0.98	0.98
S.E. of fit	1.9×10^{-4}	1.9×10^{-4}
F-Value	300	470
p-value	2.3×10^{-30}	9.3×10^{-32}

Table 3.5 *Kinetic parameters obtained for DHDPS-K161A and DHDPS-K161R using the ternary-complex model compared with wild-type DHDPS (fitted with the ping-pong model).*

Parameter	Wild-type[1]	K161A	K161R
k_{cat} (s^{-1})	45±3	0.06±0.02	0.16±0.06
Relative k_{cat} (%)	100	0.13	0.35
$K_{mPyruvate}$ (mM)	0.15±0.01	0.45±0.04	0.57±0.06
K_{mASA} (mM)	0.12±0.01	0.23±0.02	0.12±0.01
$k_{cat}/K_{mPyruvate}$ ($M^{-1}s^{-1}$)	(3.0±0.4)x10^5	(7.5±3.0)x10^3	(3.6±1.7)x10^3
k_{cat}/K_{mASA} ($M^{-1}s^{-1}$)	(3.8±0.6)x10^6	(3.8±1.5)x10^3	(7.5±3.6)x10^3

[1] As determined in Chapter two using the ping-pong model.

3.5.1 DHDPS-K161A kinetics

The initial rate data fitted the ternary-complex mechanism well, which can be seen in Figures 3.4 and 3.5, except at the lowest substrate concentrations, as observed for wild-type DHDPS (section 2.5). The R^2 values were 0.99 and the p (F) <0.01 in both instances. The k_{cat} value was found to be 0.06±0.02 s^{-1} – about 0.1% of the activity observed for the wild-type (Table 3.5). The K_m values were both found to be somewhat greater than that of the wild-type. The $K_{mPyruvate}$ was 0.45±0.04 mM and K_{mASA} was 0.23±0.02 mM, compared to 0.15±0.01 mM and 0.12±0.01 mM for the wild-type respectively.

3.5.2 DHDPS-K161R kinetics

Again, the data collected fitted the ternary-complex model well (Figures 3.6 and 3.7), except at the lowest substrate concentrations, as observed for wild-type DHDPS and DHDPS-K161A. The k_{cat} was found to be 0.16±0.06 s^{-1} – less than 0.4% of the wild-type (Table 3.5). The $K_{mPyruvate}$ was increased over 2-fold (0.57±0.06 mM), while the K_{mASA} remained the same as that of wild-type DHDPS (0.12±0.01 mM). The R^2 for both fits was 0.98 and the p (F) value was much less than 0.01.

Figure 3.4 *Kinetic analysis of DHDPS-K161A with respect to pyruvate. (A) is a direct plot, (B) is the Lineweaver-Burk plot, (C) is the Eadie-Hofstee plot, and (D) is a percentage residual plot of the data.* R^2*=0.99 and* p (F) *<0.01*

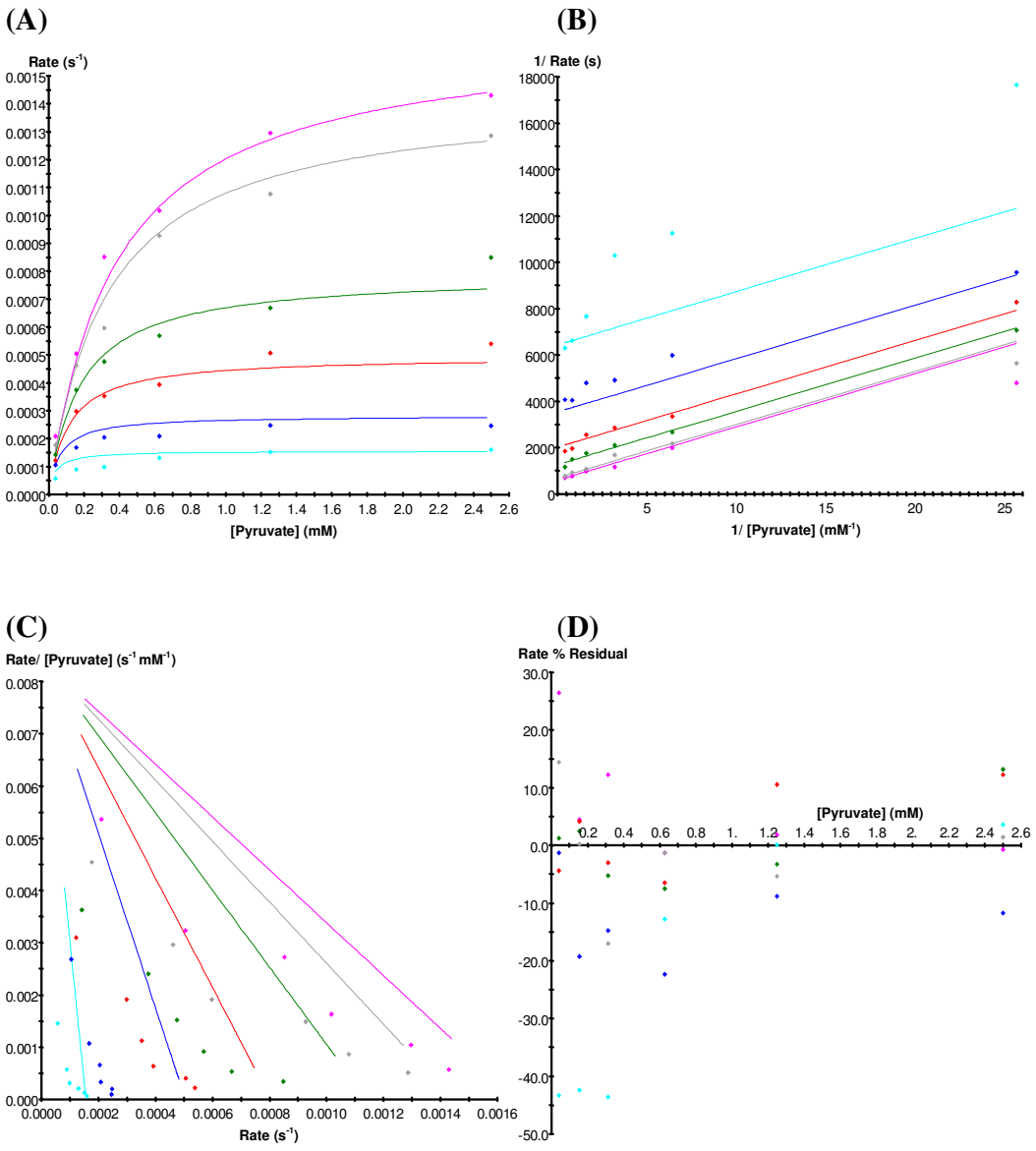

Figure 3.5 *Kinetic analysis of DHDPS-K161A with respect* (*S*)-ASA. *(A) is a direct plot, (B) is the Lineweaver-Burk plot, (C) is the Eadie-Hofstee plot, and (D) is a percentage residual plot of the data.* R^2*=0.99 and* p (F) *<0.01*

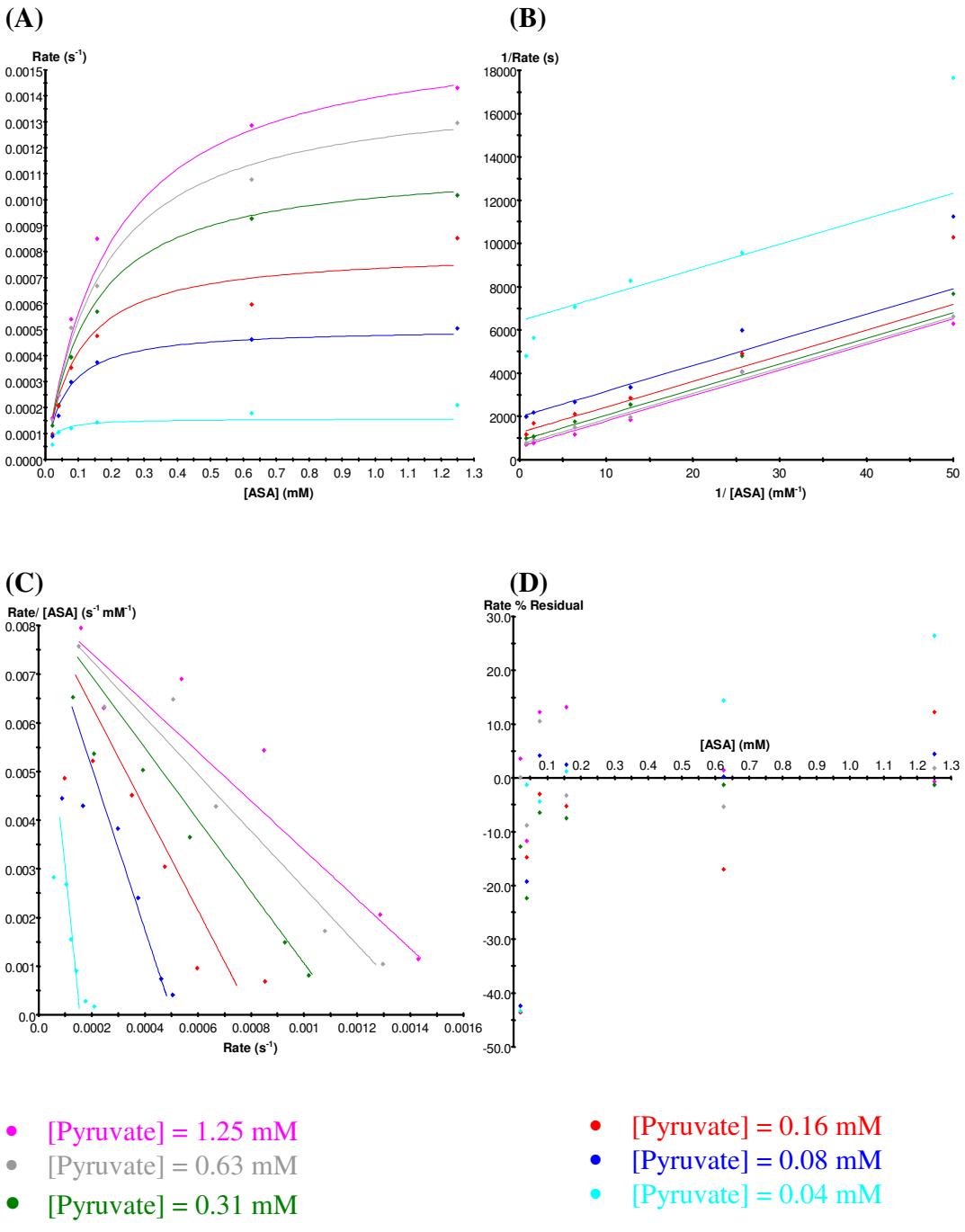

Figure 3.6 *Kinetic analysis of DHDPS-K161R with respect to pyruvate. (A) is a direct plot, (B) is the Lineweaver-Burk plot, (C) is the Eadie-Hofstee plot, and (D) is a percentage residual plot of the data.* R^2*=0.98 and* p (F) *<0.01*

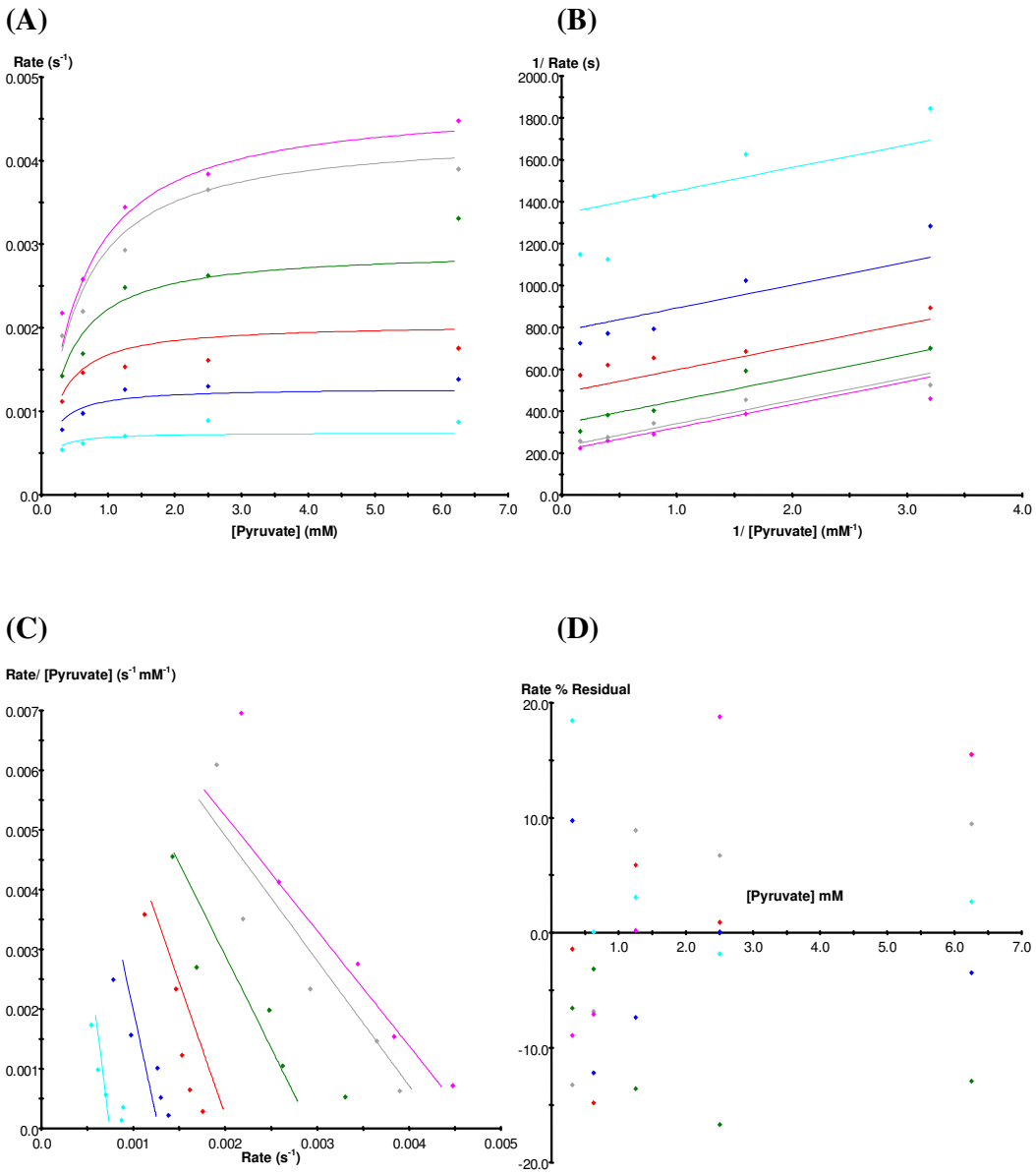

- [ASA] = 2.50 mM
- [ASA] = 0.63 mM
- [ASA] = 0.31 mM
- [ASA] = 0.16 mM
- [ASA] = 0.08 mM
- [ASA] = 0.04 mM

Figure 3.7 *Kinetic analysis of DHDPS-K161R with respect to* (S)*-ASA. (A) is a direct plot, (B) is the Lineweaver-Burk plot, (C) is the Eadie-Hofstee plot, and (D) is a percentage residual plot of the data.* R^2*=0.98 and* p (F) *<0.01*

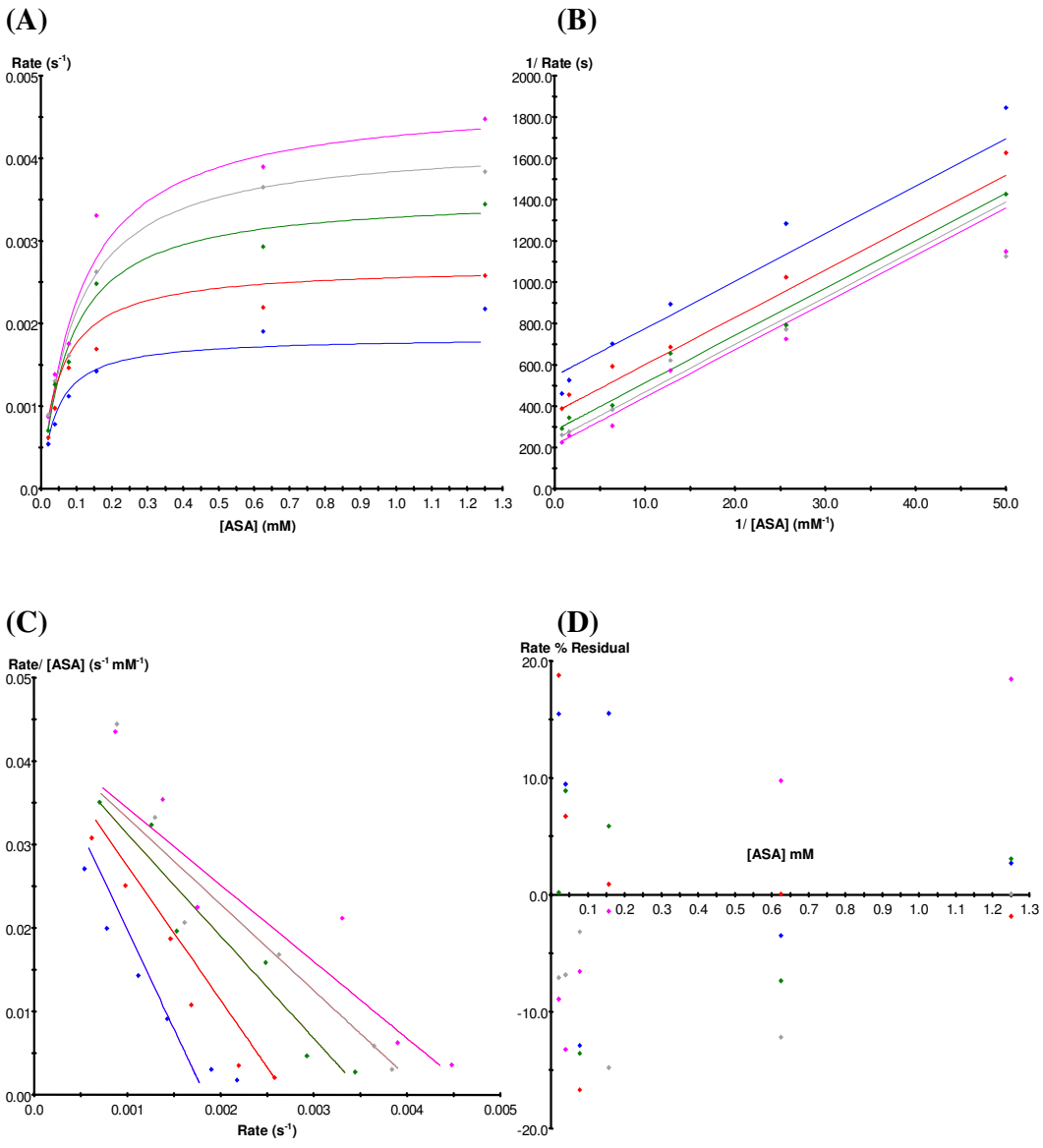

- [Pyruvate] = 1.25 mM
- [Pyruvate] = 0.31 mM
- [Pyruvate] = 0.16 mM
- [Pyruvate] = 0.08 mM
- [Pyruvate] = 0.04 mM

3.6 Lysine inhibition studies

3.6.1 DHDPS-K161A lysine inhibition

This mutant showed the same type of inhibition as the wild-type with respect to both substrates, indicating that this mutation does not interfere with the lysine binding site (Figures 3.8 and 3.9). DHDPS-K161A showed partial uncompetitive inhibition in relation to pyruvate, with a K_i value of 0.14±0.01 mM (Table 3.4), compared to 0.12 ±0.01 mM for the wild-type. The K_i value with respect to (*S*)-ASA was 0.23±0.04 mM, whereas the wild-type enzyme had a K_i value of 0.18±0.02 mM. The type of inhibition remained partial non-competitive. At saturating levels of lysine, this mutant was about 92% inhibited, exactly as observed in the wild-type (Table 3.4).

3.6.2 DHDPS-K161R lysine inhibition

Like DHDPS-K161A, this mutant behaved in a similar manner to the wild-type with regards to lysine inhibition (Figures 3.10 and 3.11). Partial uncompetitive inhibition was again observed with respect to pyruvate and partial non-competitive inhibition was observed with respect to (*S*)-ASA (Table 3.4). The K_i and the alpha values were also similar to wild-type DHDPS.

Table 3.4 *Lysine inhibition studies of DHDPS-K161A and DHDPS-K161R compared with wild-type DHDPS. The inhibition types are all partial.*

	Wild-type[1]	**K161A**	**K161R**
Varied [Pyruvate]			
Inhibition type	Uncompetitive	Uncompetitive	Uncompetitive
α (%)[2]	8±1	8±1	10±2
K_i (mM)	0.12±0.01	0.14 ±0.01	0.14±0.01
Varied [ASA]			
Inhibition type	Non-competitive	Non-competitive	Non-competitive
α (%)[2]	8±1	7±1	7±1
K_i (mM)	0.18±0.02	0.23 ±0.04	0.14±0.01

[1] As determined in Chapter two.

[2] α is the ratio of the maximal velocity without the inhibitor (V) to the maximal velocity at saturating levels of the inhibitor (V').[12]

Figure 3.8 *Lysine inhibition of DHDPS-K161A with respect to pyruvate. (A) is a direct plot, (B) is the Lineweaver-Burk plot, (C) is the Eadie-Hofstee plot, and (D) is a percentage residual plot of the data.* R^2*=0.96 and* p (F) *<0.01*

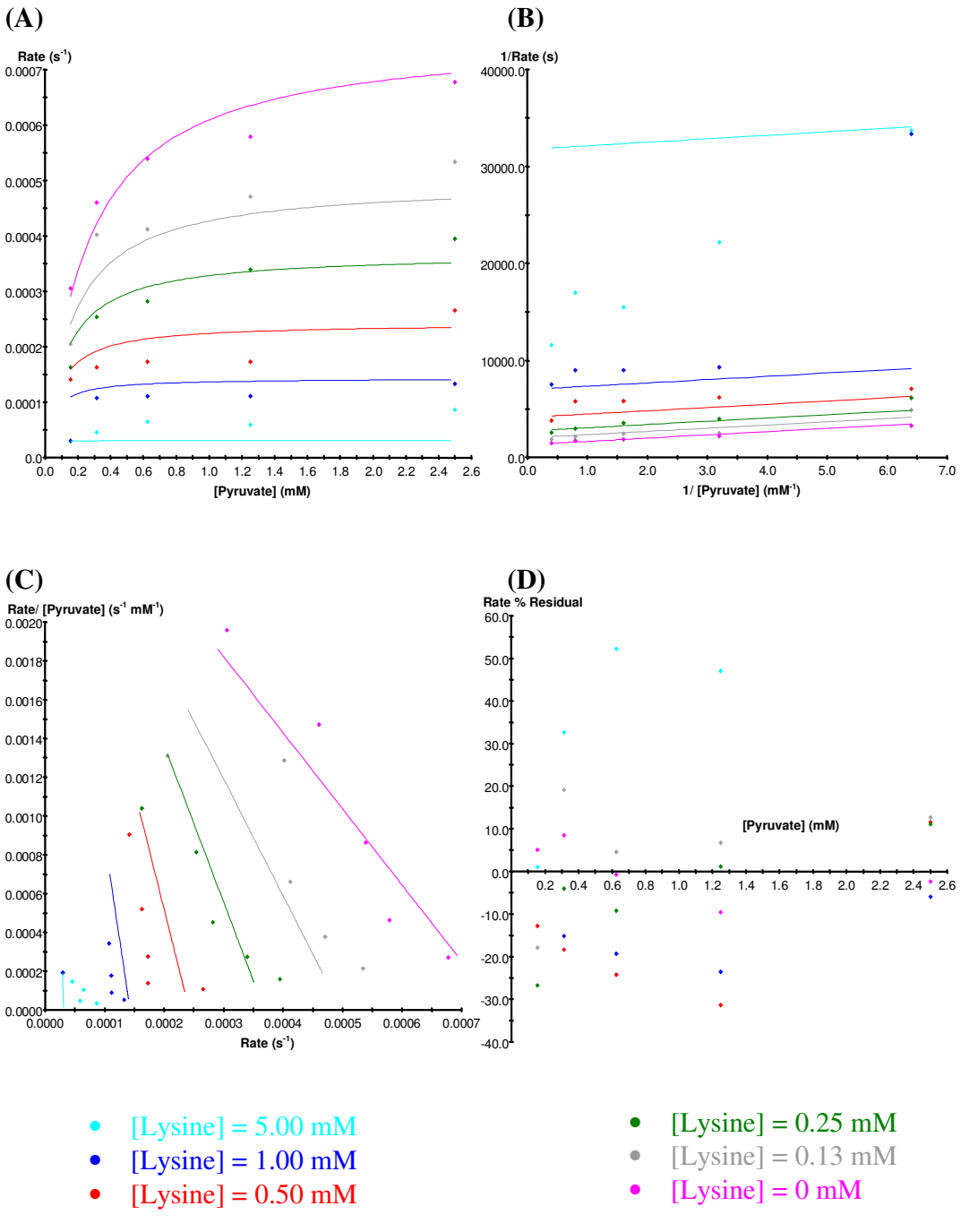

Figure 3.9 *Lysine inhibition of DHDPS-K161A with respect to* (S)*-ASA. (A) is a direct plot, (B) is the Lineweaver-Burk plot, (C) is the Eadie-Hofstee plot, and (D) is a percentage residual plot of the data.* R^2*=0.98 and* p (F) *<0.01*

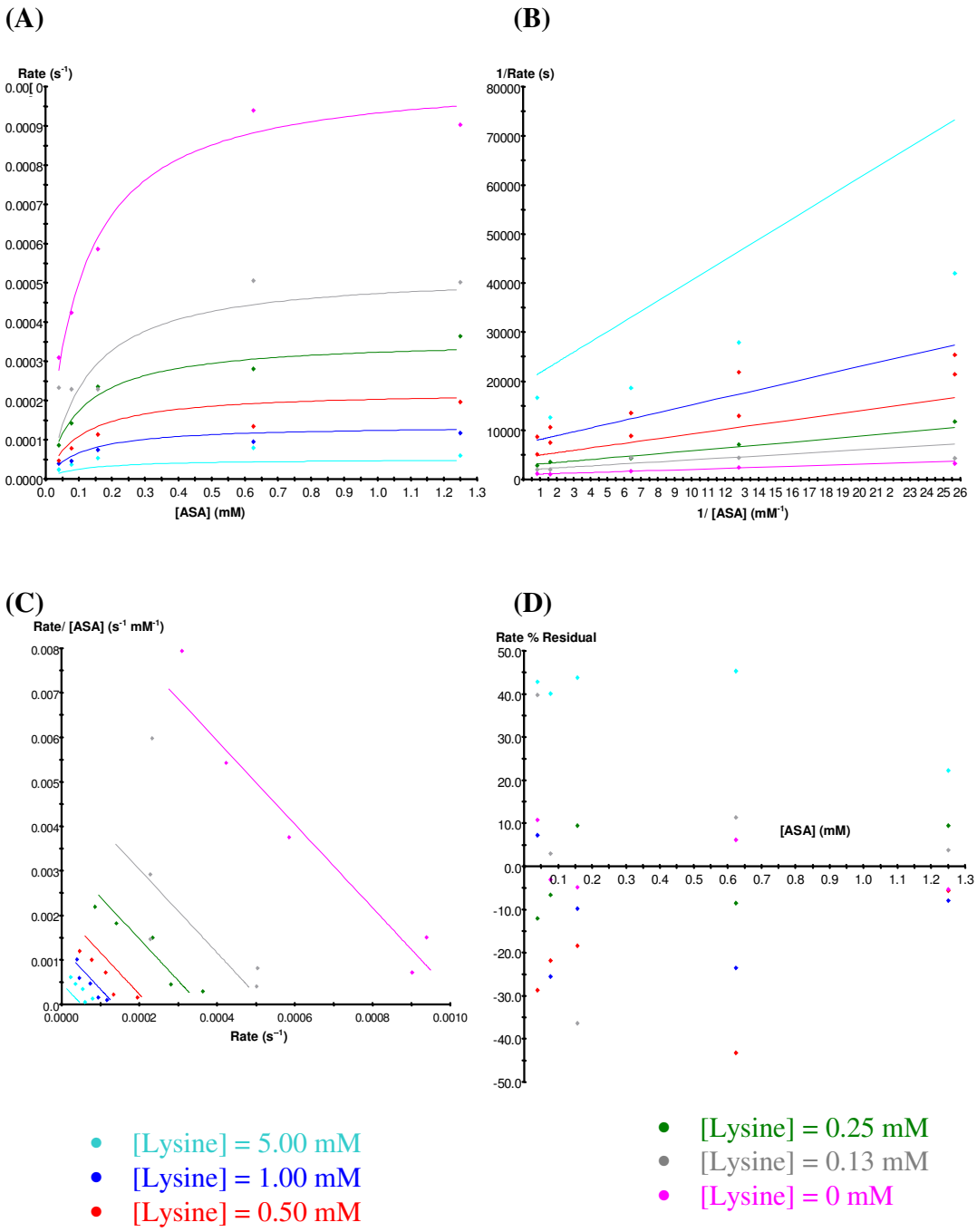

Figure 3.10 *Lysine inhibition of DHDPS-K161R with respect to pyruvate. (A) is a direct plot, (B) is the Lineweaver-Burk plot, (C) is the Eadie-Hofstee plot, and (D) is a percentage residual plot of the data.* R^2*=0.99 and* p (F) *<0.01*

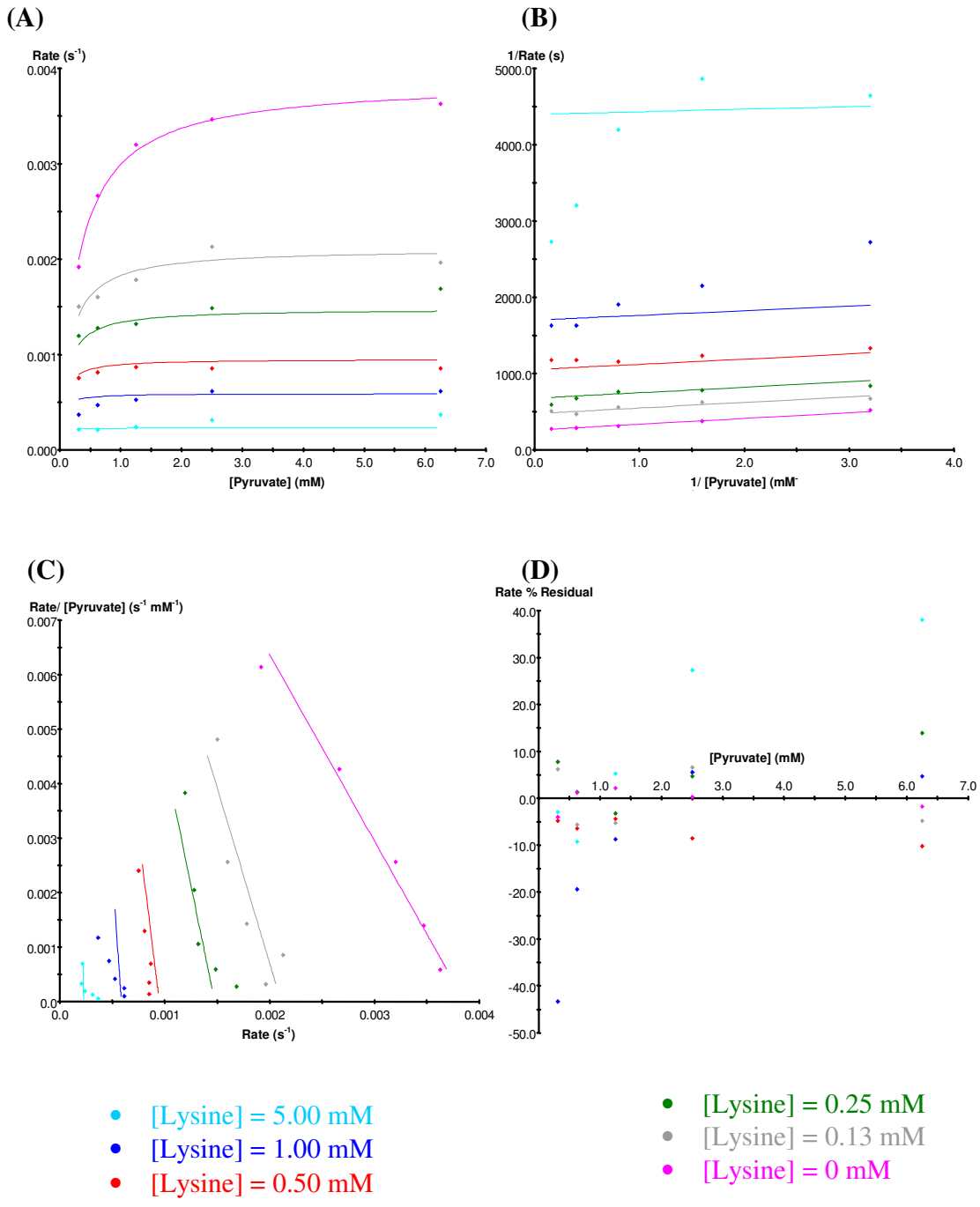

Figure 3.11 *Lysine inhibition of DHDPS-K161R with respect to (S)-ASA. (A) is a direct plot, (B) is the Lineweaver-Burk plot, (C) is the Eadie-Hofstee plot, and (D) is a percentage residual plot of the data.* R^2*=0.98 and* p (F) *<0.01*

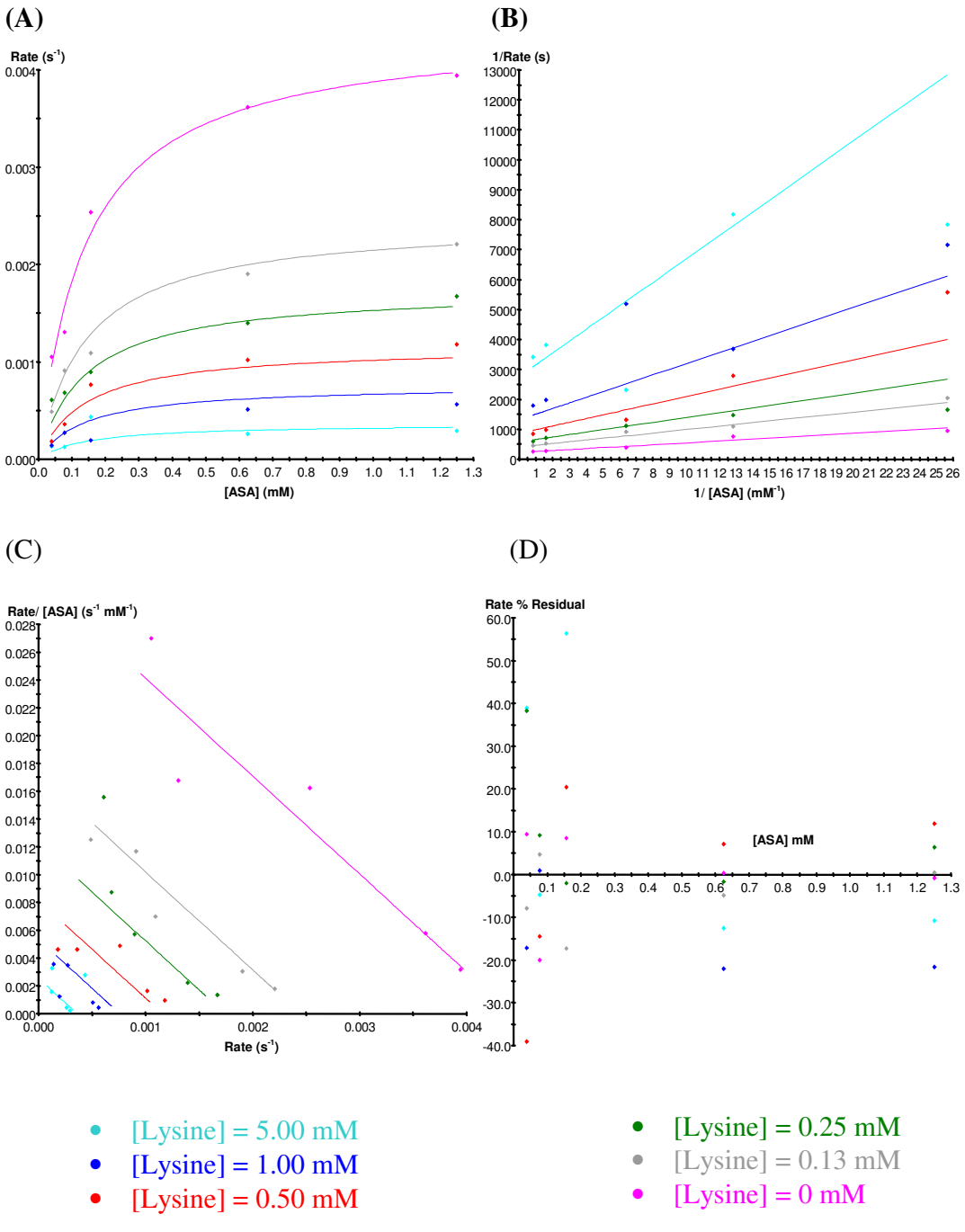

3.7 Sodium borohydride inactivation test

The reducing agent sodium borohydride can be used to detect the formation of a Schiff base between an enzyme and pyruvate by inactivation of the enzyme, due to the reduction of the C=N bond (Figure 3.12).[13] This reagent was used in this work to examine whether a Schiff base could still be formed between the first substrate pyruvate and the two K161 mutants generated. As seen in Table 3.5, the two mutants of DHDPS were not inactivated when incubated with pyruvate and the reducing agent, unlike the wild-type enzyme, suggesting that a Schiff base is not formed. In the presence of the second substrate, (*S*)-ASA, the activity remained the same for each enzyme, as expected. The difference in results obtained for the mutant enzymes and wild-type DHDPS also rules out the possibility of wild-type enzyme contamination.

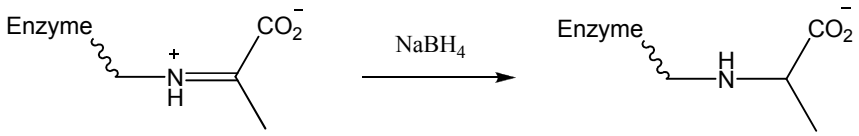

Figure 3.12 *Reduction of Schiff base by $NaBH_4$.*[13]

Table 3.5 *Percentage of activity remaining of wild-type and K161 mutants after treatment with $NaBH_4$, in the presence and absence of substrates.*

	Activity Remaining (%)		
	Wild-type	**K161A**	**K161R**
Enzyme	100	100	100
Enzyme + $NaBH_4$	91	98	97
Enzyme + $NaBH_4$ + pyruvate	0.2	84	78
Enzyme + $NaBH_4$ + (*S*)-ASA	87	93	89

3.8 Far-ultraviolet circular dichroism spectroscopy

Far-UV CD spectroscopy is a widely used technique for obtaining information about the secondary structure composition of a protein.[14] In this work, CD spectra were obtained for both mutant enzymes and they were compared to that of wild-type DHDPS, in order to establish if their secondary structure in solution had been altered upon introduction of the mutations. It is clear from Figure 3.13, which shows all spectra overlaid, that the secondary structures of DHDPS-K161A and DHDPS-K161R are similar to that of wild-type DHDPS. All three spectra are comprised of double minima at 208 nm and 222 nm, which is characteristic of a predominantly α-helical structure.[7] Thus, the introduction of the mutations at position 161 did not disrupt protein folding in solution.

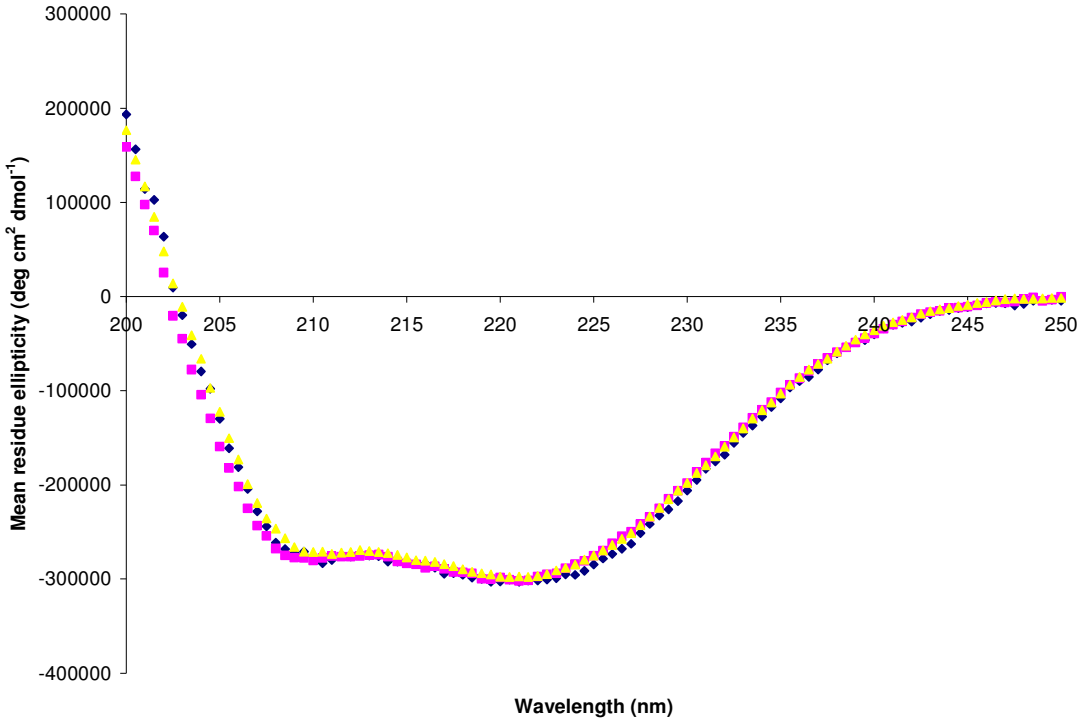

Figure 3.13 *Overlaid CD spectra of wild-type DHDPS (♦), DHDPS-K161A (■) and DHDPS-K161R (▲).*

3.9 Differential scanning fluorimetry (DSF)

DSF can be used to detect low molecular weight ligands that can bind and stabilise a particular protein.[15] The basis for this technique is that at the temperature at which a protein unfolds, its hydrophobic portions become exposed and can then interact with a fluorescent dye, which in this case was Sypro Orange. This results in a significant increase in the fluorescence emitted by the dye.[16] The higher the temperature at which this occurs, the higher the stability of the enzyme. The fluorescence then starts to decrease, probably due to precipitation of the complex formed between the fluorescent probe and the denatured protein or due to aggregation.

It has been suggested that DHDPS is stabilised by its first substrate, pyruvate, due to a tighter packing of the protein structure upon formation of the Schiff base.[17] This anecdotal observation was confirmed during this work using DSF, where the mutant enzymes were screened against a saturating concentration of pyruvate and compared to the wild-type enzyme, at temperatures ranging from 20°C to 90°C. This experiment was carried out in triplicate and the standard error was 0.10°C.

The Boltzmann model (Equation 3.1) was used to obtain the temperature midpoint for each protein unfolding transition, T_m, from the fluorescence data gathered.

Equation (3.1)

$$y = LL + \frac{(UL - LL)}{1 + \exp\left(\frac{T_m - T}{a}\right)}$$

Where y is the fluorescence intensity at temperature T, LL and UL are the values of minimum and maximum intensities, respectively, and a denotes the slope of the curve within T_m.[16]

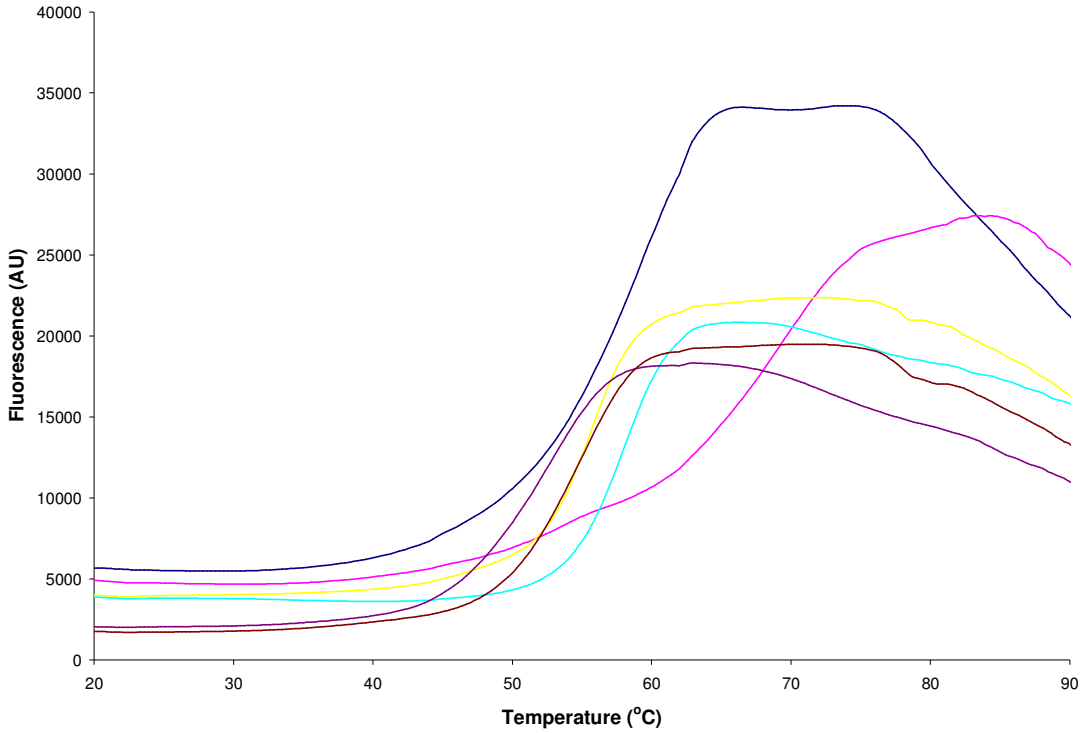

Figure 3.14 *Average thermal shift assay result for the wild-type and mutant enzymes generated screened against a saturating concentration of pyruvate (100 mM). —Wild-type DHDPS, — Wild-type DHDPS + pyruvate, —DHDPS-K161A, —DHDPS-K161A + pyruvate, —DHDPS-K161R and —DHDPS-K161R + pyruvate.*

There is a clear shift of the melting curve to the right when pyruvate is added to wild-type DHDPS (Figure 3.14). However, the shift in the curve is much smaller when pyruvate is added to the mutant enzymes. The average T_m values obtained when each enzyme was mixed with pyruvate were compared to the average T_m values obtained for the enzyme on its own. Wild-type DHDPS showed an average increase in T_m of 9.9°C in the presence of pyruvate (Figure 3.15). The melting temperature for DHDPS-K161A and DHDPS-K161R also increased upon addition of pyruvate (ΔT_m values of 2.4°C and 1.9°C respectively), but to a lesser extent than for the wild-type enzyme. This suggests that the stabilisation of *E. coli* DHDPS is largely dependent on Schiff base formation, although some stabilisation is afforded by pyruvate binding, even when the covalent adduct does not form.

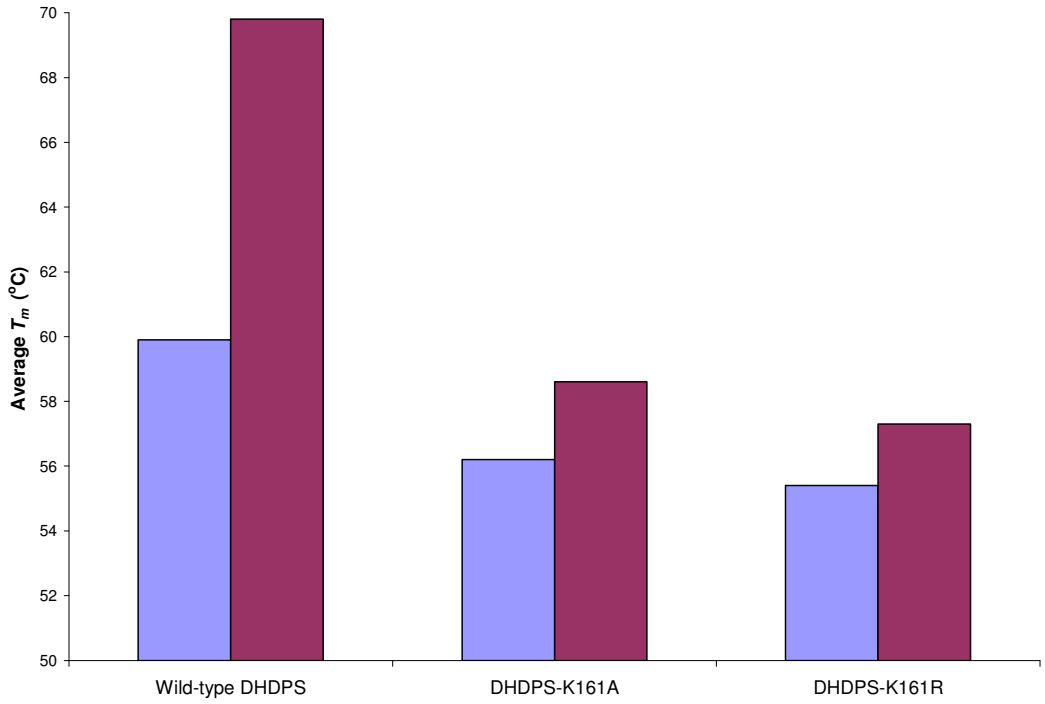

Figure 3.15 *Midpoint temperatures of the protein-unfolding transition (T_m) for wild-type DHDPS and DHDPS mutants in the absence (■) and in the presence (■) of pyruvate. Standard error < 0.10°C.*

3.10 Isothermal titration calorimetry (ITC)

ITC is a technique used to measure the energy released or absorbed during a chemical reaction between two components.[18] Interpretation of the energy change can allow the determination of the magnitude of the binding affinity (K_b) and also the magnitude of the enthalpy (ΔH) and entropy (ΔS) changes from a single experiment. ITC has thus found widespread applicability in the study of biological systems involving protein-ligand, protein-nucleic acid, and protein-protein interactions.[19]

Workers in this laboratory have found that the binding of wild-type DHDPS towards pyruvate is a low-affinity interaction.[20,21] Wiseman *et al.* noted that the shape of a binding isotherm for a simple non-interacting one-site model changes according to the product of

the association constant (K_b) and the receptor concentration ($[M]_{t(0)}$), which they referred to as the *c* value.[22] For receptors with several identical non-interacting binding sites, the *c* value is defined by Equation (3.2).

Equation (3.2) $$c = n K_b [M]_{t(0)}$$

Where *n* is the number of binding sites. A major limitation of ITC in the study of low-affinity systems such as for the interaction between DHDPS and pyruvate is the need for high protein concentrations in order to obtain *c* values between 10 and 500, which is the range of values where curve fitting is thought to produce reliable thermodynamic parameters.[23]

In a recent study, it was concluded that the difficulty in obtaining accurate thermodynamic information for low-affinity systems under low *c* values could be overcome if four criteria are met.[23] Firstly, a sufficient portion of the binding isotherm needs to be used for analysis. This was ensured by using seven equivalents of pyruvate per binding site. The binding stoichiometry must also be known, as well as the concentrations of the ligand and the protein. The second criterion, of knowing the binding stoichiometry, was met based on crystallographic studies, which show DHDPS as a tetramer with four identical binding sites for pyruvate. This gives *n* a value of four. The third criterion was also met, as the concentration of each enzyme was determined in triplicate using A_{280} and the concentration of pyruvate by dilution from a stock pyruvate solution of a known concentration. Lastly, adequate signal-to-noise was also maintained during the titration.

In this work, ITC experiments were carried out to determine the binding of both DHDPS-K161A and DHDPS-K161R to pyruvate. Titration of wild-type DHDPS at similar concentrations to both mutant enzymes was also carried out, against the same relative concentrations of pyruvate, to provide a comparison point. There was no discernible heat produced upon binding of pyruvate to the mutant enzymes compared to the wild-type enzyme (Figure 3.16). Therefore, a specific binding model for the mutant enzymes could

not be invoked. This indicates that there is no measurable binding event occurring between the mutant enzymes and the first substrate, confirming that lysine 161 plays a crucial role towards pyruvate-binding, presumably *via* the intermediacy of a thermodynamically favourable Schiff base. Furthermore, the lack of the heat evolved in response to ligand injection implies that no other external non-active site binding residues are participating in the formation of Schiff base like structures.

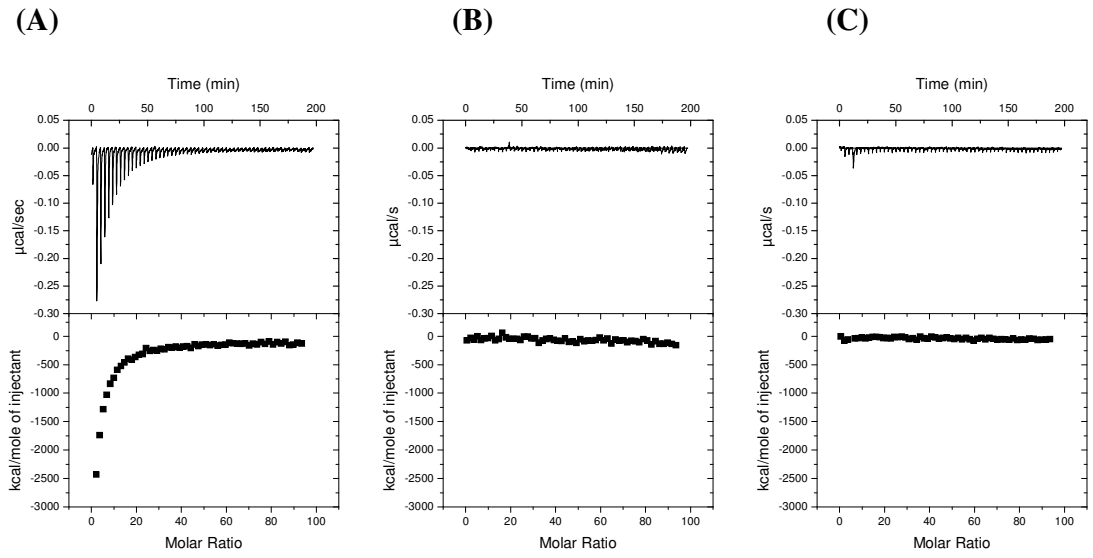

Figure 3.16 *ITC profiles obtained for titrations of pyruvate into wild-type DHDPS at 0.27 mg/mL (A), DHDPS-K61A at 0.28 mg/mL (B) and DHDPS-K161R at 0.34 mg/mL (C). The top graphs show the raw data for 55 injections of pyruvate into a 20 mM HEPES buffered DHDPS solution at 25^{o}C. The bottom graphs show heat released as a function of pyruvate added. The software accounts for the small differences in protein concentrations when attempting to fit a curve though the data. Data fitting could not be performed for the mutant enzymes due to the lack of heat generated.*

3.11 ^{1}H Nuclear magnetic resonance (NMR) spectroscopy

In the current proposed mechanism for DHDPS (Figure 1.3), the tautomerisation of the Schiff base to an enamine species creates the nucleophile that attacks (*S*)-ASA. This is followed by cyclisation, which leads to the release of HTPA from the active site. In section 3.7, it was shown by a sodium borohydride inactivation test, that the mutant enzymes are unable to form the covalent intermediate. Nevertheless, catalytic rates could still be measured, which were significantly greater than those in the absence of enzyme (section 2.5). Thus, the question arose as to which species acts as the nucleophile in the mutant enzymes, since the reaction can still proceed in the absence of the Schiff base, although at a much slower rate than with the wild-type enzyme.

In order to examine whether the enolisation of pyruvate to an enol species could explain the detection of rate enhancements, the ability of the mutant enzymes to catalyse hydrogen-deuterium exchange of pyruvate was tested using NMR. This was done in collaboration with Andrew Muscroft-Taylor. The loss of the methyl protons from pyruvate can be followed by the decrease of the hydrogen ^{1}H NMR signal as deuterium atoms are incorporated into the methyl group (Figure 3.17).[24] The development of the splitting of the methyl peak of pyruvate is a consequence of ^{1}H-^{2}D coupling, resulting in the incorporation of deuterium which has a spin isotope number of s = 1.

The chemical shift data for pyruvate and its deuterated analogues, in parts per million, are as follows: H_3-pyruvate 2.36 (singlet), H_2D-pyruvate 2.35 (triplet, J = 2.23 Hz) and D_2H-pyruvate 2.33 (quintet, J = 2.25 Hz). The large peak at 4.80 ppm, due to water in the solvent, was suppressed using a PRESAT pulse sequence, allowing adequate resolution of the signals from 0 to 4 ppm. The methyl peaks of *t*-butanol were used as internal standards for NMR measurements, referenced as a singlet at 1.24 ppm.[25] The exchange of pyruvate in D_2O in both the absence of enzyme and in the presence of an enzyme which is not known to accelerate the rate of enolisation of pyruvate were followed as negative controls. The control enzyme used in this work was DHDPR, which does not use a Schiff base intermediate for catalysis.

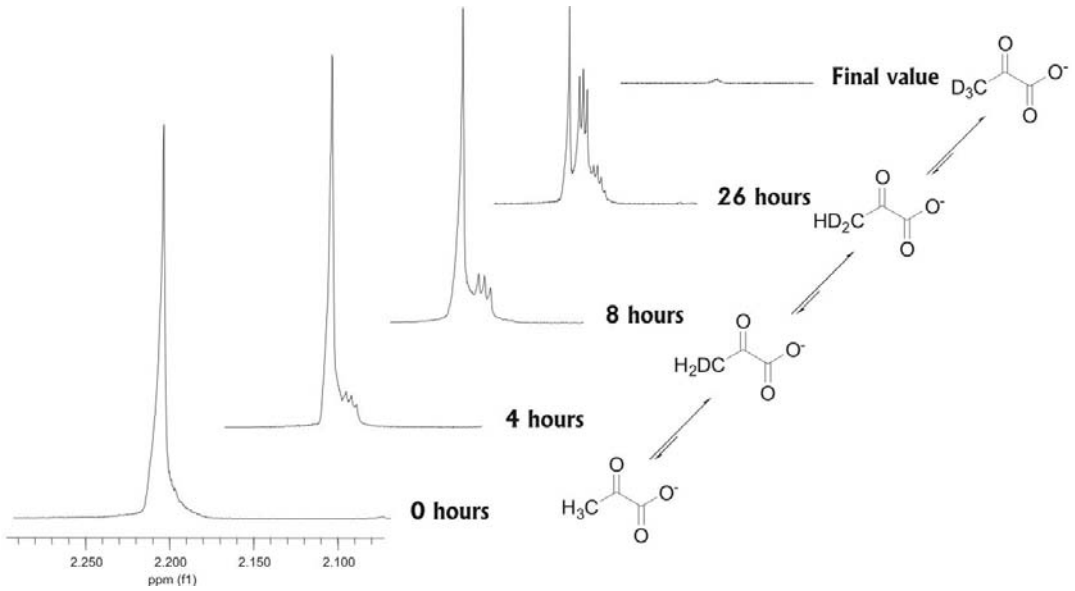

Figure 3.17 *^{1}H-NMR spectra of H_3-pyruvate in D_2O in the presence of wild-type DHDPS, illustrating ^{1}H to ^{2}D exchange at the time intervals 0 hours, 4 hours, 8 hours, 26 hours and 80 hours.*

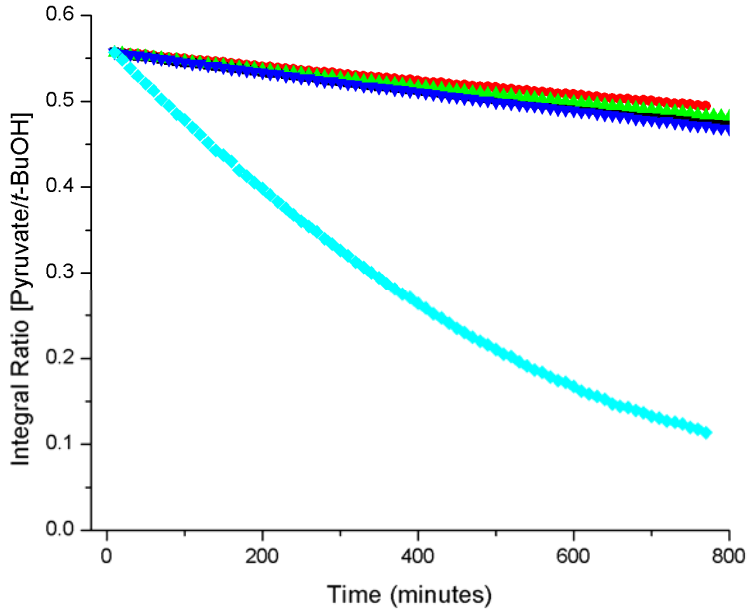

Figure 3.18 *Integral ratios from NMR spectra measured at 10 minute time intervals for pyruvate in D_2O in the presence of wild-type DHDPS (♦), DHDPS-K161A (■), DHDPS-K161R (▲), DHDPR (▼) and no enzyme (●).*

The rapid decline in the pyruvate proton integral ratio for wild-type DHDPS indicates that this enzyme is much faster at catalysing the hydrogen-deuterium exchange of pyruvate than D_2O alone (Figure 3.18). On the other hand, the mutant enzymes did not seem to catalyse the exchange of hydrogen atoms between pyruvate and D_2O, presumably because of their inability to form a Schiff base. The exchange rates observed were similar to those obtained for the control experiments (in the absence of enzyme and in the presence of the control protein, DHDPR). These results suggest that the rate of enolisation of the keto form of pyruvate to its enol tautomer is unchanged in DHDPS-K161A and DHDPS-K161R catalysed mechanism.

3.12 Discussion

As mentioned in section 3.1, lysine 161 was identified as being involved in the formation of a Schiff base intermediate with the ketone group of the first substrate, pyruvate.[1,2] The present study provides further evidence for the importance of this conserved residue, as demonstrated by the dramatic loss of activity observed in both lysine 161 mutants. The mutation of lysine 161 to an alanine resulted in an enzyme that retained only 0.1% wild-type activity. The change of lysine 161 to an arginine also resulted in a significant decrease in activity, with less than 0.4% activity remaining. However, the most surprising finding was that mutation of lysine 161 did not completely abolish enzyme activity. This contrasts with what is observed in the homologous enzyme NAL, where the K161A mutant was inactive.

An interesting finding was a shift in the kinetic mechanism, from the ping-pong to the ternary-complex mechanism, after the introduction of the mutations. This shift indicates a relaxation in the order of reaction steps during catalysis for the K161 mutants. Closer inspection of the K_m values shows that the first half reaction, which involves pyruvate binding and Schiff base formation, is slightly affected, as evidenced by a 3-fold increase in the Michaelis-Menten constant with respect to pyruvate for both mutants. An increase in the $K_{mPyruvate}$ values were expected as the Schiff base-forming residue was removed,

however the small magnitude of the increase was a surprise. The ITC experiments showed that even though both mutants still retained activity, there is no measurable energy change occurring in the reaction between the mutant enzymes and pyruvate. The kinetic and ITC data confirm that lysine 161 plays a crucial role towards pyruvate-binding and that a mutation at this position affects the first half reaction, which agrees with sequence alignment experiments as well as the crystallography data obtained for wild-type DHDPS in the presence of pyruvate. There was little or no change in K_{mASA}, indicating that the removal of lysine 161 did not affect the second half reaction, which is to be expected, since lysine 161 is not involved in (*S*)-ASA binding according to the current proposed mechanism shown in section 1.3.

Treatment with $NaBH_4$ provides evidence that a Schiff base is not formed when pyruvate associates with either of the mutant enzymes generated. This is confirmed by DSF, which shows that the mutant enzymes are stabilised to a lesser extent in the presence of pyruvate than the wild-type enzyme, presumably due to their inability to form a Schiff base. These tests, combined with the detection of residual activity, demonstrate that covalent catalysis represents only part of the total lowering of the free energy of activation of the DHDPS-catalysed reaction. Hydrogen-deuterium exchange of pyruvate *via* NMR suggests that the rate of enolisation of the keto form of pyruvate to its enol tautomer is unchanged in DHDPS-K161A and DHDPS-K161R catalysed mechanism.

The behaviour of the K161 mutants with respect to lysine inhibition was also investigated in this chapter. The mutants behaved in an entirely analogous fashion to the wild-type DHDPS. Not only were the same types of inhibition displayed and similar K_i values were observed but at saturating inhibitor levels, the enzymes were 92% inhibited as is the wild-type enzyme. This demonstrates the lack of involvement of lysine 161 in the regulation of DHDPS by (*S*)-lysine.

CD spectroscopy showed that the mutations did not grossly perturb the secondary structure of the enzyme in solution. The crystal structure of these mutants will be detailed in the following chapter in the presence and in the absence of pyruvate to allow a further

understanding of how DHDPS can perform catalysis in the absence of its key active site residue, lysine 161, and to rule out the possibility that their tertiary and quaternary structures have been altered.

3.13 References

1. Laber, B.; Gomis-Ruth, F. X.; Romao, M. J.; Huber, R., *Escherichia coli* dihydrodipicolinate synthase. Identification of the active site and crystallization. *Biochemistry Journal* **1992,** 288, (Pt 2), 691-695.
2. Blickling, S.; Renner, C.; Laber, B.; Pohlenz, H. D.; Holak, T. A.; Huber, R., Reaction mechanism of *Escherichia coli* dihydrodipicolinate synthase investigated by X-ray crystallography and NMR spectroscopy. *Biochemistry* **1997,** 36, (1), 24-33.
3. Kruger, D.; Schauer, R.; Traving, C., Characterization and mutagenesis of the recombinant *N*-acetylneuraminate lyase from *Clostridium perfringens* - insights into the reaction mechanism. *European Journal of Biochemistry* **2001,** 268, (13), 3831-3839.
4. Peracchi, A., Enzyme catalysis: removing chemically 'essential' residues by site-directed mutagenesis. *Trends in Biochemical Sciences* **2001,** 26, (8), 497-503.
5. Gerrard, J. A. Studies on dihydrodipicolinate synthase. D. Phil. Thesis. Oxford University, 1992.
6. Stratagene, *Quickchange site-directed mutagenesis kit: Instruction manual*. 1998.
7. Fersht, A. R., *Structure and mechanism in protein science - a guide to enzyme catalysis and protein folding*. Freeman & Co: New York, 1999.
8. Dobson, R. C. Investigating the catalytic and regulatory mechanism of dihydropicolinate synthase. D. Phil. Thesis. University of Canterbury, 2003.
9. Cornish-Bowden, A., *Fundamentals of enzyme kinetics*. Portland Press, London: 1999.
10. Michaelis, L.; Davidsohn, H., The effect of hydrogen ions on invertin. *Biochemische Zeitschrift* **1911,** 35, 386-412.

11. Selwyn, M. J., A simple test for enzyme inactivation of an enzyme during assay. *Biochimie et Biophysica Acta* **1965,** 105, 193-195.
12. Dobson, R. C.; Griffin, M. D.; Roberts, S. J.; Gerrard, J. A., Dihydrodipicolinate synthase (DHDPS) from *Escherichia coli* displays partial mixed inhibition with respect to its first substrate, pyruvate. *Biochimie* **2004,** 86, (4-5), 311-315.
13. Shedlarski, J. G.; Gilvarg, C., The pyruvate-aspartic semialdehyde condensing enzyme of *Escherichia coli*. *Journal of Biological Chemistry* **1970,** 245, 1362-1373.
14. Yang, J. T.; Wu, C. S. C.; Martinez, H. M., Calculation of protein conformation from circular-dichroism. *Methods in Enzymology* **1986,** 130, 208-269.
15. Niesen, F. H.; Berglund, H.; Vedadi, M., The use of differential scanning fluorimetry to detect ligand interactions that promote protein stability. *Nature Protocols* **2007,** 2, (9), 2213-2221.
16. Ericsson, U. B.; Hallberg, B. M.; DeTitta, G. T.; Dekker, N.; Nordlund, P., Thermofluor-based high-throughput stability optimization of proteins for structural studies. *Analytical Biochemistry* **2006,** 357, 289-298.
17. Griffin, M. D. Why is dihydrodipicolinate synthase a tetramer? D. Phil. Thesis. University of Canterbury, 2005.
18. Leavitt, S.; Freire, E., Direct measurements of protein binding energetics by isothermal titration calorimetry. *Current Opinion of Structural Biology* **2001,** 11, (5), 560-566.
19. Ababou, A.; Ladbury, J. E., Survey of the year 2005: literature on applications of isothermal titration calorimetry. *Journal of Molecular Recognition* **2007,** 20, 4-14.
20. Domigan, L. Characterisation on dihydrodipicolinate synthase (DHDPS) from *Bacillus anthracis*. B. Sc. Hons. Thesis. University of Canterbury, 2007.
21. Muscroft-Taylor, A., *Personal communications*, 2007.
22. Wiseman, T.; Williston, S.; Brandts, J. F.; Lin, L. N., Rapid measurement of binding constants and heats of binding using a new titration calorimeter. *Analytical Biochemistry* **1989,** 179, (1), 131-137.

23. Turnbull, W. B.; Daranas, A. H., On the value of c: can low affinity systems be studied by isothermal titration calorimetry? *Journal of the American Chemical Society* **2003,** 125, (48), 1459-1466.

24. Kosicki, G. W., Oxaloacetate decarboxylase from cod. Catalysis of hydrogen-deuterium exchange in pyruvate. *Biochemistry Journal* **1968,** 7, (12), 4310-4314.

25. Gottlieb, H. E.; Kotlyar, V.; Nudelman, A., NMR chemical shifts of common laboratory solvents as trace impurities. *Journal of Organic Chemistry* **1997,** 62, (21), 7512-7515.

Chapter Four

Crystal structures of DHDPS-K161A and DHDPS-K161R

4.1 Introduction

The results from Chapter three showed a dramatic decrease in enzyme activity when lysine 161 is replaced by either an alanine or an arginine in DHDPS. CD spectroscopy confirmed that the secondary structures of the mutant enzymes were identical to that of the wild-type enzyme. In this chapter, X-ray crystallography was used to determine their structure in order to rule out the possibility that this decrease in activity was due to gross alterations in their tertiary or quaternary structures. The structural information obtained from X-ray crystallography has proved to be a key factor in the investigation of enzyme mechanisms. This technique allows the construction of an electron density map that shows the arrangement in space of the atoms in a protein, using the information obtained from the X-ray diffraction patterns of suitable crystals.[1] Protein crystallography is not a trivial task, as protein crystals of sufficient size and quality are needed, so that interpretable diffraction patterns can be obtained.

This chapter details the structures of both DHDPS-K161A and DHDPS-K161R, and compares them to the structure of the wild-type enzyme that had previously been solved by Dobson *et al.*[2] to a resolution of 1.9 Å. However, in order to fully understand how an enzyme works, it is necessary to determine the structure of not only the enzyme but also the structures of the complexes of the enzyme with its substrates. In this chapter, the structure of DHDPS-K161A and DHDPS-K161R are characterised, both in native form

and in the presence of the first substrate, pyruvate. It was shown in the previous chapter, by using a sodium borohydride inactivation test, that pyruvate does not form a Schiff base with either DHDPS-K161A or DHDPS-K161R despite being accepted as a substrate and that there is no measurable binding event occurring between the mutant enzymes and pyruvate, as assessed by ITC. Therefore, these ligand-bound structures provide further insight into which residues are close to this substrate and what structural changes occur in the substrate and enzyme upon binding.

I carried out the work in this chapter in the laboratory of Professor Geoff Jameson (Massey University, Palmerston North).

4.2 Crystallisation and diffraction data collection

Crystals were obtained using the hanging drop-vapour diffusion method as described by Mirwaldt *et al.* (1995)[3] but at 12°C. Diffraction data sets were processed and scaled using the programme *CrystalClear*.[4] All crystals diffracted to beyond 2.4 Å and they belonged to the same space group as the wild-type enzyme, $P3_121$, with minor differences in the cell dimensions. The R_{merge} values were 0.091, 0.088, 0.139 and 0.114 for DHDPS-K161A, pyruvate-bound DHDPS-K161A, DHDPS-K161R and pyruvate-bound DHDPS-K161R, respectively (Table 4.1).

4.3 Structure determination and refinement

The structures were solved using the molecular replacement method, as incorporated in the programme *MolRep*,[5] based on the structure of the wild-type enzyme found in the RCB Protein Data Bank, entry 1YXC. Refinement rounds were performed using *REFMAC5*.[5] Electron density maps were interpreted with the aid of *COOT*. Structure quality was assessed using *PROCHECK*[6] and other validation tools in *COOT*.[7] The data collected and refinement statistics are shown in Table 4.1.

Table 4.1 *Data collection and refinement statistics for DHDPS-K161A and DHDPS-K161R crystal structures with and without pyruvate bound.*

	K161A	**K161A + pyruvate**	**K161R**	**K161R + pyruvate**
Data collection				
Number of crystals	1	1	1	1
Oscillation range (°)	0.25	0.25	0.20	0.25
Number of images	361	225	368	494
Exposure time (sec)	660	570	606	240
Camera length (mm)	130.1	130.1	130.1	135.2
Data processing				
Space group	$P3_121$	$P3_121$	$P3_121$	$P3_121$
Unit cell[a] *a*, *b*, *c* (Å)	121.04, 121.04, 110.05	120.88, 120.88, 110.50	121.02, 121.02, 110.95	121.44, 121.44, 111.05
α, *β*, *γ* (°)	90, 90, 120	90, 90, 120	90, 90, 120	90, 90, 120
Resolution (outer shell) (Å)	1.99 (2.07-1.99)	2.30 (2.38-2.30)	2.40 (2.48-2.40)	2.10 (2.18-2.10)
Number of reflections (unique)	268,357 (63,475)	136,247 (39,830)	157,741 (36,802)	381,650 (53,975)
Completeness (outer shell, %)	99.4 (96.7)	95.0 (97.3)	98.9 (97.4)	97.2 (100)
I/σ (I) (outer shell)	7.1 (2.3)	7.4 (2.8)	6.5 (2.5)	8.8 (3.3)
Redundancy (outer shell)	4.23 (4.02)	3.42 (3.27)	4.29 (4.21)	7.07 (7.04)
R_{merge}[b] (outer shell)	0.091 (0.453)	0.088 (0.350)	0.139 (0.454)	0.114 (0.443)
Refinement				
R_{free}[c] (outer shell)	0.2386 (0.385)	0.2319 (0.268)	0.2344 (0.336)	0.2350 (0.356)
R_{Cryst}[d] (outer shell)	0.2022 (0.304)	0.1845 (0.254)	0.2032 (0.291)	0.1977 (0.295)
Solvent molecules	408	180	208	387
Glycerol molecules	5	8	3	6
Pyruvate molecules	0	2	0	2
Potassium ions	4	4	4	4
Mean *B*-value (Å^2)	31.53	34.21	28.54	30.89
root mean square deviation				
Bond lengths (Å)	0.012	0.023	0.014	0.011
Bond angles (°)	1.403	2.006	1.601	1.361

[a] Wild-type cell dimensions were $a=b=121.87$ Å, $c=110.19$ Å.[2]

[b] $R_{merge}= \Sigma |I-\langle I\rangle| / \Sigma\langle I\rangle$.

[c] R_{free} based on 5% of the total reflections with the same set of reflections transferred from the original wild-type structure, common to all four structures.

[d] $R_{Cryst} = \Sigma(|F_{obs}|-|F_{calc}|) / \Sigma|F_{obs}|$.

4.4 General features of the DHDPS mutants

The final models were made up of two monomers, A and B, with 292 amino acid residues each. The tetramer can be generated from these by crystallography symmetry. Each monomer is composed of two domains: the N-terminal domain that folds into a $(\beta/\alpha)_8$ barrel (residues 1-224) and the C-terminal α-helical domain (residues 225-292) (Figure 1.2). As described in Chapter one, the active site is found at a cavity formed by the two monomers, where the residue at position 161 is found on a hydrophobic scaffold, leaving only one side accessible to the solvent (Figures 1.2 and 4.1). Y133 is positioned directly above it and T44 is hydrogen bonded to both Y133 and Y107 (from the adjacent monomer in the dimer), forming the catalytic triad. R138 is situated at the entrance of the active site cavity, where it is believed to be involved in binding the carboxyl group of (*S*)-ASA.[8,9]

The R_{free} values for the final refined structures were: 20.2% for DHDPS-K161A, 18.5% for DHDPS-K161A with pyruvate, 20.3% for DHDPS-K161R, and 19.8% for DHDPS-K161R with pyruvate (Table 4.1). The Ramachandran plot[10] for each structure showed that all residues fell within favoured regions, except for Y107. It has been suggested that this is the case because its conformational strain is associated with function.[2,3,11]

The NCS constraints used for all four structures varied from medium, for both the main chains and the side chains, for the initial rounds of refinement, to loose for the side chains in the later rounds. There was very well defined electron density for the main chain residues from the carboxy-terminal to the amino-terminal, except for the N-terminal methionine at position 1. The conformation of some side chain residues could not be resolved, either because there was no electron density to guide the rebuilding, or because the residue appeared to hold several different conformations—these side chains were assigned 0% occupancy in the final PDB files.

Overall, the mutant enzymes showed no major changes in their structures when compared to the structure of wild-type DHDPS (Figure 4.1), indicating that the attenuated catalytic

activities observed in Chapter three were not due to any major structural changes induced by the mutations.

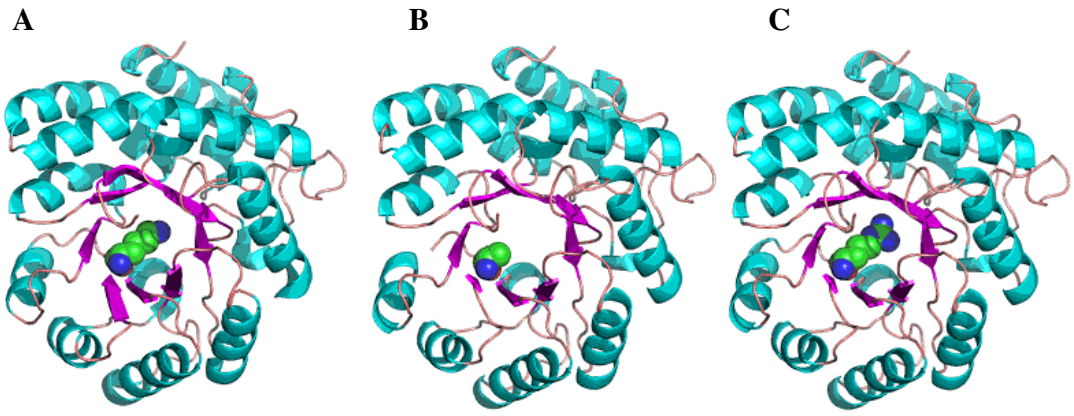

Figure 4.1 *Tertiary structure of the monomer:* ***A****, Wild-type DHDPS;* ***B****, DHDPS-K161A;* ***C****, DHDPS-K161R. The residue at position 161, found in the centre of the barrel, is highlighted in green and blue. The β-sheets are coloured in purple and the α-helices are coloured in cyan. This and subsequent figures in this chapter were produced using PyMol, unless otherwise stated.*[12]

4.5 Active site of DHDPS-K161A

The structure of DHDPS-K161A showed very well-defined electron density around alanine at position 161 (Figure 4.2). The orientation and position of the active site residues found in monomer A were very similar to those found in monomer B (Figure 4.3). The distances between the functional groups of the main active site residues in both monomers were also very similar (Table 4.2). Due to the high similarity between the monomers within the asymmetric unit, the pictures generated show monomer A only.

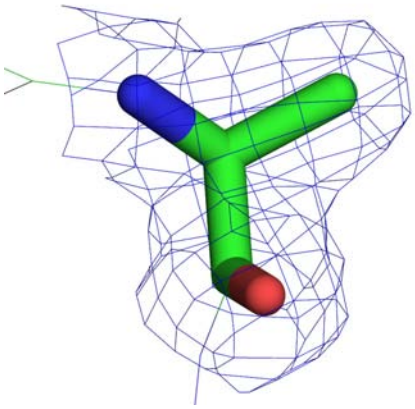

Figure 4.2 *Residue A161 of DHDPS-K161A covered by 2Fo-Fc electron density (blue), which is contoured at 1σ.*

Table 4.2 *Comparison of the distance between key groups within the active site of wild-type DHDPS and DHDPS-K161A.*

			Wild-type[a]	Monomer A DHDPS-K161A	Monomer B DHDPS-K161A
Protein distances (Å)	OH_Y133	NH_2_K161	2.9	-	-
	OH_Y133	CH_3_A161	-	6.7	6.6
	OH_Y133	OH_T44	2.6	3.2	3.3
	OH_T44	OH_Y107	2.6	2.8	2.7
	OH_Y133	OH_107	3.7	4.3	4.5
	OH_Y133	X	2.6	-	-
	N^{ε}_R138	X	3.2	-	-

[a] As reported by Dobson *et al.*[2]

The overlay of the structures of the wild-type enzyme and DHDPS-K161A (rmsd = 0.154 Å) showed very little change within the active site (Figure 4.4). The conformations of the active site residues T45, Y106, Y107, R138, G186 and I203 are completely conserved in the structure of this mutant enzyme relative to wild-type DHDPS. Whilst the main chain atoms of Y133 are positioned similarly, the aromatic ring was twisted slightly in DHDPS-K161A relative to the wild-type enzyme for both subunits A and B. Y133 is thought to be central for DHDPS function. It is positioned directly above the residue at position 161 and it is part of a hydrogen bond network with T44 and Y107 in the wild-

type enzyme. This motif makes up the catalytic triad, which facilitates Schiff base formation.[8,11]

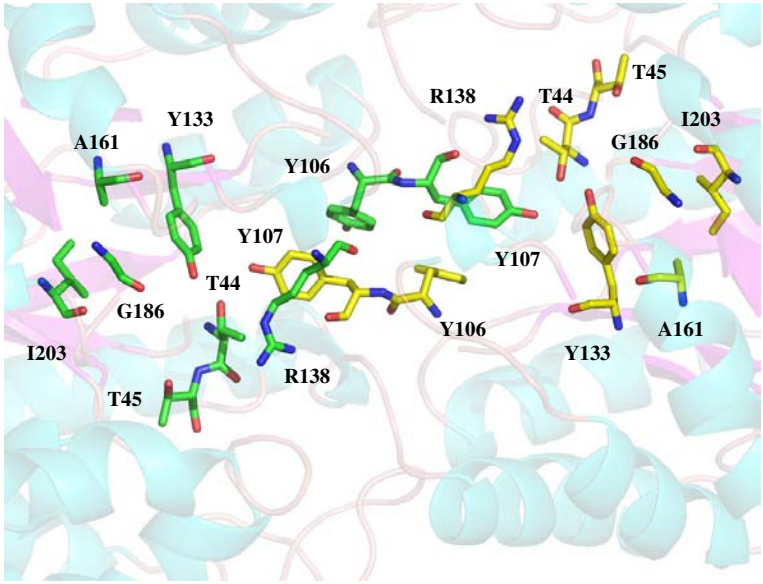

Figure 4.3 *Active site residues of monomer A (green) and monomer B (yellow) of DHDPS-K161A.*

The twist in the aromatic ring results in a slightly longer distance between the hydroxyl group of Y133 and those of T44 and Y107 compared to the wild-type enzyme (Table 4.2). Nevertheless, the distance still allows the formation of hydrogen bonds between the hydroxyl groups of T44 and Y133 (3.2 Å), and between T44 and Y107 (2.8 Å) as in the wild-type, where the distances are both 2.6 Å. This is important because Y133, although no longer involved in Schiff base formation in this enzyme, is still presumably involved in the binding of the hydrate (*S*)-ASA.[11] This is thought to be achieved by a proton transfer to the leaving hydroxyl group.

The larger distance between the T44 and Y133 OH groups can also be accounted for by a small movement in the loop bearing T44, which results in a shift of its hydroxyl group away from Y133 by approximately 0.2 Å, compared to the wild-type enzyme.

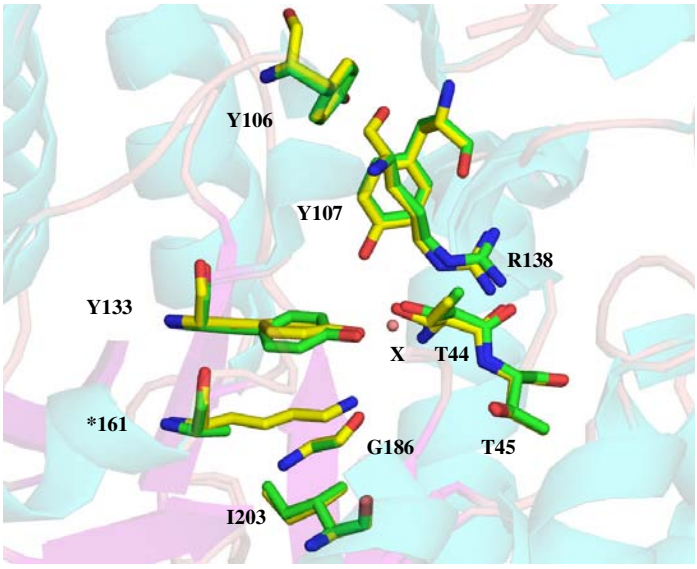

Figure 4.4 *Overlay of active site of the wild-type DHDPS (yellow) and DHDPS-K161A (green) from monomer A. X is a water molecule (pink) present in the wild-type structure only. Notice the small twist in orientation of the aromatic ring of Y133 and the small displacement of T44.*

An interesting feature of the wild-type structure is the presence of a water molecule (Figure 4.4, molecule X) that bridges the hydroxyl group of Y133 (2.6 Å) and the N^{ε} atom of R138 (3.2 Å). This water molecule is absent in the structure of this mutant enzyme. This water bridges Y133 with the cationic guanidium group of R138, which makes the hydroxyl group a better acid. This is particularly important in the first half reaction, which involves Schiff base formation, as described in section 1.3.3. When absent, as in the wild-type structure with pyruvate bound, the hydroxyl group becomes a weaker acid (and perforce a stronger base), which is important in the binding of (*S*)-ASA.[2] This hypothesis is confirmed by mutagenic experiments, where the change of Y133 to a phenylalanine residue increases K_m by 100-fold for both pyruvate and (*S*)-ASA, whereas the T44V and Y107F mutations only result in K_m values that are substantially higher with respect to pyruvate.[11]

4.6 Active site of DHDPS-K161R

The crystal structure of DHDPS-K161R confirmed that arginine had successfully been introduced at position 161, as evidenced by the well-defined electron density around the skeleton of this residue (Figure 4.5). There is no major difference between monomers A and B in terms of orientation of residues (Figure 4.6) or distances between the residues that make up the catalytic triad (Table 4.3). Therefore, the pictures were generated using monomer A only.

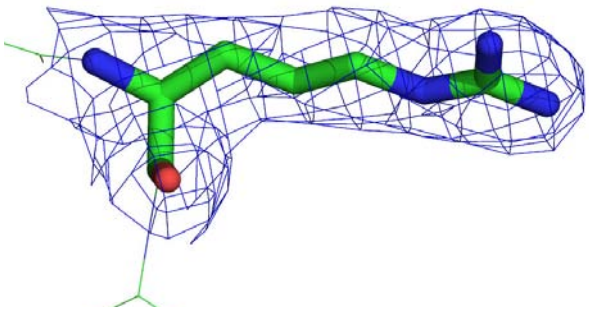

Figure 4.5 *Residue R161 of DHDPS-K161R covered by 2Fo-Fc electron density (blue), which is contoured at 1σ.*

Table 4.3 *Comparison of the distance between key groups within the active site of wild-type DHDPS and DHDPS-K161R.*

			Wild-type[a]	Monomer A DHDPS-K161A	Monomer B DHDPS-K161A
Protein distances (Å)	OH_Y133	NH_2_K161	2.9	-	-
	OH_Y133	CH_3_A161	-	3.4	3.5
	OH_Y133	OH_T44	2.6	3.3	3.4
	OH_T44	OH_Y107	2.6	2.7	2.5
	OH_Y133	OH_107	3.7	4.1	4.1
	OH_Y133	X	2.6	-	-
	N^{ε}_R138	X	3.2	-	-

[a] As reported by Dobson *et al.*[2]

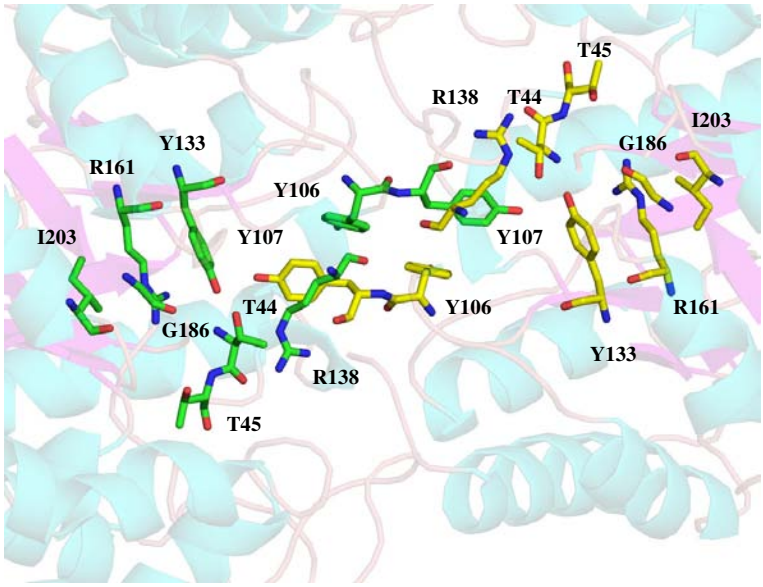

Figure 4.6 *Active site residues of monomer A (green) and monomer B (yellow) of DHDPS-K161R.*

The alignment of the asymmetric subunit containing monomers A and B of DHDPS-K161R and that of the wild-type enzyme resulted in a rmsd of 0.215 Å. There is little re-organisation of the side chains of the residues in the vicinity of the mutation (Figure 4.7). The side chain of R161 adopts a similar fully extended conformation to that of K161 in the wild-type enzyme. As in the structure of DHDPS-K161A, the aromatic ring of Y133 appears to be slightly twisted. T44 has also moved away from Y133 by about 0.5 Å and rotated by ~20^{o}, which results in a larger distance between the OH groups of Y133 and T44 in both monomers (Table 4.3). These changes are quite significant as the hydrogen bond between the hydroxyl groups of T44 and Y133, which are involved in moving protons in and out of the active site, is much weaker than in the wild-type enzyme. However, the hydroxyl group of Y107 is still positioned similarly and can interact with T44 *via* hydrogen bonds. The remaining residues in the active site are found in the same orientation as the wild-type enzyme (Figure 4.7). The water molecule (Figure 4.7, molecule X), which connects Y133 and R138 in the wild-type, is also missing in DHDPS-K161R.

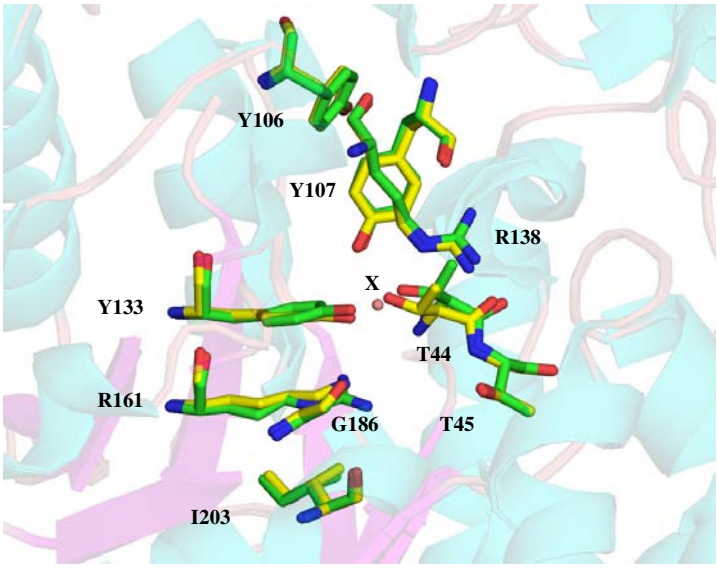

Figure 4.7 *Overlay of the active site of wild-type DHDPS (yellow) and DHDPS-K161R (green) from monomer A. X is a water molecule (pink) present in the wild-type structure only. Notice the small twist in orientation of the aromatic ring of Y133 and the movement and rotation of T44.*

4.7 Active site of DHDPS-K161A with pyruvate bound

In order to understand how pyruvate, which is no longer involved in Schiff base formation, is binding at the active site of DHDPS-K161A, X-ray data were collected from crystals of the protein co-crystallised with pyruvate. Pyruvate was found bound at the active site of both subunits, with an occupancy of 50% in subunit A (Figure 4.8) and 100% in subunit B. A comparison of the pyruvate-bound and pyruvate-free forms of DHDPS-K161A reveals that, after pyruvate binding, the structure of the enzyme remains predominantly as it was in the pyruvate-free form. Apart from a small rotation of T44 away from pyruvate upon binding, the remaining active site residues are in the same orientation, resulting in a rmsd for the asymmetric unit alignment of 0.176 Å (Figure 4.9).

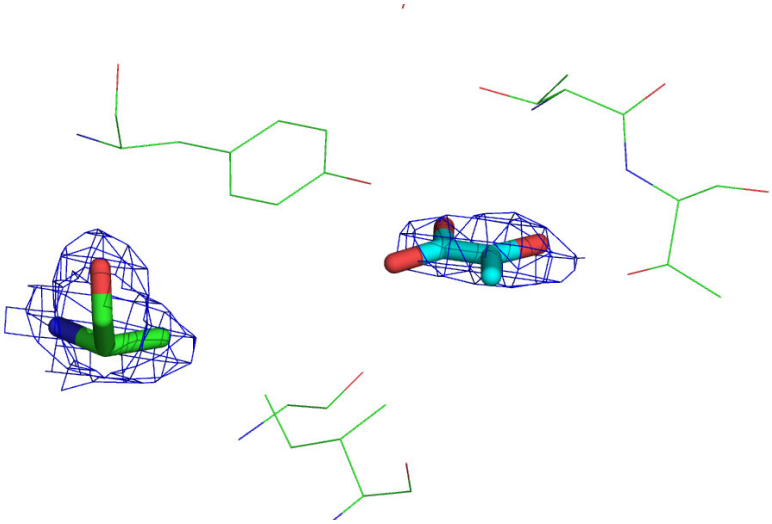

Figure 4.8 *2Fo-Fc electron density (blue) contoured at 1σ around pyruvate (cyan) and alanine at position 161 (bold and green) at the active site of monomer A of pyruvate-bound DHDPS-K161A. Note that the occupancy of pyruvate is 50%.*

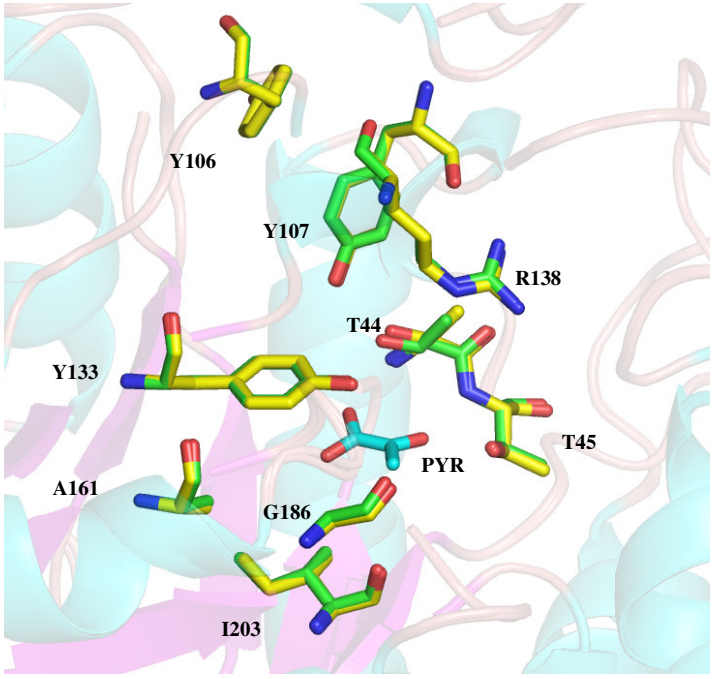

Figure 4.9 Overlay of the monomer A active site of DHDPS-K161A (green) and pyruvate-bound DHDPS-K161A (yellow). Pyruvate (PYR) is shown in cyan.

4.8 Comparison of the active site of wild-type DHDPS and DHDPS-K161A with pyruvate bound

The alignment of the asymmetric unit of wild-type and DHDPS-K161A, both obtained in the presence of pyruvate, resulted in a rmsd of 0.187 Å. The structure of the pyruvate-bound DHDPS-K161A reveals that the free pyruvate has rotated ~90^{o} clockwise from where it is found in the wild-type enzyme as part of a Schiff base (Figure 4.10). The connections that pyruvate makes to the active site of DHDPS-K161A are shown in Table 4.4.

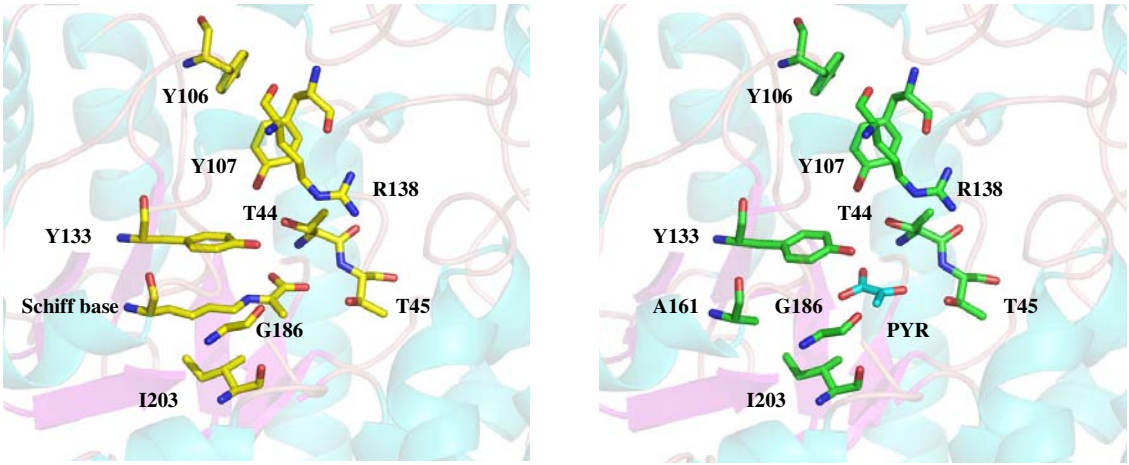

Figure 4.10 *Comparison of the monomer A active site residues of wild-type DHDPS (yellow) and DHDPS-K161A (green) in the presence of pyruvate (PYR), which is shown either as part of a Schiff base or in cyan.*

Table 4.4 *Connections and distances between pyruvate and DHDPS-K161A.*

Pyruvate	Residue	Distance (Å)
O1	OG1_T45	2.7
O1	N_T44	3.3
O2	OG1_Y133	4.1
O2	N$^{\varepsilon}$_T45	3.0
O3	-	-

In the wild-type enzyme, O1 is covalently bound to the amino group of K161 to form the Schiff base. In the structure of DHDPS-K161A, the pyruvate molecule has adopted a different orientation, where O1 is now oriented towards T44 and T45, allowing stabilisation by hydrogen bonds to the backbone amino group of T44 (3.3 Å) and to the hydroxyl group of T45 (2.7 Å) (Table 4.4).

In the wild-type enzyme, the O2 and O3 atoms of the carboxylate group of the bound pyruvate are oriented toward Y133 (3.3 Å), T44 (2.8 Å) and T45 (2.8 Å). In this mutant, the O2 atom is still facing T45 (3.0 Å) but it is too far away from the hydroxyl group OG1_Y133 to enable the formation of any hydrogen bonds. The O3 atom of pyruvate is now oriented towards the hydrophobic cavity where K161 is usually located and it is not in close proximity to any residue or solvent to make hydrogen bond contacts. It is likely that this oxygen is protonated. Interestingly, the methyl carbon retains approximately the same spatial positioning as in the wild-type enzyme. Figure 4.11 shows all the stabilising connections pyruvate makes to the active site residues of DHDPS-K161A.

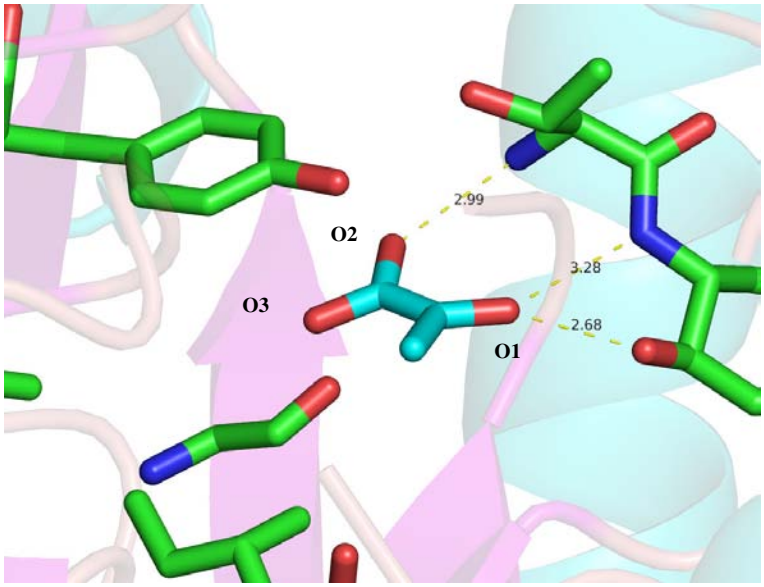

Figure 4.11 *Hydrogen bonds stabilising pyruvate (cyan) bound at the active site of monomer A of DHDPS-K161A.*

4.9 Active site of DHDPS-K161R with pyruvate bound

The active sites of both subunits A and B show bound pyruvate molecules, with occupancy of 70% in both cases (Figure 4.12). The overlay of the pyruvate-bound and pyruvate-free forms of DHDPS-K161R reveals that, apart from a rotation of the loop bearing T44 away from pyruvate upon binding, the remaining active site residues are in the same orientation as in the pyruvate-free form of the enzyme, resulting in a rmsd for the asymmetric unit alignment of 0.168 Å (Figure 4.13).

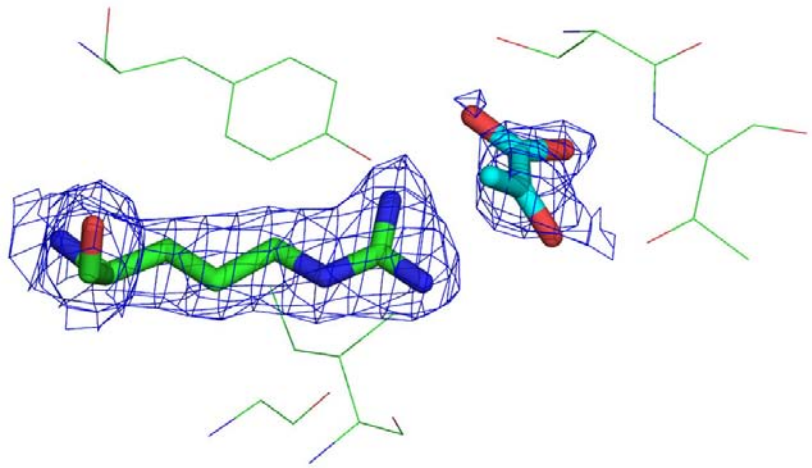

Figure 4.12 *2Fo-Fc electron density (blue) contoured at 1σ around pyruvate (cyan) and arginine at position 161 (bold and green) at the active site of monomer A of DHDPS-K161R. Note that the occupancy of pyruvate is 70%.*

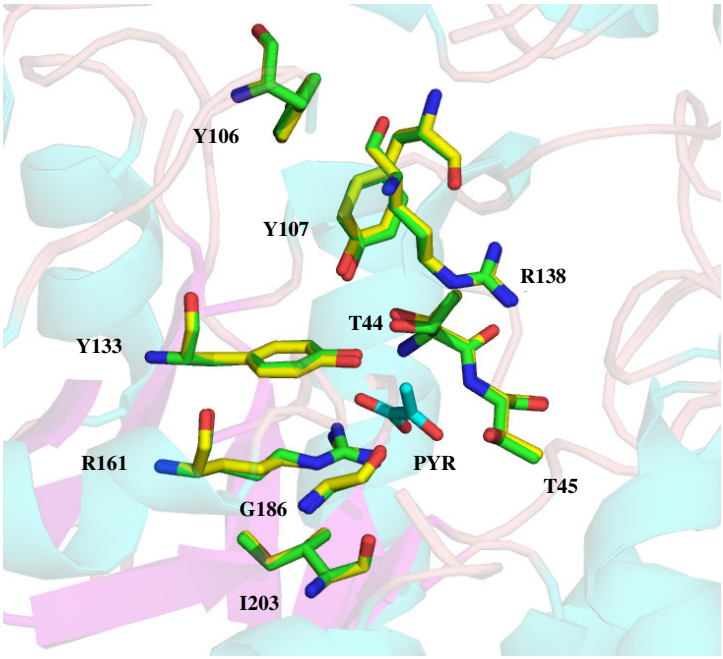

Figure 4.13 *Overlay of the active site residues of DHDPS-K161R (green) and pyruvate-bound DHDPS-K161R (yellow) from monomer A. Pyruvate (PYR) is shown in cyan.*

4.10 Comparison of the active site of wild-type DHDPS and DHDPS-K161R with pyruvate bound

The pyruvate bound at each active site of DHDPS-K161R has rotated ~30^{o} clockwise from where it binds in DHDPS-K161A. The connections that the pyruvate makes to the active site of this mutant enzyme are shown in Table 4.5.

Table 4.5 *Connections and distances between pyruvate and DHDPS-K161R.*

Pyruvate	Residue	Distance (Å)
O1	OG1_T45	2.1
O1	NH_2_R161	3.3
O2	N_T44	3.1
O3	N^{ε}_T45	3.0

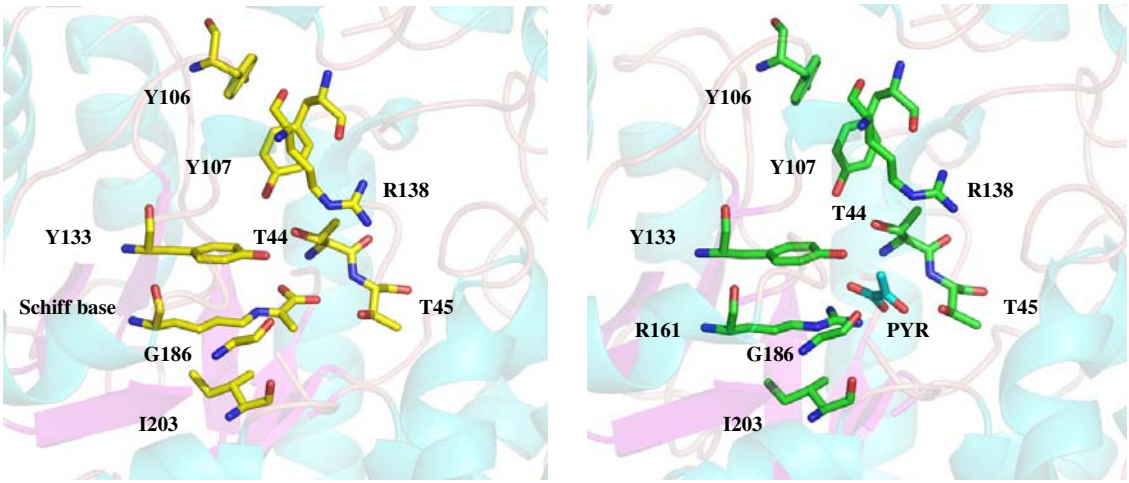

Figure 4.14 *Comparison of the active sites of wild-type DHDPS (yellow) and DHDPS-K161R (green) from monomer A in the presence of pyruvate (PYR), which is either shown as part of the Schiff base or in blue.*

The O1 atom is now closer to the hydroxyl group of T45 (2.1 Å) than in the other mutant structure (2.7 Å), allowing stronger hydrogen bonds to be formed. O1 also makes a strong electrostatic interaction with the positively charged amino group of the arginine residue introduced at position 161, which is 3.3 Å away. The short distance of pyruvate O1 to OG1_T45 and the rather long distance to NH_2_R161 could be an artifact of the very strong planarity restraints placed on the pyruvate molecule. A small twist about C1-C2 would lead to a distance of ~2.6 Å to T45.

O2 of the carboxylate group is stabilised by the amino group on the side chain of residue T44 (3.1 Å). O3 is the same distance from the backbone amino group of T45 (3.0 Å) as O2 is in DHDPS-K161A. The methyl group on pyruvate is facing the hydrophobic cavity between R161 and Y133. Figure 4.15 shows all the stabilising connections pyruvate makes to the active site residues of DHDPS-K161R.

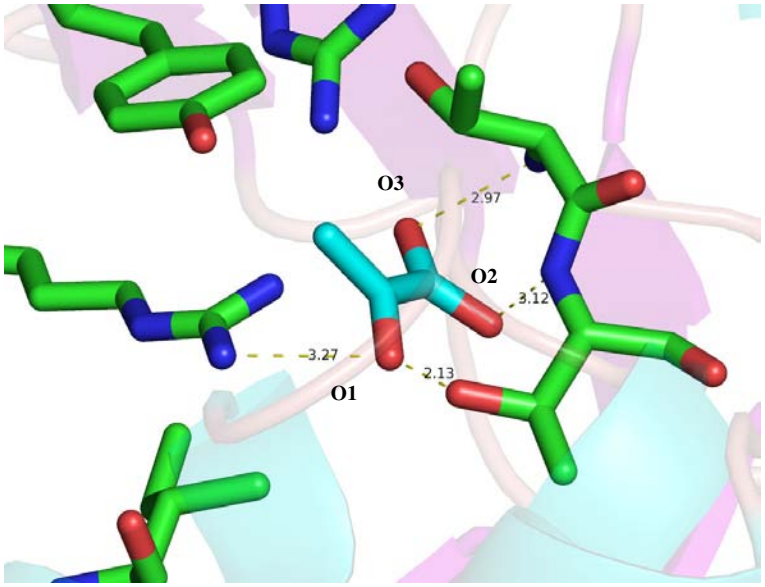

Figure 4.15 *Hydrogen bonds stabilising pyruvate (cyan) bound at the active site of monomer A of DHDPS-K161R.*

4.11 Lysine binding site of DHDPS-K161A and DHDPS-K161R

Structurally, the allosteric binding site of both mutants is identical to that of the wild-type enzyme (Figure 4.14). Y107 is still solvent accessible to bulk solvent through a number of hydrogen bonds to well ordered water molecules leading to the lysine binding site. The distance between these water molecules in both mutant enzymes is no more than 3.0 Å.

The aromatic stack formed by Y106 and the Y107 residue from the other monomer, which links both active sites to the allosteric binding site, remains intact. It would be expected that lysine would bind in a very similar manner to DHDPS-K161A and DHDPS-K161R, as observed for wild-type DHDPS. This is entirely consistent with the kinetic data obtained in Chapter three.

A **B**

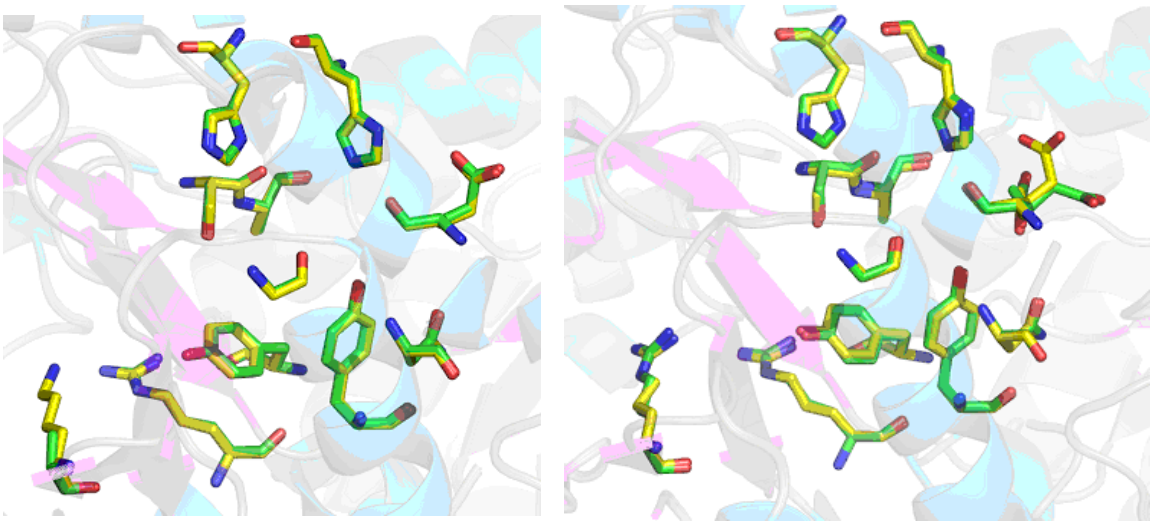

Figure 4.14 ***A*** *Overlay of the lysine binding site of wild-type DHDPS (yellow) and DHDPS-K161A (green) from monomer A;* ***B*** *Overlay of the lysine binding site of wild-type DHDPS (yellow) and DHDPS-K161R (green) from monomer A.*

4.12 Summary

The X-ray crystal structures of both DHDPS-K161A and DHDPS-K161R were solved to resolutions of 2.0 and 2.4 Å respectively, and they were compared to the structure of the wild-type enzyme solved by Dobson *et al.* (2005).[2] There were no significant changes in the tertiary or quaternary structures, including the catalytic and regulatory motifs, upon the introduction of the mutations. The mutant enzymes belonged to the same space group as the wild-type, $P3_121$, with very similar cell dimensions. This observation confirms that the attenuated catalytic activity of the mutant enzymes generated was not due to alterations in their structure but due to the absence of the Schiff base-forming residue, lysine 161.

The crystal structures of the mutants were also solved with pyruvate bound to resolutions of 2.3 and 2.1 Å for DHDPS-K161A and DHDPS-K161R respectively. These ligated structures confirm the inability of the mutant enzymes to form a Schiff base. Free

pyruvate is found bound at the active site of both subunits in each enzyme, where it can be stabilised by surrounding residues. The allosteric site remains intact for DHDPS-K161A and DHDPS-K161R.

4.13 References

1. Fersht, A. R., *Structure and mechanism in protein science - a guide to enzyme catalysis and protein folding*. Freeman & Co: New York, 1999.
2. Dobson, R. C.; Griffin, M. D.; Jameson, G. B.; Gerrard, J. A., The crystal structures of native and (*S*)-lysine-bound dihydrodipicolinate synthase from *Escherichia coli* with improved resolution show new features of biological significance. *Acta Crystallographica Section D-Biological Crystallography* **2005,** 61, (Pt 8), 1116-1124.
3. Mirwaldt, C.; Korndorfer, I.; Huber, R., The crystal structure of dihydrodipicolinate synthase from *Escherichia coli* at 2.5 Å resolution. *Journal of Molecular Biology* **1995,** 246, (1), 227-239.
4. Pflugrath, J. W., The finer things in X-ray diffraction data collection. *Acta Crystallographica Section D-Biological Crystallography* **1999,** 55, 1718-1725.
5. CCP4, The CCP4 suite: programs for protein crystallography. *Acta Crystallographica Section D-Biological Crystallography* **1994,** D50, 760-763.
6. Laskowsky, R.; MacArthur, M.; Thornton, D., *PROCHECK*: a program to check the stereochemical quality of protein structures. *Journal of Applied Crystallography* **1993,** 26, 283-291.
7. Emsley, P.; Cowtan, K., Coot: model-rebuilding tools for molecular graphics. *Acta Crystallographica Section D-Biological Crystallography* **2004,** 60, 2126-2132.
8. Blickling, S.; Renner, C.; Laber, B.; Pohlenz, H. D.; Holak, T. A.; Huber, R., Reaction mechanism of *Escherichia coli* dihydrodipicolinate synthase

investigated by X-ray crystallography and NMR spectroscopy. *Biochemistry* **1997,** 36, (1), 24-33.

9. Dobson, R. C.; Devenish, S. R.; Turner, L. A.; Clifford, V. R.; Pearce, F. G.; Jameson, G. B.; Gerrard, J. A., Role of arginine 138 in the catalysis and regulation of *Escherichia coli* dihydrodipicolinate synthase. *Biochemistry* **2005,** 44, (39), 13007-13013.
10. Rachamandran, G.; Sasisekharan, V., Conformation of polypeptides and proteins. *Advances in Protein Chemistry* **1986,** 23, 283-437.
11. Dobson, R. C. Investigating the catalytic and regulatory mechanism of dihydropicolinate synthase. D. Phil. Thesis. University of Canterbury, 2003.
12. DeLano, W. L. *The PyMOL Molecular Graphics System.* DeLano Scientific: San Carlos, 2002.

Chapter Five

Discussion and conclusions

5.1 Introduction

DHDPS catalyses the first reaction unique to lysine biosynthesis, the condensation of (*S*)-ASA with pyruvate to form an unstable heterocyclic molecule, currently believed to be HTPA, *via* a ping-pong mechanism. The major hallmark of this mechanism is the formation of a Schiff base intermediate between lysine 161 and the first substrate, pyruvate. Although lysine 161 is thought to be the key active site residue in DHDPS, no-one had yet confirmed this using a site-directed mutagenesis approach. This is probably because it was predicted that the enzyme would lose all of its activity upon removal of this residue.

The aim of this thesis, as set out in Chapter one, has been to test the assumption that lysine 161 is absolutely essential for catalysis by DHDPS. This project was undertaken in light of results published by Kruger *et al.* (2001)[1] on a mechanistically and structurally related enzyme, NAL, where the mutation of the equivalent residue to an alanine completely abolished enzyme activity.

This chapter will discuss the kinetic and structural work presented in Chapters three and four and propose a new mechanism for catalysis by DHDPS deprived of lysine 161. The results obtained also hint at the evolutionary relationship between DHDPS and NAL.

5.2 Significant decrease in catalytic activity for mutants

The kinetic results presented in Chapter three showed that the catalytic activity of both mutants was dramatically decreased when compared to the wild-type enzyme. The k_{cat} values were decreased by 300–800-fold upon the introduction of an alanine or arginine at position 161. These results confirm the importance of lysine 161 in the catalytic mechanism of DHDPS. However, the detection of rate enhancements compared to the background rate (section 2.5) was unexpected.

The crystal structures of these mutants revealed, firstly, that the desired mutations were introduced, and secondly, that no significant changes in the arrangement of the active site had occurred. CD spectroscopy showed that the mutations introduced did not alter the secondary structure of the mutant enzymes in solution compared to wild-type DHDPS. Hence, the dramatic decrease in activity was due to the removal of the Schiff base-forming residue and not due to gross alterations in the structure of the mutant enzymes.

As mentioned earlier, the mutation of the corresponding lysine residue in NAL to an alanine completely abolished activity of the enzyme.[1] However, the NAL arginine mutant still retained 3% activity. It was proposed that residual activity could be detected because the guanidinium group of arginine should still allow the formation of the Schiff base, but at a much slower rate than with the amino group of lysine 161. Although arginine has been shown to allow Schiff base formation by Morris *et al.* (1996)[2] using sodium borohydride to trap this intermediate, no experimental work was conducted by Kruger *et al.* (2001)[1] to confirm this proposal.

In this work, treatment of DHDPS-K161A and DHDPS-K161R with the reducing agent sodium borohydride and pyruvate did not result in enzyme inactivation, indicating that the Schiff base is not formed with either mutant. The crystal structure of the mutant enzymes in the presence of pyruvate further confirmed their inability to form a Schiff base. Therefore, the activity detected in the DHDPS mutants cannot be attributed to the formation of the covalent intermediate.

5.3 Binding affinities with substrates

Surprisingly, the mutations did not have a major impact on the ability of the enzyme to bind its substrates as judged by the kinetic parameters. The $K_{mPyruvate}$ values (0.45±0.04 mM for DHDPS-K161A and 0.57±0.06 mM for DHDPS-K161R) increased by only 3-fold compared to the wild-type enzyme (0.15±0.01 mM). An increase in the Michaelis-Menten constants with respect to pyruvate was expected since this substrate is no longer involved in Schiff base formation. However, the magnitude of the increase was much lower than expected for both enzymes. This indicates that other active site residues apart from K161 are involved in the initial binding of this substrate, which is observed in the crystal contacts made in the wild-type enzyme.

The K_{mASA} value for DHDPS-K161R was identical to that of the wild-type enzyme (0.12±0.01 mM), while for the alanine mutant, there was only a 2-fold increase (0.23±0.02 mM). This observation agrees with the current proposed mechanism of DHDPS, where K161 plays no role in (*S*)-ASA binding. Assuming that the hydrate of (*S*)-ASA is the relevant species, Y133 is in position to protonate one of the hydroxyl groups after the dehydration reaction, while G186 is in position to coordinate the other one. The catalytic triad is involved in the stabilisation of the tyrosine anion *via* a proton relay to bulk solvent.[3,4]

5.4 Subtle shift in kinetic mechanism

The statistical values obtained from both the ping-pong and the ternary-complex models were very similar for both DHDPS-K161A and DHDPS-K161R. Based on the *F*-value and *p*-value for each fit, it was decided that the ternary-complex mechanism gave a slightly better fit than the classical wild-type ping-pong mechanism. In the ping-pong mechanism, the substrates bind in a defined order *via* a covalently bound enzyme-substrate intermediate and two independent products are released.[5] In the case of wild-

type DHDPS, water is released as the first product of the reaction mechanism upon formation of the enamine, before (*S*)-ASA can bind.

For the mutants generated in this work, both substrates can be present simultaneously at the active site prior to product formation. This is not surprising since these enzymes are unable to form a Schiff base and consequently, unable to release water as the first product.

5.5 Schiff base enhances stability of wild-type DHDPS

It has been suggested that DHDPS is stabilised by its first substrate, pyruvate.[6] This anecdotal observation was confirmed during this work using differential scanning fluorimetry. The addition of saturating concentrations of pyruvate to wild-type DHDPS resulted in a 9.9^{o}C increase in the melting temperature (T_m). This increase in stability was hypothesised to be attributed to a tighter protein packing upon the formation of the Schiff base.

The T_m values of the mutants with pyruvate only increased by ~2^{o}C, showing that the stabilisation of DHDPS by pyruvate is largely, but not entirely, dependent on Schiff base formation. This is further confirmed by an increase in the *B*-values from the crystal structures upon binding of pyruvate in both DHDPS-K161A (31.53 Å^2 compared to 34.21 Å^2 in the presence of pyruvate) and DHDPS-K161R (28.54 Å^2 compared to 30.89 Å^2). The mean *B*-value for wild-type DHDPS in the presence of pyruvate remains exactly the same as in the pyruvate-free form (19.9 Å^2). However, the lower resolutions of the crystal structures obtained in this work, compared to that of the wild-type enzyme, could account for some of the differences in the *B*-values.

5.6 Lysine 161 is not involved in the regulatory mechanism

Evidence from kinetic and structural studies have supported the idea that lysine is an allosteric inhibitor of wild-type DHDPS;[3,7-9] however, the exact mechanism by which lysine exerts its regulatory effect is still open to debate.

Both DHDPS-K161A and DHDPS-K161R showed very similar behaviour in relation to lysine sensitivity when compared to the wild-type: at saturating concentrations of the inhibitor, the mutant enzymes were still 7-10% active and they displayed the same type of inhibition. There was also little change in their K_i values. The structure of the lysine binding site of the mutants is identical to that of the wild-type. The aromatic stack formed by Y106 and the Y107 residue from the other monomer, which links both active sites to the allosteric binding site, remains intact. It would be expected that lysine would bind in a very similar manner to DHDPS-K161A and DHDPS-K161R as observed for wild-type DHDPS. It is clear from the kinetic and structural studies presented in this work that lysine 161 is not involved in the regulatory mechanism of DHDPS.

5.7 Binding of pyruvate

The mutation of the nucleophilic lysine 161 residue had significant consequences for DHDPS activity by precluding the formation of the covalent intermediate, which is an important step in the catalytic mechanism. Nevertheless, the detection of residual activity suggests that pyruvate is still binding and interacting with other residues, since considerable rate enhancement compared to the background rate is observed when (*S*)-ASA and pyruvate are mixed together in the presence of both K161 mutant enzymes. This emphasises the idea that enzymes lacking key catalytic groups are still good catalysts.[10] Similar residual activities were observed when Y133 and T44, which are part of the catalytic triad of DHDPS, were mutated to a phenylalanine and a valine respectively.[4] The slight increase in stability of the mutant enzymes upon addition of

pyruvate observed in the DSF experiments also demonstrates that pyruvate is still binding to these enzymes, despite their inability to form a Schiff base.

The structure of DHDPS-K161A and DHDPS-K161R that had been co-crystallised with pyruvate revealed that one free pyruvate molecule binds at each active site of both enzymes. Obviously, the position of the pyruvate molecules is different from that found in the wild-type enzyme, since this substrate is no longer part of a Schiff base. Nevertheless, each enzyme still retained a well defined binding site for pyruvate that is not dependent on lysine 161. The structure of the pyruvate-bound DHDPS-K161A reveals that the free pyruvate has rotated ~90^{o} clockwise from its orientation in the wild-type enzyme. Pyruvate is located near the amide N_T44, N$^{\varepsilon}$_T45 and the hydroxyl group OG1_T45, at hydrogen-bonding distances of 3.3 Å, 3.0 Å and 2.7 Å, respectively. The pyruvate is bound at each active site of DHDPS-K161R in a slightly different orientation from where it binds in DHDPS-K161A. However, pyruvate is still stabilised by the same groups: N_T44 (3.1 Å), N$^{\varepsilon}$_T45 (3.0 Å) and OG1_T45 (2.1 Å). In addition, it makes a strong electrostatic interaction with the positively charged guanidinium group of the arginine residue introduced at position 161, which is 3.3 Å away. This additional electrostatic interaction could explain why the arginine mutant was found to have a slightly higher catalytic activity than the alanine mutant.

A comparison of the pyruvate-bound and pyruvate-free forms of the mutant enzymes reveals that, after pyruvate binding, the active site residues remain predominantly as they were in the pyruvate-free form. The main change observed is the small movement of the loop bearing T44 away from pyruvate upon binding in both enzymes, which is also observed in the wild-type enzyme. The lack of heat production associated with the binding of pyruvate to the mutant enzymes observed in the ITC experiments is consistent with the lack of conformational change upon pyruvate binding. Pyruvate is held at the active site in the mutant enzymes through favourable electrostatic interactions, which are much weaker than the covalent bond that is formed in the wild-type enzyme. It is likely that the energy released when pyruvate binds is offset by the energy required to move solvent molecules out of the active site in order to accommodate this substrate.

5.8 Alternative mechanism

The existence of a covalent intermediate between pyruvate and the active site lysine 161 residue has been shown by trapping the intermediate with sodium borohydride,[11] by electrospray ionisation mass spectrometry,[12] and by X-ray crystallography.[3] However, site-directed mutagenesis had not been employed to confirm this. It can be concluded from the kinetic and structural data gathered for DHDPS-K161A and DHDPS-K161R, that although lysine 161 is important for catalysis, it is not absolutely essential. The current proposed catalytic mechanism must therefore be reconsidered and expanded.

There are a number of mechanisms that can be employed by enzymes to lower the free energy of activation of a reaction. Such mechanisms include electrostatic and geometric complementarity to the transition state in order to reduce the enthalpy of transition state formation, and the use of binding energy for precise positioning of the substrates for lowering the entropy of activation.[13] It has been shown that by simply bringing substrates together and correctly positioning two reactants in an enzyme active site, a rate enhancement of up to 10^8-fold compared to 1 M reactants in free solution can be achieved.[14]

It is hard to understand how an enzyme that employs a ping-pong mechanism can still function without its catalytic nucleophile. This is because a ping-pong mechanism implies that the first half of the reaction, which in this case involves pyruvate binding and Schiff base formation, must be completed before the binding of the second substrate. Thus, an enzyme variant lacking a nucleophile necessary for its original activity may catalyse a different chemical transformation by using a mechanism that had previously been superseded by the nucleophilic attack on the substrate.[15]

In the current proposed mechanism, the tautomerisation of the Schiff base to an enamine species creates the nucleophile that attacks (*S*)-ASA. This is followed by cyclisation, which leads to the release of HTPA from the active site (Figure 1.3). Since the Schiff

base is no longer being formed with these mutant enzymes, another nucleophilic species must be present that can still react with the second substrate.

Here, it is proposed that the enol form of pyruvate, which exists in equilibrium with its keto tautomer, can fulfill the role of the enamine species (Figure 5.1). Enols are the oxygen analogues of enamines, but their formation from ketones is less thermodynamically favourable than enamine formation from Schiff bases.[16] NMR studies from Chapter three suggest that the rate of enolisation of the keto form of pyruvate to its enol tautomer is unchanged in DHDPS-K161A and DHDPS-K161R catalysed mechanism, ruling out the possibility that the enolisation process could be the rate-determining step. ITC experiments show that in the absence of Schiff base formation, enthalpic contributions may not be responsible for the observed enzymatically accelerated reaction of these two substrates as no measurable binding event occurs between the mutant enzymes and pyruvate. It is likely that substrate orientation and favourable charge interactions may facilitate interaction of an active site bound pyruvate with (*S*)-ASA and may be the major catalytic devices operating in DHDPS-K161A and DHDPS-K161R. Future work should investigate this mechanism further, perhaps using labelled substrates and monitoring kinetic isotope effects to explore the rate-determining step.

It is proposed that for DHDPS-K161A and DHDPS-K161R, the oxygen atom on the enol is stabilised by the hydrogen bond contact it makes with the hydroxyl group of T45 in both enzymes. The carboxylate is stabilised primarily by the backbone amino group of T44. The binding of (*S*)-ASA and subsequent cyclisation and product release is proposed to occur in exactly the same fashion as in wild-type DHDPS. Y133 in both DHDPS-K161A and DHDPS-K161R are in a similar position as in the wild-type enzyme, despite being slightly twisted. This allows this residue to still be able to protonate one of the hydroxyl groups of (*S*)-ASA, while G186, whose position is in both mutant enzymes is exactly the same as in wild-type DHDPS, can still coordinate to the other hydroxyl group.

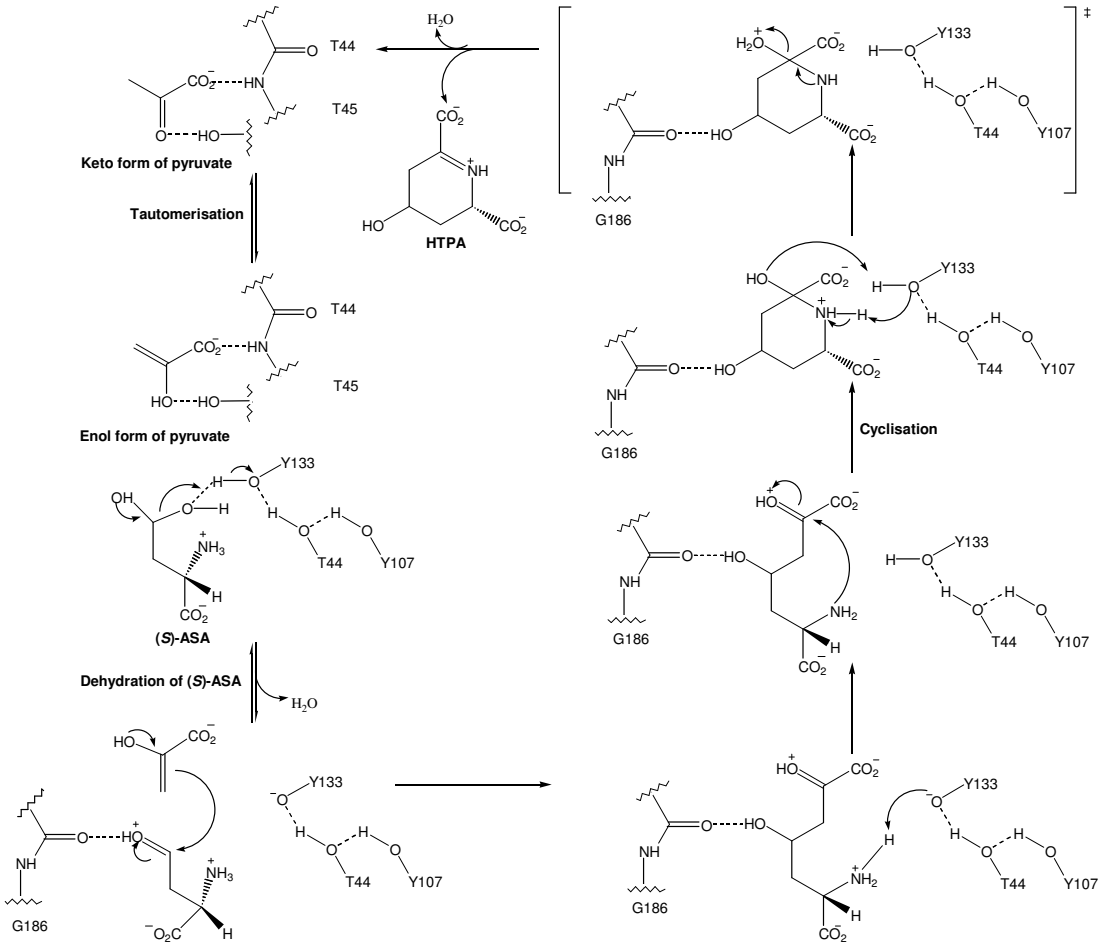

Figure 5.1 *Proposed mechanism for how DHDPS lacking lysine 161 catalyses the condensation reaction between (*S*)-ASA and pyruvate to form HTPA.*

The crystal structures showed that T44 moved away from Y133 in both mutant enzymes, resulting in a larger distance (an increase of ~0.6 Å) between the OH groups of Y133 and T44. The distance, however, is still small enough to allow the formation of a hydrogen bond between the hydroxyl groups of these residues, which are involved in moving protons in and out of the active site. The hydroxyl group of Y107 is still positioned similarly in both mutant enzymes and can interact with T44 *via* hydrogen bonds. So it is likely that the catalytic triad is still operating in DHDPS-K161A and DHDPS-K161R by stabilising the tyrosine anion *via* a proton relay to bulk-solvent. Y133 is also still believed

to be involved in coordinating the attacking amine group in this alternative mechanism, which facilitates cyclisation and product release.

The ternary-complex mechanism can operate in an ordered or random fashion in terms of substrate binding.[5] Unfortunately, this can not be determined by looking at the kinetic data alone. So even though the scheme outlined in Figure 5.1 shows pyruvate binding at the active site first, it is possible that (*S*)-ASA is the first substrate to bind.

The detection of residual activity in site-directed mutants of enzymes from other families, which lack their key active site residue, has been observed in many cases[14,17-19] This suggests that it is not uncommon for enzymes to use more than one mechanism to enhance their rate of reactions. Removal of the Schiff base-forming residue in DHDPS could not impede catalysis completely because of the existence of a 'back-up' mechanism, in which lysine 161 plays no part. This 'back-up' mechanism seems not to be present in the NAL enzyme, where mutation of the equivalent residue to an alanine abolished all activity.

5.9 Evolutionary relationship between DHDPS and NAL

DHDPS belongs to a sub-family of the $(\alpha/\beta)_8$ proteins, whose members also include NAL, *trans-o*-hydroxybenzylidenepyruvate hydratase-aldolase (HBPHA), D-5-keto-4-deoxyglucarate dehydratase (DOGDH), *trans*-2'-carboxybenzalpyruvate hydratase-aldolase (CBPHA) and D-2-keto-3-deoxygluconate aldolases (KDGA). The MosA protein is also thought to belong to this sub-family.[20] These enzymes all share common structural features but they catalyse different reactions on separate biochemical pathways.[21] It has been proposed that these enzymes share a unifying step in their reaction pathway, namely the Schiff base formation between a strictly conserved lysine residue and the C2 carbon of the common α-keto acid moiety of the substrate.[20]

Out of the seven members, only DHDPS and NAL have been well-characterised in terms of function and structure. The crystal structures of both of these enzymes have been determined for a range of organisms.[3,20,22-24] NAL and DHDPS show the hallmarks of an enzyme sub-family: a low level of sequence identity (<24% between the two *E. coli* enzymes), but a similar fold with similar active site architecture.[25] In particular, sequence alignments indicates that the Schiff base-forming residue (K161), as well as the other active site residues (T44, T45, Y133, G186, Y107 and I203), have the same spatial positioning. This led to the conclusion that the mechanism of Schiff base formation and the subsequent aldol reaction is likely to be conserved in both enzymes.[3]

The results in this thesis give further insights into the evolutionary relationship between NAL and DHDPS. The NAL-K161A enzyme was completely inactive but the DHDPS-K161A enzyme still retains some activity. Based on these results and the central metabolic role of DHDPS, it is reasonable to speculate that DHDPS evolved before NAL. The ancestral form of DHDPS probably lacked the lysine 161 residue and performed catalysis through the alternative mechanism proposed in this thesis, where orientation and non-covalent substrate binding are major catalytic devices (Figure 5.2). On the other hand, NAL activity evolved after the appearance of the Schiff base-forming residue, which facilitates catalysis because it is more nucleophilic than the enol form of pyruvate. These results may thus provide fresh insights into the mechanism and evolution of enzymatic activities of other class I aldolases.

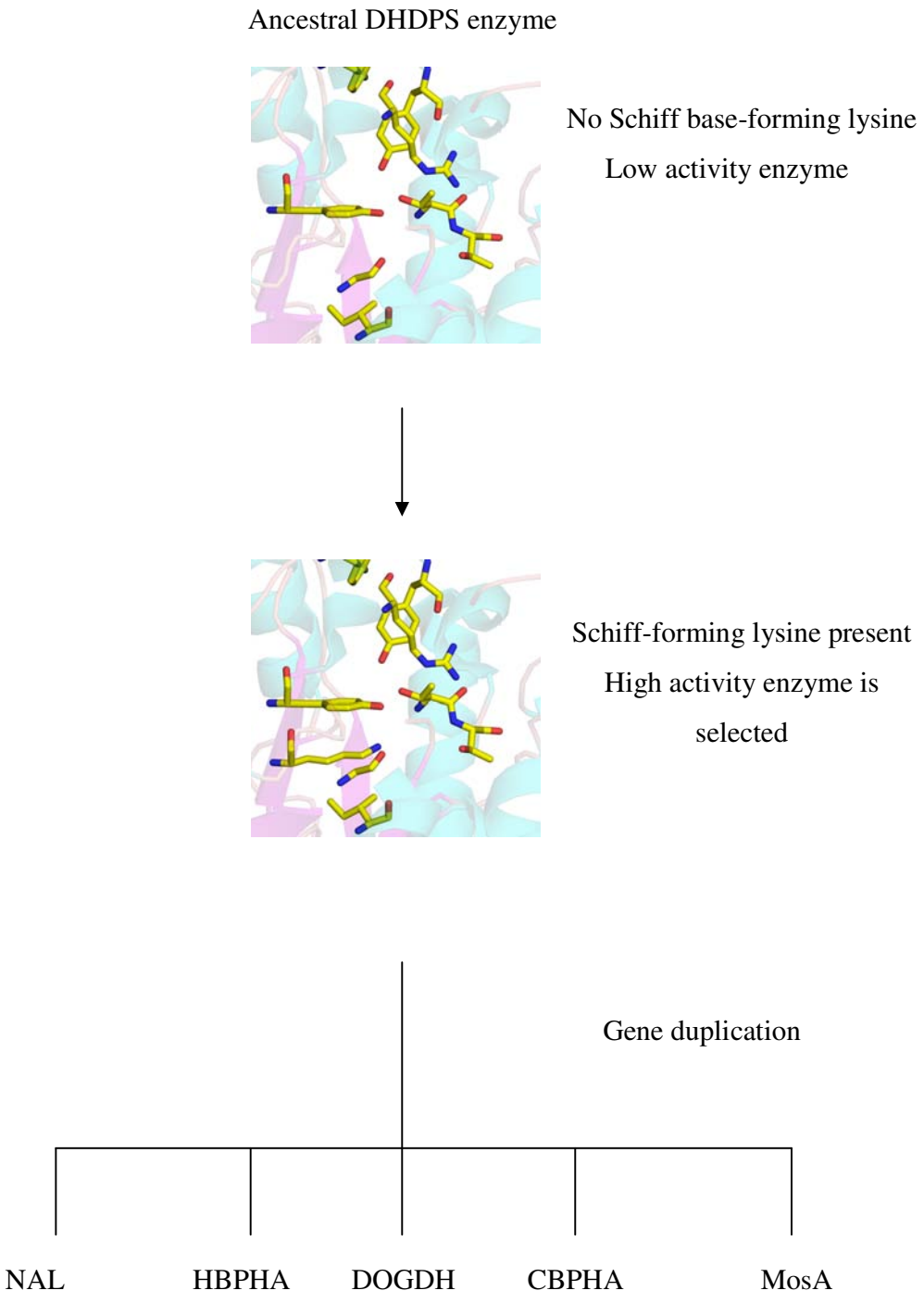

Figure 5.2 *Proposed evolution of enzymatic activity in the DHDPS sub-family.*

5.10 Summary

Site-directed mutagenesis confirmed the involvement of lysine 161 in DHDPS Schiff base formation. Nevertheless, the mutant enzymes still displayed residual activities, implying that Schiff base formation is not absolutely essential for DHDPS activity. DHDPS deprived of lysine 161 can still catalyse the condensation reaction between (*S*)-ASA and pyruvate, using orientation and proximity as major catalytic devices. Such results underscore the sophistication of enzyme catalysis and the functional plasticity of enzyme active sites.

5.11 References

1. Kruger, D.; Schauer, R.; Traving, C., Characterization and mutagenesis of the recombinant *N*-acetylneuraminate lyase from *Clostridium perfringens* - insights into the reaction mechanism. *European Journal of Biochemistry* **2001,** 268, (13), 3831-3839.
2. Morris, A.; Davenport, R. C.; Tolan, D. R., A lysine to arginine substitution at position 146 of rabbit aldolase changes the rate-determining step to Schiff base formation. *Protein Engineering* **1996,** 9, (1), 61-67.
3. Blickling, S.; Renner, C.; Laber, B.; Pohlenz, H. D.; Holak, T. A.; Huber, R., Reaction mechanism of *Escherichia coli* dihydrodipicolinate synthase investigated by X-ray crystallography and NMR spectroscopy. *Biochemistry* **1997,** 36, (1), 24-33.
4. Dobson, R. C. Investigating the catalytic and regulatory mechanism of dihydropicolinate synthase. D. Phil. Thesis. University of Canterbury, 2003.
5. Cornish-Bowden, A., *Fundamentals of enzyme kinetics*. Portland Press: London, 1999.
6. Griffin, M. D. Why is dihydrodipicolinate synthase a tetramer? D. Phil. Thesis. University of Canterbury, 2005.

7. Yugari, Y.; Gilvarg, C., The condensation step in diaminopimelate synthesis. *Journal of Biological Chemistry* **1965,** 240, 4710-4716.
8. Laber, B.; Gomis-Ruth, F. X.; Romao, M. J.; Huber, R., *Escherichia coli* dihydrodipicolinate synthase. Identification of the active site and crystallization. *Biochemistry Journal* **1992,** 288, (Pt 2), 691-695.
9. Blickling, S.; Knablein, J., Feedback inhibition of dihydrodipicolinate synthase enzymes by *L*-lysine. *Biological Chemistry* **1997,** 378, (3-4), 207-210.
10. Fersht, A. R., *Structure and mechanism in protein science - a guide to enzyme catalysis and protein folding*. Freeman & Co: New York, 1999.
11. Shedlarski, J. G.; Gilvarg, C., The pyruvate-aspartic semialdehyde condensing enzyme of *Escherichia coli*. *Journal of Biological Chemistry* **1970,** 245, 1362-1373.
12. Borthwick, E. B.; Connell, S. J.; Tudor, D. W.; Robins, D. J.; Shneier, A.; Abell, C.; Coggins, J. R., *Escherichia coli* dihydrodipicolinate synthase: characterization of the imine intermediate and the product of bromopyruvate treatment by electrospray mass spectrometry. *Biochemistry Journal* **1995,** 305, (Pt 2), 521-524.
13. Kraut, D. A.; Carroll, K. S.; Herschlag, D., Challenges in enzyme mechanism and energetics. *Annual Review of Biochemistry* **2003,** 72, 517-571.
14. Peracchi, A., Enzyme catalysis: removing chemically 'essential' residues by site-directed mutagenesis. *Trends in Biochemical Sciences* **2001,** 26, (8), 497-503.
15. Toscano, M. D.; Woycechowsky, K. J.; Hilvert, D., Minimalist active-site redesign: teaching old enzymes new tricks. *Angewandte Chemie International Edition* **2007,** 46, 3212-3236.
16. Page, M.; Williams, A., *Organic & Bio-organic Mechanisms*. Addison Wesley Longman: London, 1997.
17. Mitchell, L. W.; Volin, M.; Martins, J.; Jaffe, E. K., Mechanistic implications of mutations to the active site lysine of porphobilinogen synthase. *Journal of Biological Chemistry* **2001,** 276, (2), 1538-1544.
18. Schorken, U.; Thorell, S.; Schurmann, M.; Jia, J.; Sprenger, G. A.; Schneider, G., Identification of catalytically important residues in the active site of *Escherichia coli* transaldolase. *European Journal of Biochemistry* **2001,** 268, 2408-2415.

19. Reither, S.; Li, F.; Gowher, H.; Jeltsch, A., Catalytic mechanism of DNA-(cytosine-C5)-methyltransferases revisited: covalent intermediate formation is not essential for methyl group transfer by the Murine Dnmt3a enzyme. *Journal of Molecular Biology* **2003,** 329, 675-684.

20. Lawrence, M. C.; Barbosa, J.; Smith, B. J.; Hall, N. E.; Pilling, P. A.; Ooi, H. C.; Marcuccio, S. M., Structure and mechanism of a sub-family of enzymes related to *N*-acetylneuraminate lyase. *Journal of Molecular Biology* **1997,** 266, (2), 381-399.

21. Barbosa, J.; Smith, B. J.; DeGori, R.; Ooi, H. C.; Marcuccio, S. M.; Campi, E. M.; Jackson, W. R.; Brossmer, R.; Sommer, M.; Lawrence, M. C., Active site modulation in the *N*-acetylneuraminate lyase sub-family as revealed by the structure of the inhibitor-complexed *Haemophilus influenzae* enzyme. *Journal of Molecular Biology* **2000,** 303, (3), 405-421.

22. Mirwaldt, C.; Korndorfer, I.; Huber, R., The crystal structure of dihydrodipicolinate synthase from *Escherichia coli* at 2.5 Å resolution. *Journal of Molecular Biology* **1995,** 246, (1), 227-239.

23. Dobson, R. C.; Griffin, M. D.; Jameson, G. B.; Gerrard, J. A., The crystal structures of native and (*S*)-lysine-bound dihydrodipicolinate synthase from *Escherichia coli* with improved resolution show new features of biological significance. *Acta Crystallographica Section D-Biological Crystallography* **2005,** 61, (Pt 8), 1116-1124.

24. Pearce, F.G.; Perugini, M.A.; McKerchar, H.J.; Gerrard, J.A., Dihydrodipicolinate synthase from *Thermotoga maritima*. *Biochemical Journal* **2006,** 400, 359-366.

25. Joerger, A. C.; Mayer, S.; Fersht, A. R., Mimicking natural evolution *in vitro*: An *N*-acetylneuraminate lyase mutant with an increased dihydrodipicolinate synthase activity. *Proceedings of the National Academy of Sciences of the United States of America* **2003,** 100, (10), 5694-5699.

Chapter Six

Experimental

6.1 Materials

Chemicals were purchased, unless otherwise stated, from Sigma-Aldrich (Castle Hill, Australia). Media for bacterial cultures and SDS-PAGE gels were purchased from Invitrogen (Christchurch, New Zealand). Bio-Rad protein assay kit and DNA ladders were purchased from Bio-Rad Laboratories (Auckland, New Zealand). Column chromatography media were purchased from GE Healthcare (Auckland, New Zealand) as Hi-Trap pre-packed columns or as a loose gel.

pH measurements were made using a standard pH meter with a Russell combination (Tris compatible) electrode type number TR/CMAW711/TB.

Sonication was performed using a Sonics Vibra Cell sonicator (50 Watts, 4 minutes total on, pulsing 2 seconds on, 9.9 seconds off).

Centrifugation was performed in an Eppendorf centrifuge 5430, on a small scale (less than 1.5 mL) at up to 14000 rpm using a F45-30-11 rotor, and on a large scale (less than 50 mL) at up to 4000 rpm using an A-4-81 rotor at 4^{o}C.

Columns were run using the GE Healthcare ÄKTA process system with UNICORN software control and a GE Healthcare Frac-950 fraction collector.

Polyacrylamide gel electrophoresis (PAGE) was run on an Invitrogen electrophoresis unit, using an Invitrogen power pack.

Ultraviolet (UV) spectroscopy was performed on a Hewlett Packard 8452A diode array spectrophotometer with a circulating water bath to maintain a constant temperature.

Far –UV circular dichroism spectra were recorded from 200 nm to 250 nm at 20^{o}C using a Jasco CD J-185 spectrophotometer.

Differential scanning fluorimetry was done using the iCycler iQ Real Time PCR detection system from Bio-Rad.

^{1}H NMR spectra were recorded on a Varian INOVA 500 spectrometer, operating at 500 MHz and temperature regulated at 23°C. A PRESAT solvent suppression algorithm was used to moderate the HOD solvent peak at 4.65 ppm. Samples were referenced to *t*-butanol as an internal standard.

Protein crystallisation was performed with equipment supplied by Hampton Research. Intensity data were collected at 110 Kelvin using an R-AXIS IV++ image-plate detector coupled to a Rigaku Micromax 007 X-ray generator, operating at 40 kV and 20 mA.

6.2 Molecular biology and microbiology techniques

The methods found in this section were based on protocols in "Molecular cloning: a laboratory manual" by Sambrook *et al.* (1990).[1]

6.2.1 Strains and plasmids

The two strains used in this work were *E. coli* XL-1 Blue (Strategene) and *E. coli* AT997 recA^{-} (*dap*A^{-}, Tet^{r}).

The plasmids used (Table 6.1) were based on the vector pBluescript KS+ and pETM11. The gene *dap*A encodes dihydrodipicolinate synthase and *dap*B encodes dihydrodipicolinate reductase.

Table 6.1 *Plasmids used for protein expression and their genotypes.*

Plasmids	Relevant genotype
pJG001	:: *dap*A, Amp^r
pSD002	:: *dap*B, Kan^r
pTC-K161A	:: *dap*A-lys161ala, Amp^r
pTC-K161R	:: *dap*A-lys161arg, Amp^r

6.2.2 Bacterial cultures

The cultures were grown under sterile conditions and were transferred in a laminar flow hood. All media and equipment were bought sterile or autoclaved at 121^{o}C for 20 min. Solutions were prepared in sterile distilled water. Standard sterile techniques were used in all manipulations of bacterial cultures and each experiment included a set of controls to detect any contamination.

6.2.3 Media

Luria-Bertani medium (LB) LB base was supplied by Invitrogen in a ready to use powdered form. To a litre of water, 20 g of LB base was added. The pH was then adjusted to 7 by addition of NaOH, and the resulting medium was sterilised by autoclave.

NZY$^+$ broth To a litre of water, 10 g of NZ amine, 5 g of yeast extract and 5 g of NaCl were added. The pH was adjusted to 7 by addition of NaOH, and the medium was autoclaved. Following autoclaving, filter-sterilised $MgCl_2$ (1 M, 12.5 mL), $MgSO_4$ (1 M, 12.5 mL), and glucose (20%, 20 mL) were added.

SOC The following were added to dH_20 (to a final concentration): bactotryptone (2% w/v), yeast extract (0.5% w/v), NaCl (10 mM), KCl (2.5 mM), $MgCl_2$ (10 mM), $MgSO_4$ (10 mM), and glucose (36% w/v). The resulting medium was then autoclaved.

6.2.4 Antibiotics and nutritional supplements

Stock solutions of antibiotics and supplements (1000x) were sterilised by filtration, where required, and stored at -20°C. The final concentrations used for selection are shown in Table 6.2.

Table 6.2 *Concentration of supplements used for bacterial selection.*

Supplement	**[Stock]** mg mL^{-1}	**[Working]** µg mL^{-1}
Ampicillin	100	100
Tetracycline	25	25
meso-Diaminopimelate	10	50

6.2.5 Plate preparation

For every 1 mL of molten LB media, 1 µL of antibiotic and 5 µL of *meso*-diaminopimelate were supplemented. The resulting medium was poured directly into sterile petri dishes close to a flame. The plates were then flamed to get rid of any bubbles formed before they had hardened. The plates were placed in a laminar flow hood to remove condensation and once dry, they were ready for use.

6.2.6 Colony growth

Agar plates were streaked with *E. coli* (from a glycerol freeze, an overnight culture, or a single colony on an agar plate) using a flamed sterilised nichrome wire. The plates were incubated overnight at 37°C. Single colonies were selected and used to inoculate LB liquid medium (10 mL). Starter cultures were grown overnight in a shaker incubator (37°C, 180 rpm) and subsequently used to inoculate larger quantities of media.

6.2.7 Preparation of glycerol freeze stocks for storage

An aliquot (1.5 mL) from an overnight culture was centrifuged (14.5 rpm for 3 min). The pellet was re-suspended in 750 µL of the cells, followed by addition of glycerol (sterile 50% v/v, 500 µL). The stock was vortexed before being frozen and stored at -80°C.

6.2.8 Competent cell preparation and transformation of AT997recA$^-$ by electroporation

An overnight culture was inoculated with a single colony of *E. coli* from an agar plate, and the culture was incubated at 37°C overnight. This inoculum was used to seed 1 L of media, which was grown until A_{600} = 0.8. The culture was chilled on ice for 15 min and then centrifuged in cold rotor (4000 g at 4°C for 15 min). The pellet was re-suspended in cold water (1 L) and centrifuged as before. The pellet was washed with cold sterile water (500 µL) and centrifuged again. The latter step was repeated once more. A final wash was performed with glycerol/water (20 mL, sterile, 10% v/v) and the cells were collected by centrifugation. The resulting pellet was re-suspended in 3 mL of cold glycerol/water (10% v/v), from which 40 µL aliquots were stored at -80°C.

When required, competent cells were removed from the freezer and defrosted on ice prior to electroporation. Plasmid DNA (2 µL) in low ionic strength buffer was added to the cells before placed in a pre-chilled cuvette.

Electroporation was performed on a Bio-Rad Gene Pulser set to 2.5 kV at 25 µF with the pulse controller set at 200 Ω. After pulsing, 1 mL of cold SOC was added immediately to re-suspend the cells. The cells were then transferred to an Eppendorf and incubated at 37°C with gentle shaking (100 rpm for 1 hour). Transformants were spread on LB agar plates, with the appropriate antibiotics and supplements, and incubated overnight.

6.2.9 Standard plasmid preparation by alkaline lysis

Solution one	50 mM glucose, 10 mM EDTA, 25 mM Tris.HCl (pH 8.0)
Solution two	0.2 M sodium hydroxide, 1% (w/v) SDS

Solution three 3 M sodium acetate (pH 4.8), 11.5% (w/v) glacial acetic acid

A single bacterial colony was used to inoculate LB broth (10 mL) with appropriate antibiotics and nutrients and incubated overnight (37°C, 180 rpm). An aliquot (1.5 mL) of the culture was added into an Eppendorf and centrifuged (14000 g at 4°C for 30 s). The supernatant was discarded and the bacterial pellet was re-suspended in ice-cold solution one (100 µL) by vigorous vortexing. Freshly prepared solution two was added, mixed with gentle inversion and chilled on ice (5 min). Ice-cold solution three was added, the solution was vortexed gently, and the tube was chilled on ice (5 min). The tube was centrifuged (14000 g at 4°C for 5 min) and the supernatant was transferred to a fresh tube.

The double stranded DNA in solution was precipitated with ethanol (900 µL) at room temperature and mixed by vortexing. The mixture was allowed to stand at room temperature (2 min) and centrifuged once more (14000 g at 4°C for 5 min). The pellet was rinsed with ethanol (70%, 1 mL at 4°C), centrifuged (14000 g at 4°C for 5 min) and the supernatant was removed. The pellet of DNA was allowed to dry in the air (10 min), re-dissolved in water (30 µL) and stored at -80 °C.

6.2.10 PCR site-directed mutagenesis

The Stratagene QuikChange site-directed mutagenesis kit[2] was used to introduce the mutations.

Primer design

Complementary primers were designed to introduce the specific amino acid mutations into the DHDPS gene. The primers were 42 bases in length with a minimum GC content of 40% and terminated in one or more CG bases. The melting temperature (T_m) was required to be greater than 78°C. Equation (6.1) was used to estimate the melting temperature of the primer.

Equation (6.1)[2] $T_m = 81.5 + 0.41(\%GC) - 675/N - \%$ mismatch

Where *N* is the primer length in base pairs. As an example, the lysine to alanine mutation is illustrated. The *dap*A sequence, either side of K161 (highlighted in bold), is shown in the following page.

$^{5'}$ G GCG AAA GTA AAA AAT ATT ATC GGA ATC **AUA** GAG GCA ACA GGG $^{3'}$
K161

The generation of the amino acid change lysine to alanine required a single mutation from AUA to GCA. Thus the primers were:

Primer 1
$^{5'}$ G GCG AAA GTA AAA AAT ATT ATC GGA ATC **GCA** GAG GCA ACA GGG $^{3'}$
(28) K161 (12)

Primer 2
$^{3'}$ C CGC TTT CAT TTT TTA TAA TAG CCT TAG **CGT** CTC CGT TGT CCC$^{5'}$
(28) K161 (12)

Primers were from Invitrogen and they were purified using polyacrylamide gel electrophoresis (PAGE).

PCR conditions

The template DNA, pJG001, was diluted to two concentrations, 0.5 ng/µL and 5 ng/µL and the primers were diluted with dH_2O to 10 ng/µL (Table 6.3). The reversion mutation of pWhitescript with the primers designed was used as a control because this plasmid has a point mutation in the *lac*Z' gene (β-galactosidase), generating a stop codon at position nine of the coding region. The mutagenic primers should replace the stop codon with a glutamine codon, thus restoring activity of the enzyme. The efficiency of the mutations was determined by the proportion of blue/white colonies on IPTG/X-Gal LB plates.

Table 6.3 *Concentration of reagents used for mutagenesis reactions.*

Reagent (Stock concentration)	Control reaction (Final amount)	Sample reaction 1 (Final amount)	Sample reaction 2 (Final amount)
10x reaction buffer	5 µL	5 µL	5 µL
pWhitescript 4.5 kb control plasmid (5 ng/ µL)	2 µL (10 ng)	-	-
Oligonucleotide control primer#1 34-mer	1.25 µL (125 ng)	-	-
Oligonucleotide control primer#2 34-mer	1.25 µL (125 ng)	-	-
dsDNA template (0.5 ng/ µL)	-	10 µL (5 ng)	-
dsDNA template (5 ng/ µL)	-	-	10 µL (50 ng)
Oligonucleotide primer 1 (10 ng/ µL)	-	12.5 µL (125 ng)	12.5 µL (125 ng)
Oligonucleotide primer 2 (10 ng/ µL)	-	12.5 µL (125 ng)	12.5 µL (125 ng)
dNTP mix	1 µL	1 µL	1 µL
dH_2O	38.5 µL	8 µL	8 µL
Pfu Turbo DNA polymerase (2.5 / µL)	1 µL	1 µL	1 µL

Once the PCR steps described in Table 6.4 were completed, the amplification of the parental plasmid was verified by running an agarose gel electrophoresis using the equivalent amount of starting template DNA as a control.

Template digestion

In order to digest methylated parental DNA, endonuclease enzyme *Dp*nI (1 µL, 10 Units μL^{-1}) was added to the reaction products, mixed, centrifuged, and incubated at 37°C for 1

hour. *Dpn*I digests parental (non-mutated) supercoiled dsDNA, leaving newly synthesised DNA unaffected.

Table 6.4 *PCR cycling parameters for mutagenesis reaction.*

Control reaction			**Sample reaction**		
Step	Temperature (^{o}C)	Time (min)	Step	Temperature (^{o}C)	Time (min)
1	95	0.5	1	95	0.5
2	95	0.5	2	95	0.5
3	55	1	3	55	1
4	68	12	4	68	12
5	Steps 2-4 eleven times		5	Steps 2-4 eleven times	

DNA sequencing

DNA sequencing reactions were performed at the Auckland Genomics Facility. Plasmids to be sequenced were quantified using a spectrophotometer and sequenced using the dideoxynucleic acid chain termination method, using the IR-labelled primers T3 and T7.

6.2.11 Agarose gel electrophoresis

Loading dye 30% (v/v) glycerol, 0.25% (w/v) bromophenol blue, 0.25% (w/v) xylene cyanol

TAE buffer 40 mM Tris-acetate (pH 8.0), 1 mM EDTA

The gel (TAE buffer 30 mL, agarose 0.3 g) was cooled to ~50^{o}C, poured into a gel casting tray, and the well comb inserted. The comb was only removed when the gel had set completely. The casting tray was transferred into a gel tank containing electrophoresis TAE buffer. The gel was loaded with DNA (1 µL), which had been mixed with loading buffer (1 µL), along with a DNA ladder. The gel was run at 60 V for ~2 hours. The gel

was stained with ethidium bromide (0.5 $mgmL^{-1}$, 20 min) and the DNA fragments were visualized under UV radiation (302 nm).

6.3 Biochemistry techniques

Unless otherwise stated, enzymes were manipulated on ice or at 4°C to reduce denaturation. All enzymes were routinely stored in 20 mM Tris.HCl pH 8.0 at 4°C (buffer A) at -20°C in 1 mL aliquots.

6.3.1 Preparation of the crude

The cultures incubated overnight were placed on ice (20 min), and the cells were harvested by centrifugation (4000 rpm at 4°C for 10 min) and re-suspended in buffer A. The cells were sonicated (20 min) to release protein and centrifuged (4000 rpm at 4°C for 20 min). The supernatant (crude) was either stored at -20°C or applied to a column for purification.

6.3.2 Purification of DHDPR

Affinity chromatography

The crude was loaded onto a His-Trap column. The column was washed with an extraction buffer (50 mM NaH_2PO_4, pH 8.0, 50 mM imidazole, 300 mM NaCl) for 3 column volumes and then protein was eluted with elution buffer (50 mM NaH_2PO_4, pH 8.0, 500 mM imidazole, 300 mM NaCl). Fractions containing DHDPR activity were pooled, dialysed against buffer A and stored at -20° C.

6.3.3 Purification of DHDPS

Heat shock

Aliquots of the crude (1 mL) were added to centrifuge tubes, heat shocked at 70°C for 2 min. The tubes were immediately cooled on ice before centrifugation (14000 rpm at 4°C for 10 min). The supernatants were collected and pooled.

Ion exchange chromatography

The pooled sample from heat shock was loaded onto a Q-Sepharose column (bed volume 75 mL, 15 x 2.6 cm) that had been pre-equilibrated with 5 bed volumes of buffer A. The column was then washed with 5 bed volumes of the same buffer and the enzyme was eluted with a 0-1 M NaCl gradient in buffer A. The column was washed with three bed volumes of the regeneration buffer (1 M NaCl in buffer A). Eluted fractions were tested for DHDPS activity using the *o*-aminobenzaldehyde assay (Table 6.5).

Table 6.5 *Reagents used in* o*-aminobenzaldehyde assay.*

	[Initial] mM	**Volume µL**	**[Final] mM**
Tris.HCl pH 8.0 at 25°C, pyruvate	200,40	150	166,33
o-aminobenzaldehyde	400	5	10
DHDPS test solution	-	5	-
(*S*)-ASA	40	5	
Total volume		165	

The assay mix was incubated (30°C for 30 min) and the reaction was quenched by the addition of TCA (10%, 100 µL). Active fractions showed purple coloration and were pooled. Control assays without substrate or enzyme were also prepared.

Hydrophobic interaction chromatography

Ammonium sulfate was added to the pooled fractions from the ion exchange step to a concentration of 0.5 M. This was loaded onto a phenyl-Sepharose column (bed volume 25 mL, 7 x 2.6 cm) that had been pre-equilibrated with five bed volumes of 0.5 M ammonium sulfate in buffer A. The column was then washed with five bed volumes of the start buffer (0.5 M ammonium sulfate, buffer A) and the enzyme was eluted with an ammonium sulfate gradient (0.5-0 M) in buffer A. The column was washed with three bed volumes of buffer A. Eluted fractions were tested for DHDPS activity using the *o*-aminobenzaldehyde assay described earlier in this section.

Size exclusion chromatography

The pooled sample from hydrophobic interaction chromatography was loaded onto a size exclusion chromatography column that had been pre-equilibrated with five bed volumes of buffer A. The fractions were once again tested for DHDPS activity using the *o*-aminobenzaldehyde assay.

6.3.4 Sodium dodecyl sulfate polyacrylamide gel electrophoresis (SDS-PAGE)

Table 6.6 *Sample preparation for SDS-PAGE.*

Reagent	**Volume (µL)**
Sample	x
NuPAGE® LDS sample buffer (4X)	2.5
NuPAGE® reducing agent (10X)	1
dH_20	To 6.5
Total volume	10

Electrophoresis tank buffer	NuPAGE ® MOPS SDS running buffer (Invitrogen)
Coomassie blue stain	1% (w/v) Coomassie blue, 50% (v/v) methanol, 10% (v/v) glacial acetic acid
Destain	5% (v/v) methanol, 10% (v/v) glacial acetic acid

Pre-cast 4-12% gradient gels were used for analysis. Samples had to be diluted with buffer to allow the loading of ~20 µg of total protein, and then mixed with equal volume of sample treatment buffer. Samples were heat shocked at 70°C for 10 min before being loaded into the wells of the gel. The gel was run at 200 V for 50 min and it was stained with Coomassie blue for 30 min, followed by destaining.

6.3.5 Bradford assay

Protein concentration was determined using the standard Bradford procedure (Table 6.7).[3] The samples were diluted to give absorbance readings at 595 nm between 0.1 and 1.0.

Table 6.7 *Volume of solutions used for the Bradford assay*

Assay solutions	Volume (µL)
Sample	80
H_2O	720
Bio-Rad protein solution dye	200

The assays were incubated at room temperature for exactly 10 min before measuring the absorbance at 595 nm, blanked against a solution containing 800 µL dH_2O and 200 µL of Bio-Rad solution. Each measurement was performed in triplicate. The protein concentrations were obtained from a calibration curve generated in parallel using BSA.

6.3.6 Kinetic studies of DHDPS

All components shown in Table 6.8, except the test solution, were added to the cuvette and incubated at 30°C for 15 min. The test solution was added with quick mixing using the pipette tip after the incubation period. The change in absorbance at 340 nm was recorded over 60 seconds, blanked against water. Controls against no substrate, and controls lacking DHDPS were also carried out. This method was adapted from Coulter *et al.* (1999)[4] and Dobson (2003).[5]

Data analysis

The initial rate data collected were analysed using the Enzfitter programme available from Biosoft (Cambridge, UK). The models used to fit the data were chosen based on R^2 values and the lowest standard errors associated with the fit. When these parameters were similar, the model was chosen based on the lowest *F*- and *p*-values.

Table 6.8 *Coupled assay to measure the initial rate of DHDPS-catalysed reaction.*[5]

Stock	[stock] mM	Volume µL	[cuvette] mM
HEPES pH 8.0 at 4°C	200	400	100
NADPH	5.4	30	0.203
DHDPR		50	
dH_2O		230	
Pyruvate	100	20	2.5
[(*S*)-ASA]	100	20	2.5
dH_2O		40	
Test solution		10	
Total		800	

6.3.7 Sodium borohydride inactivation test

Each enzyme (0.3-1.0 mg/mL) was incubated (30 min, 25°C) with pyruvate (20 mM) or (*S*)-ASA (5 mM) in the presence of Tris.HCl (200 mM, pH 8.0, 4°C). Samples were then placed on ice, followed by addition of $NaBH_4$ (25 µL, 100 mM made up with Tris.HCl (200 mM, pH 8.0, 4°C) for a total period of 15 min. After that, the samples were placed on ice for a further 30 min and then dialysed against 100 volumes of buffer A overnight. The activity of DHDPS after treatment with $NaBH_4$ was assessed using the coupled assay.

6.3.8 Far-UV circular dichroism spectroscopy

Purified wild-type DHDPS, DHDPS-K161A and DHDPS-K161R, which were all stored in 20 mM Tris.HCl (pH 8.0), were first applied to a de-salting column against the assay buffer (20 Mm $NaPO_4$, 150 mM NaF, pH 8.0) at 4°C. Final concentrations of the proteins were determined using a NanoDrop (Thermo Fischer Scientific) reading at A_{280} to be ~0.3 mg/mL. CD spectra were recorded from 200 nm to 250 nm at 0.5 nm increments, using a 1 mm path length quartz cell. The reported spectra were the average of two scans that were corrected for buffer blanks.

6.3.9 Differential scanning fluorimetry

DSF was performed using the iCycler iQ Real Time PCR detection system from Bio-Rad, with methods based on those of Niesen *et al.* (2007).[6] Solutions of Sypro orange (20 µL, 1000x concentrate), protein (80 µL, 0.1-2.0 mg/mL) and pyruvate (5 mM) were added to the wells of a 96-well thin-wall PCR plate (Bio-Rad). Water was added instead to protein in the control sample and for each well containing pyruvate, there was one without it for comparison. The plates were sealed with optical quality sealing tape (Bio-Rad) and heated in an iCycler iQ Real Time PCR detection system from 20 to 90°C, in increments of 0.30°C.

The Boltzmann model (Equation (6.2)) was used to obtain the temperature midpoint for each protein unfolding transition, T_m, from the fluorescence data gathered.

Equation (6.2)[6]

$$y = LL + \frac{(UL - LL)}{1 + \exp\left(\frac{T_m - T}{a}\right)}$$

Where y is the fluorescence intensity at temperature T, LL and UL are the values of minimum and maximum intensities, respectively, and a denotes the slope of the curve within T_m.[7]

6.3.10 Isothermal titration calorimetry

ITC experiments were performed using a VP-ITC calorimeter (MicroCal, Inc.) as described previously.[8] All experiments were conducted at 25°C. Purified wild-type DHDPS, DHDPS-K161A and DHDPS-K161R, which were all stored in 20 mM Tris.HCl (pH 8.0), were first applied to a de-salting column against the assay buffer (20 mM HEPES, pH 8.0) at 4°C. Final concentrations of DHDPS-K161A and DHDPS-K161R in 20 mM HEPES were determined using a NanoDrop (Thermo Fischer Scientific) reading at A_{280} to be 0.3 mg/mL and 0.4 mg/mL respectively. A portion of the buffer was used to make up the pyruvate solutions to minimise the heats of dilution. The concentration of pyruvate in the syringe used in the DHDPS-K161A experiment was 0.9 µM and 1.4 µM

for DHDPS-K161R. Prior to titration, all the solutions were degassed under vacuum for 5 min at 23°C.

The titration schedule consisted of an initial injection of 2 μL, followed by 55 consecutive injections of 5 μL of pyruvate solution over a period of 10 sec into the reaction cell (volume = 1.5 mL), at an interval of 210 s to allow heat equilibration, using a syringe rotating at 307 rpm. The initial injection of 2 μL for all samples and third injection of 5 μL for DHDPS-K161R were excluded from attempted data fitting due to anomalous values.

Efforts to increase the heat generated per injection of pyruvate into DHDPS-K161A and K161R were not attempted due to consideration of the heat generated for the binding of pyruvate to wild-type DHDPS at similar protein concentrations.

6.3.11 ^{1}H NMR spectroscopy

Deuterated phosphate buffer (Na_3PO_4, 20 mM, pD 8.16) was prepared *via* the addition of Na_2HPO_4 (66.2 mg) and NaH_2PO_4 (4.1 mg) to 5 mL of 99.9% D_2O. Conversion of pH to pD values was done using Equation (6.3).

Equation (6.3) $$pD = 0.929\ pH^* + 0.42$$

Where pH* is a direct reading in a D_2O solution of the H_2O-calibrated pH-meter.[9]
An internal standard solution of *t*-butanol was prepared by diluting *t*-butanol (8 μL) into D_2O (200 μL). Pyruvate solution (20 mM) was prepared immediately prior to spectra acquisition by dissolving the desired amount of sodium pyruvate in the deuterated phosphate buffer (Na_3PO_4, 20 mM, pD 8.16).

Experimental samples for data acquisition were prepared *via* the addition to a 5 mm NMR tube of *t*-butanol standard solution (10 μL), aqueous protein solution (10 μL) and sodium pyruvate (20 mM, 400 μL) in deuterated phosphate buffer solution. The tube was

inverted a number of times to facilitate mixing and spectra acquisition commenced immediately.

The experiment was repeated for several enzyme concentrations. Data recording runs were conducted either discretely or continuously. Discrete collection was performed on three replicates, with spectra recorded at 1 hour time intervals for the first 6 hours, and subsequently at extended intervals for a period of 4 days. Continuous collection was done as a single arrayed experiment for a period of 16 hours, acquiring spectra every 10 minutes to generate 78 unique data points. Proton-deuterium exchange of the enolisation of pyruvate α-protons was quantified by comparison of the integral values of pyruvate peak area relative to the *t*-butanol standard.

6.3.12 Crystallisation

Crystallisation and X-ray data collection

The crystals were grown at 12°C using the hanging drop-vapour diffusion method as described by Mirwaldt *et al.* (1995).[10] The crystal trays were set up as it is described in Table 6.9.

The reservoir contained K_2HPO_4 buffer (1 mL, 1.8 M, pH 10.0). The crystals appeared after 2 days and they were soaked in a cryoprotectant solution (K_2HPO_4, 1.8 M, pH 10.0, 20% glycerol (v/v)) prior to being flash-frozen in liquid nitrogen when data was required. Some crystals were also grown in the presence of pyruvate (20 mM), which was added to the buffer solution. Diffraction data sets were processed and scaled using the programme *CrystalClear*.[11]

Structure determination and refinement

The structure of each mutant enzyme was solved using *MolRep*,[12] The wild-type enzyme structure found in the RCB Protein Data Bank, entry 1YXC, was used to get the preliminary structures. Further refinements were done using *REFMAC5*.[12] Electron density maps were interpreted with the aid of *COOT*. Structure quality was assessed using *PROCHECK*[13] and other validation tools in *COOT*.[14]

Table 6.9 *Crystal tray set-up for crystallography experiments.*

		Column 1	**Column 2**	**Column 3**	**Column 4**	**Column 5**
Row 1	Protein (µL)	3	3	3	3	3
	Buffer (µL)	1.2	1.1	1	0.9	0.8
	N-OG (µL)	0.45	0.45	0.45	0.45	0.45
	H_2O (µL)		0.1	0.2	0.3	0.4
	Total volume (µL)	4.65	4.65	4.65	4.65	4.65
Row 2	Protein (µL)	2.25	2.25	2.25	2.25	2.25
	Buffer (µL)	1.2	1.1	1	0.9	0.8
	N-OG (µL)	0.45	0.45	0.45	0.45	0.45
	H_2O (µL)	0.25	0.35	0.45	0.55	0.65
	Total volume (µL)	4.15	4.15	4.15	4.15	4.15
Row 3	Protein (µL)	1.5	1.5	1.5	1.5	1.5
	Buffer (µL)	1.2	1.1	1	0.9	0.8
	N-OG (µL)	0.45	0.45	0.45	0.45	0.45
	H_2O (µL)	0.5	0.6	0.7	0.8	0.9
	Total volume (µL)	3.65	3.65	3.65	3.65	3.65

Where the protein concentration was ~7.5 mg/mL

The buffer used was K_2HPO_4 (1.8 M, pH 10.0)

N-OG was used at a concentration of 6% (w/v).

6.4 References

1. Sambrook, J.; Fritsch, E.; Maniatis, T., *Molecular cloning: a laboratory manual* Cold Spring Harbor Press: New York, 1990.
2. Stratagene, *Quickchange site-directed mutagenesis kit: instruction manual*. 1998.

3. Bradford, M., A rapid and sensitive method for the quantification of microgram quantities of protein utilizing the principle of protein-dye binding. *Analytical Biochemistry* **1976,** 72, 248-254.
4. Coulter, C. V.; Gerrard, J. A.; Kraunsoe, J. A. E.; Pratt, A. J., *Escherichia coli* dihydrodipicolinate synthase and dihydrodipicolinate reductase: kinetic and inhibition studies of two putative herbicide targets. *Pesticide Science* **1999,** 55, 887-895.
5. Dobson, R. C. Investigating the catalytic and regulatory mechanism of dihydropicolinate synthase. D. Phil. Thesis. University of Canterbury, 2003.
6. Niesen, F. H.; Berglund, H.; Vedadi, M., The use of differential scanning fluorimetry to detect ligand interactions that promote protein stability. *Nature Protocols* **2007,** 2, (9), 2213-2221.
7. Ericsson, U. B.; Hallberg, B. M.; DeTitta, G. T.; Dekker, N.; Nordlund, P., Thermofluor-based high-throughput stability optimization of proteins for structural studies. *Analytical Biochemistry* **2006,** 357, 289-298.
8. Turnbull, W. B.; Daranas, A. H., On the value of c: can low affinity systems be studied by isothermal titration calorimetry? *Journal of the American Chemical Society* **2003,** 125, (48), 1459-1466.
9. Krężel, A.; Bal, W., A formula for correlating pK_a values determined in D_2O and H_2O. *Journal of Inorganic Biochemistry* **2004,** 98, (1), 161-166.
10. Mirwaldt, C.; Korndorfer, I.; Huber, R., The crystal structure of dihydrodipicolinate synthase from *Escherichia coli* at 2.5 Å resolution. *Journal of Molecular Biology* **1995,** 246, (1), 227-239.
11. Pflugrath, J. W., The finer things in X-ray diffraction data collection. *Acta Crystallographica Section D-Biological Crystallography* **1999,** 55, 1718-1725.
12. CCP4, The CCP4 suite: programs for protein crystallography. *Acta Crystallographica Section D-Biological Crystallography* **1994,** D50, 760-763.
13. Laskowsky, R.; MacArthur, M.; Thornton, D., PROCHECK: a program to check the stereochemical quality of protein structures. *Journal of Applied Crystallography* **1993,** 26, 283-291.

14. Emsley, P.; Cowtan, K., Coot: model-rebuilding tools for molecular graphics. *Acta Crystallographica Section D-Biological Crystallography* **2004,** 60, 2126-2132.